Combining a Physics-based Model and Spatial Interpolation of Scarce Bed Topography Data in Meandering Alluvial Rivers

Dimitrios Ioannis Zervakis

Technische Universiteit Delft

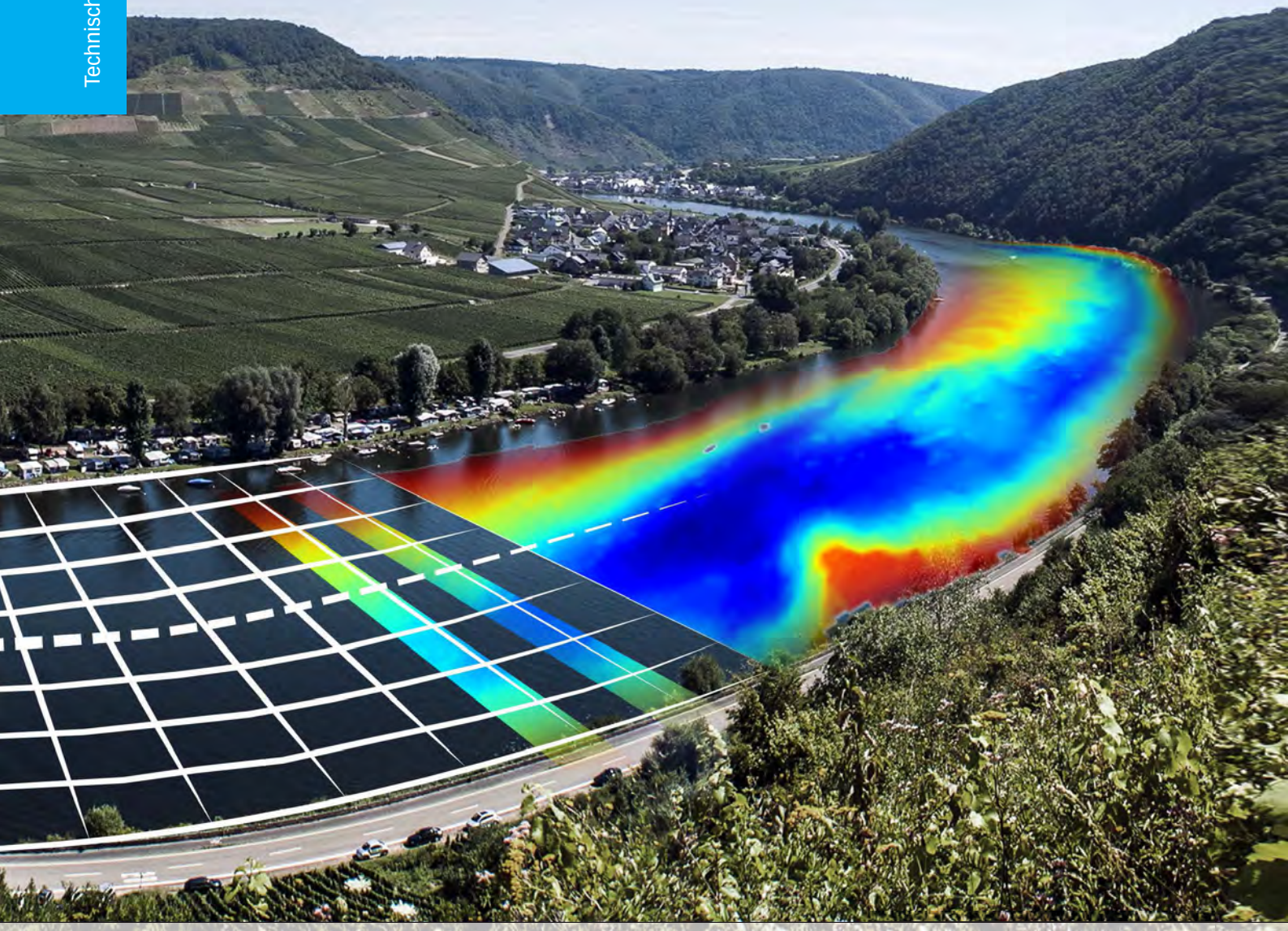

TU Delft Delft University of Technology

Deltares Enabling Delta Life

Challenge the future

Combining a Physics-based Model and Spatial Interpolation of Scarce Bed Topography Data in Meandering Alluvial Rivers

by

Dimitrios Ioannis Zervakis

Student number: 4312775

E-mail: zerbakis@gmail.com

in partial fulfillment of the requirements for the degree of

Master of Science
in Geomatics

at the Delft University of Technology,
to be defended publicly on Friday November 6, 2015 at 14:45 AM.

Supervisors: Dr. Ir. B.M. (Martijn) Meijers
Prof. Dr. Ir. P.J.M. (Peter) van Oosterom
Dr. Ir. E. (Erik) Mosselman

An electronic version of this thesis is available at: http://repository.tudelft.nl/

For further information regarding the current state of the project contact
Ymkje.Huismans@deltares.nl or Koen.Berends@deltares.nl

TU Delft Delft University of Technology

Deltares
Enabling Delta Life

On cover:

Mosel River, Beilstein, Germany. [*50°06'26.3"N 7°14'09.5"E (WGS84)*]

Photo by: "*donnosch*", https://interfacelift.com/wallpaper/details/3527/mosel_river_curve.html

Adaptation by: *Rusnė Šilerytė*

Abstract

All human life is dependent on fresh water and activities related to monitoring its availability have become crucial for financial and survival reasons. Most rivers are being constantly investigated today by both the private and public sector using various means. In advanced countries, the researches cover extensively the riverbed in order to fully assess its topography. However, there are quite often cases where the data collected are disorderly scarce, resulting in questionable assumptions and interpolated predictions.

The purpose of this thesis is to provide a new method for reconstructing the riverbed topography when data are scarce, so as to achieve better results than the ones conventional methods currently give. The chosen course of action involves a combination of the datasets outputted by a simplified physics-based model and spatial interpolation of the available scarce topography data.

The surrounding research involves numerous aspects of mathematics, physics and spatial analysis, which together are called in to provide a complete solution to an existing problem. The focus lies on meandering alluvial rivers, whose planform style is the most common in human-populated river basin areas. Three rivers of different extent and interest are explored, namely the Danube (Romanian area), IJssel (Netherlands) and Kootenai (United States). The study cases comprise river areas extracted from each of them, in order to focus on bends and mildly widening or narrowing parts of the rivers.

The final outcome of this Master Graduation Thesis project was achieved through literature research, exploration and implementation of ideas and scientific methods, made possible through cooperation with the Deltares independent institute for applied research. The proposed method combines scarce riverbed topography data with the basics of river morphology and spatial interpolation techniques to come to a new method that achieves a result of higher value in the complex field of river and geomatics engineering. The method is further assessed and evaluated and will ideally be incorporated in the Rapid Assessment Tool for Inland Navigation (*RAT-IN*) which is currently under development at Deltares.

Acknowledgements

This thesis has been carried out with the kind support and help of many individuals. I would like to extend my sincere thanks to all of them.

First, I would like to thank my supervisors at the TU Delft, Martijn Meijers and Peter van Oosterom for their skilful guidance and critical and constructive comments on my work. Their involvement in both feedback and directions has been invaluable.

I would also like to thank my supervisors at Deltares, Koen Berends and Ymkje Huismans for their support, motivation and outmost attention they showed throughout the completion of my thesis. Working with them has been a pleasure and a great inspiration.

Furthermore, a big thank you goes to my co-reader Erik Mosselman, who has always been willing to advise and clarify any conundrums I came across in theory and practice.

My gratitude extends to Ryan Fosness of USGS for information regarding data and Alessandra Crosato for her work that helped immensely this thesis, along with the very informative meeting I had with her.

Of course, I want to thank my friends and colleagues in both my Geomatics group and Deltares for many interesting and enjoyable talks through pressured and relaxed times. Special thanks to Rusnė Šilerytė for the beautiful cover and other kinds of support.

Last, but most importantly, I wish to wholeheartedly thank my parents Evangelos and Victoria and my sister Maria for always standing by my side even though the physical distance kept us apart most of the time.

Thank you all.

Contents

Acronyms

CRS	Coordinate Reference System
DEM	Digital Elevation Model
EPSG	European Petroleum Survey Group
EIDW	Elliptical Inverse Distance Weighting
GIS	Geographic Information System
IDW	Inverse Distance Weighting
MAT	Medial Axis Transform
NHWS	Normalized Half-Width Slope
RAT-IN	Rapid Assessment Tool for Inland Navigation
RBF	Radial Basis Function
RMSE	Root Mean Square Error
TIN	Triangulated Irregular Network
TPS	Thin Plate Spline
USGS	United States Geological Survey

1 Introduction

It is a common case that river bathymetry data are limited due to the way they are collected. Subsequent interpolation methods applied do not provide an accurate representation of the riverbed in such cases, therefore physical or computational models are used, with the need for expert assessment. This process is usually highly time-consuming and also does not take full advantage of any knowledge acquired from the collected data.

In this thesis, a complete method for combining a physics-based model and spatial interpolation results is proposed as a solution to the above problem. The first chapter provides the motivation (§1.1), formulates the problem (§1.2) and relates it to the field of Geomatics (§1.3). The scope (§1.4) and research objectives (§1.5) are stated, along with the research questions (§1.6) that govern the process described. Finally, the outline of the remainder of the document is presented in §1.7.

1.1 Motivation

It has always been common practice for people to inhabit places with close access to fresh water. Today nearly 50% of the global population lives closer than 3 km to surface fresh water [*Kummu et al. 2011*], mainly including rivers and streams. Furthermore, the economic viability and competitiveness of ports has a lifeline link to the waterway network, which mainly comprises rivers. Therefore, river monitoring is of utmost importance for flood safety, water availability and safe navigation of ships, the latter of which can be compromised by the natural behaviour of rivers to form shoals and sharp bends. To this extent, the riverbed morphology and topography needs to be well-updated regularly to provide reliable information.

Unfortunately, bathymetric river data usually do not cover the whole channel bed in order to allow for its precise depiction, but are instead limited and scarcely spread. To mediate the lack of data, interpolation methods are applied, which, depending on the data available, can be highly inaccurate [*Merwade 2009*]. Their output can be extremely smoothed-out and in cases, the overall result dissuades their extended use.

Therefore, physics-based models and flow dynamics are sometimes called in, in order to reach a more natural riverbed topography representation. However, these models can be difficult to formulate, they are subject to a number of pre-defined conditions and in the case of Computational Fluid Dynamics (CFD) they require large computational times and power.

In situations where a more expert assessment is required, the ultimate solution is manual interpolation. Experts in river morphology can provide a graceful insight on what is expected behaviour in river channels and together with whatever limited data are available, they can come close to a real representation of the riverbed. As it is obvious though, this procedure is time-consuming and bad on managing human resources.

Considering the above issues, an automatized method that can make use of such limited data and also "fill in the gaps" by applying the physical aspects of river morphology in a rapid assessment of the riverbed topography is a wanted advancement towards solving this data scarcity problem.

1.2 Problem Statement

A variety of numerical modelling efforts related to hydrodynamics, sediment transport, vegetation and geomorphic analyses require an accurate representation of riverbed topography. However, the applicability of the numerical models can be impaired due to the low availability of bathymetric data. Many reasons may pose a hindrance for acquiring full riverbed coverage, among those being low funding, river accessibility, crew and equipment unavailability and even the dynamic environment of rivers itself, which is constantly changing. Therefore, river data collection usually results in limited information, upon which interpolation techniques need to be applied to acquire an overall representation.

A number of spatial interpolation methods are available, like Inverse Distance Weighting, Kriging, Spline and others. It has been proven [*Merwade et al. 2006*] that transforming the data to a flow-oriented coordinate system and applying anisotropic spatial interpolation techniques outperforms significantly isotropic ones in both the Cartesian and flow-oriented coordinate systems.

This procedure however is only suitable if the data points gathered are relatively dense, closely-spread or regularly sparse. On the other hand, if only scarcely-spread data are available, such techniques cannot be directly applied, since they result in wrong predictions about bed topography in river bends and where the river widens or narrows. Furthermore, they may smooth out crucial bed formations or result in solutions governed by noise.

Such scarce data are common to be originating from for example single-beam echo sounder data, mainly gathered along a vessel's trajectory ("trackline") or expeditions on chosen cross-sections. The difficulty of the problem is to couple the physics of the river morphology with a spatial interpolation technique that can be applied upon such scarce datasets.

1.3 Relevance to Geomatics

Geomatics Engineering is the science and study concerned with the collection, manipulation and presentation of the natural, social and economic geography of natural and built environments [*Lemmens 2011*]. Geographical information plays an important role in activities such as environmental monitoring, management of land and marine resources, and real-estate transactions. In such manner, river data contain geographical information that, depending on the application, can be of high interest.

An accurate representation of the riverbed topography can be vital in a wide range of applications, including studies which relate to monitoring and investigating rivers for flood safety, water availability, navigability and dredging. Developing a way of extracting useful information from limited resources and creating new knowledge is one of the main actions performed within the multidisciplinary field of Geomatics. Extending this procedure to an automatized process that helps the researcher or general user and provides a faster result is also a golden goal to aim at.

1.4 Thesis Scope

The focus of this project is on the implementation and assessment of a method that couples a spatial interpolation technique together with the impact of physics in riverbed morphology in order to provide an acceptable solution when collected data are scarce. River bathymetry data come in many forms, but the wording of 'scarce' in the current context is defined as data insufficient to provide a very good estimation for the riverbed topography. These data may be single-beam tracklines derived from ship trajectories collected in a 'zig-zag' pattern, or even cross-sections collected at areas of interest [Figure 1.1].

Figure 1.1. Scarce single-beam echo-sounder data. Cross-sections are formed when data are collected transversely of the river's direction. "Trackline" data follow trajectories of the ships along a river (Danube River, Romania. *Bing maps, 2015*).

The river areas of special interest are defined as single river channel bends and parts where the river narrows or widens without sudden changes. The aim of this choice is to examine the ability of an algorithm to predict the areas of small water depth (point bars) and the bathymetry in general. The type of rivers examined in this context is meandering alluvial rivers without extreme natural impacts or human interventions (i.e. waterfalls, big discharge, islands, bifurcations, dams etc.). Meandering rivers are chosen as they are the most common planform type of rivers in populated areas [*Crosato 2008*], therefore in the wider social context are of a greater importance. The method could be extended to include bifurcation cases; however, that would require further implementation in terms of grid alignment, space tessellation, data averaging and a re-established physics-based model. Hence, bifurcations are considered out of scope.

The governing theory applied [*Crosato 2008*] allows as a first relaxation to the non-linear equations that define the water flow a zero-order approximation under the assumption of an infinitely long

straight channel. This basically assumes that the flow cross-section remains constant, providing a basis for the riverbed level of a mildly varying in width channel. Furthermore, as a rule for the prediction of bed topography in river bends, the axi-symmetric solution of the derived equations can be estimated assuming mildly curved channels. Other physics-based models [*Frascati & Lanzoni 2013*] make more detailed assumptions about the impact of varying widths in rivers, but due to their complexity and the general ambiguity of where river banks are really situated, they are not considered. Furthermore, out of scope are any physics related to bank erosion/failure (bank accretion/advance), vegetation and floods. In order to deal with the presence of river banks, a simpler static geometrical profile is assumed.

Within the thesis scope, a number of existing spatial interpolation techniques are considered, through which the final algorithm is made possible and to which it is compared. Currently, the most notable ones are Elliptical Inverse Distance Weighting (EIDW) [*Merwade et al. 2006*] and anisotropic ordinary kriging [*Eriksson & Siska, 2000*]. However, the latter one is shown to produce erroneous results when available data are scarce. In addition, state of the art techniques such as those used by GIS software cannot be implemented, but can only be used for assessment and comparisons. From the ones implemented, the best performing one is used for the definite comparison with the proposed method. Ideally, the river areas would be able to be segmented in parts, evaluated as to their geometrical and physical properties and the data available and the best spatial interpolation method would be chosen for each segment. This however extends beyond the scope of the thesis into a separate field of research. The proposed method can nevertheless be used in a scheme that includes the aforementioned partitioning and evaluation. By this decision, the partitioning of the river areas is not of significance and as such, any kind of effort for classification and semantics of rivers is considered out of scope as well.

The evaluation is made in a trilateral sense. In hard numerical terms, the use of a Root Mean Square Error (RMSE) evaluator allows to compare a 'ground-truth' and a derived 'test' dataset for the combined method for each case. Furthermore, for a visual inspection, Error Maps are presented to qualitatively assess the results in pictures. Finally, the transverse slope of the half-width along the centerline of the river is investigated, in order to receive a more center-targeted evaluation of the results.

The implementation and assessment of all processes were fully developed as Python code, maintaining an open-source friendly profile. The classes, modules and scripts can be further assessed to be incorporated into the Rapid Assessment Tool for Inland Navigation (RAT-IN). This tool is currently in development at Deltares [*Institute; Deltares*] and aims to "*rapidly assess a river's suitability for inland navigation based on state-of-the-art scientific knowledge and freely available data sources*". Therefore, the main application field for the proposed method is the navigability of channels that fit into the above scope description.

In terms of efficiency, the proposed method aims to provide a tool for the researcher or the general user to aid him or her in research and greatly reduce the time required compared to what it would be if the same process was performed manually. However, techniques for computational efficiency such as parallelization (multi-core computing), efficient storage and accessing of datasets, data structures for efficient performance of each interpolation method and the evaluation by computational time are excluded from this research, since they lie more in the optimization of the method than the method itself.

1.5 Objectives

To set the covered issues into perspective, the objectives of the thesis need to be defined. These range from hard requirements that are intertwined with the thesis purpose to intermediate goals that were required to be completed in order to reach the final result.

Therefore, the hard requirements are as stated:

- Develop a method for combining a spatial interpolation technique with the physical impacts of riverbed morphology.
- Consider the zero-order approximation of water flow and axi-symmetric solutions of bed topography in river bends.
- Describe data in a flow-oriented coordinate system.

The first two are inter-connected towards the completion of the project, while the third allows for a better final result.

High-priority objectives are considered the following:

- Define ground-truth and test datasets.
- Compare results with other spatial interpolation methods for evaluation.
- Provide a 'goodness-of-fit' model for evaluation.
- Incorporate final method into the RAT-IN tool.

The above are fully covered at the completion of the project, except the last one, which requires an extra assessment by the party interested (Deltares). The current status is to extend the RAT-IN tool with further features and options before release.

Further aims needed for completion of the project are:

- Create a way of obtaining a curvilinear grid upon which the data are projected.
- Propose a way for representing the raw data on the grid.
- Acquire realistic hydrographical/geometric values that relate to the chosen rivers. These values are numbers related to parameters required in order to use the equations of the physics-based model. These include discharge, mean grain size, slope, widths and other coefficients.

The latter three aims are desired research, closely related to the topic and are resolved within the overall procedure. However, these objectives are not the core of this thesis and as such the solutions proposed are not definite, complete or necessarily the best ones.

The objectives listed above clearly define the implementation aims of the thesis, but towards the resulting outcome, a number of additional procedures are considered without naming them here. These can nevertheless be important to the completion process, yet not strictly defined as objectives. This is due to the fact that their functional use does not affect the methodology and they can be achieved in a variety of ways.

1.6 Research Questions

The main research question that directed the progress of this thesis is the following:

> *"How can a spatial interpolation method be coupled with river morphology physics in order to approximate better* the riverbed topography when input data are scarce**?"*

*: By the notion of '*better*' a numerical form of assessing quality (in example, Root Mean Square Error) or other form of quality flag evaluation is meant. The comparison is made to existing spatial interpolation methods, which are chosen in terms of state-of-the-art and relation to the topic.

**: The term '*scarce*' is related back to the origins of the problem, which as described in §1.4, includes 'trackline' data or simple cross-sectional data.

In addition to the governing research question, a number of issues will be addressed, to provide completeness on the project's results:

1. *What is an objective function to measure 'goodness-of-fit' of the method?*

2. *What coordinate system allows for better predictions on riverbed topography?*

3. *How much of the full data can be thinned out and still have a successful outcome?*

The above questions are answered with the delivery of the solution and the experimental results. Further research can be performed to cover a wider extent of each question and to ultimately arrive at a deeper understanding of the problem field.

1.7 Thesis Outline

The structure of the remainder of the thesis is as follows:

- Chapter *2* provides the reader with the related work that encompasses the thesis scope and implementation. The approximations taken into account related to riverbed morphology physics are presented along with an overview of spatial interpolation methods and related literature.
- Chapter *3* covers the methodology followed in the thesis and gives insight on the concept of the proposed method.
- Chapter *4* presents the actual approach and implementation procedure for every step of the methodology. The issues related to successfully complete each step of the process are covered along with the overall process pipeline. One of the study cases is chosen as the example that follows the whole procedure.
- Chapter *5* features selected final results and through a discussion compares them to a range of outputs from a variety of different study cases. Also, the evaluation and the methods of assessment are discussed.
- Chapter *6* finishes with conclusions, recommendations and future work that can be done to advance the field.

Additionally, three Appendices supplement this thesis. These concern the construction of the river polygon centerline (Appendix A), the aggregation of the point data on the grid (Appendix B) and additional results not presented in the body of the thesis (Appendix C).

2 Related Work

The relevant concepts and theories encompassing the field of the study subject can be considered as vast, complex and developing. Much of the information related to the river environment still lie in the theoretical scope and few physics-based models currently account for factors related to river morphology. Nevertheless, the last decade has allowed for better representations of the river dynamics using 2D and 3D models (unstructured nested grid in SSIIM by [*Olsen 2003*], the morphodynamic model of Delft3D by [*Lesser et al. 2004*], meander migration model MIANDRAS by [*Crosato 2008*]), which also unlocked hidden areas of research.

Riverbed topography is still subject to numerous influences, which even if they are partially accounted for in numerical modelling may result in wrong predictions. This is due to insubstantial data, variable information or physical effects not yet incorporated in the models. As a best practice for the scope of this research and for producing an acceptable outcome, is assuming approximations related to the flow, sediment transportation and bank migration. These approximations are based upon the research performed in [*Crosato 2008*].

Spatial interpolation techniques are also widely explored in general, with varying results depending on the application. For the study field of riverbed topography, only few consider the case of limited datasets, in order to incorporate rules deriving from riverbed morphology. Therefore, scientific interest lies in accomplishing a successful coupling of interpolation algorithms together with specifics of the physical impacts that may be present. In theory, the more general cases can be extended with additional rules. However, the choice of the spatial interpolation technique is always vital to what results the fused method yields.

Other than the main focus of the thesis, a number of processes require some sort of theoretical basis in order to reach a well-produced result. These processes can be achieved in a number of ways, but they are indeed important for completion. Procedures like centerline and grid construction, averaging data on the grid and smoothing are structural components towards realizing a full implementation of the method proposed. Furthermore, the evaluation that follows the implementation is also based upon past research, theory and practices.

In this chapter, the literature research is reported together with any other background information related (§2.1). Spatial interpolation techniques are mentioned and the most promising choices are presented (§2.2). Furthermore, the basis of the additional processes performed for the completion of the project is also made known (§2.3). The chapter closes with a conclusion of the prior parts (§2.4).

2.1 River Physics Framework

As a natural flowing watercourse, rivers are a result of numerous and even chaotic natural processes [*Frascati & Lanzoni 2010*]. In order to derive some knowledge about their creation, migration and

stability, researchers tend to examine them according to the direction of the main water flow or its vertical. Since they are also analysed in a three-dimensional space, these directions are usually clarified as the *longitudinal* direction of the water flow or the major axis and the *transverse* direction. Transverse "slices" of the river form its *cross-sections,* which are often used for understanding better the behaviour of riverbed topography and the geometrical parameters that define it, such as the water flow area, the channel and bankfull width, the wetted perimeter and the hydraulic radius [Figure 2.1]. In meandering rivers, they are all of high importance since they make up most of the values used for modelling the bathymetry alongside the hydrographical parameters.

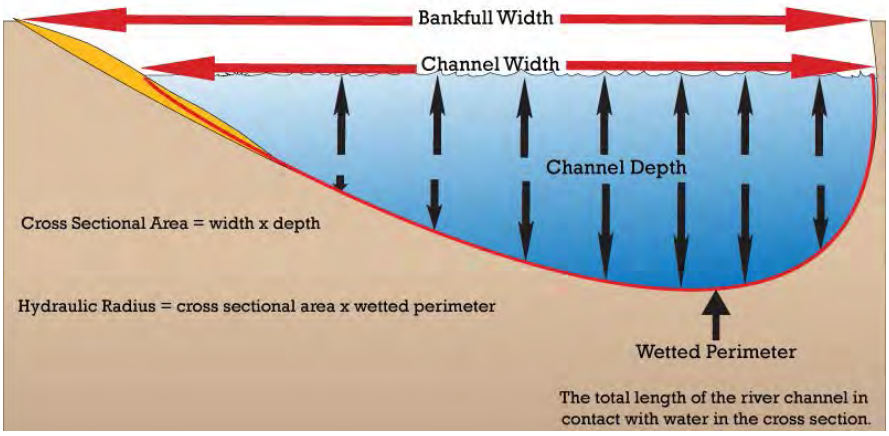

Figure 2.1. River cross-section and measurements (non-commercial use: *www.i-study.co.uk*).

A river channel's actual widths are quite ambiguous because they depend on the water levels which are rising and falling, mainly influenced by floods that may be present during a water year. Of significance is the bankfull width, which defines the borders for which if the flow rises above them, the water enters the active (topographic) floodplain [Figure 2.2]. The greater amount of material transported over time in general is achieved at bankfull flow, forming and maintaining the channel shape with an effective discharge [*Leopold 1994*]. In meandering rivers, changes on the bed level and the impacts of bank erosion and accretion influence the cross-sectional channel width [*Parker 1978, Mosselman 1992, Allmendiger et al. 2005*]. Assuming however, a counter-balance of erosion and accretion between opposite banks, an equilibrium bankfull width can be considered as correct representation of the river.

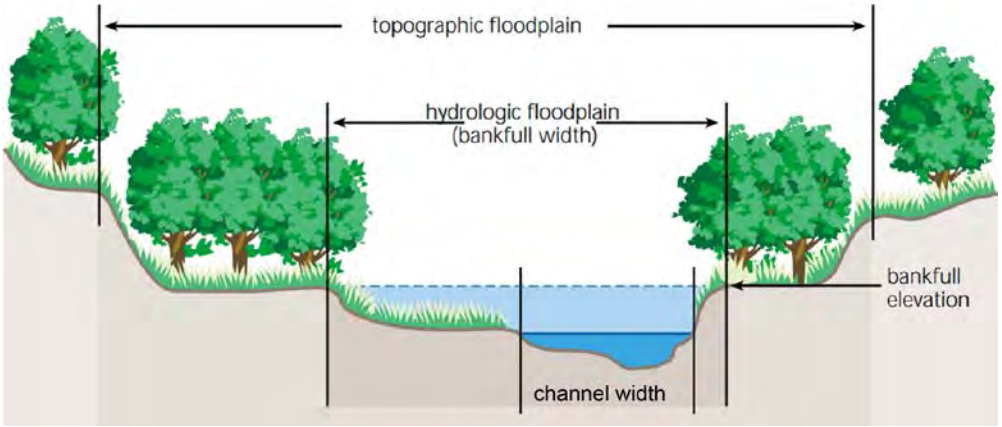

Figure 2.2. River cross-section with bankfull width and active (topographic) floodplain (non-commercial use: *http://www.usda.gov/stream_restoration*).

To further this equilibrium basis, only rivers of mild curvature are reviewed so that there are less instability issues. To define this, the curvature ratio (γ) can quantify a bend's sharpness. The ratio is equal to the bankfull channel width (B) divided by the radius of curvature of the channel centreline (R_c):

$$\gamma = \frac{B}{R_c} \qquad \text{(Eq. 2.1)}$$

R_c is a varying measure that equals to the distances from the centers of the tangent-fitted circles to the centerline points [Figure 2.3]. It can be used as a first evaluation for channel stability, since large values signify a stable channel and small values forecast temporal changes [*Bagnold 1960*]. In respect to the curvature ratio, mildly curved channels display a value of γ with an order of magnitude 0.1 or smaller, whereas sharper bends have one of 1 [*Crosato 2008*]. The behaviour of highly curved meandering rivers exceeds the scope of this thesis, since considerations about cutoffs and influence of vegetation should be taken.

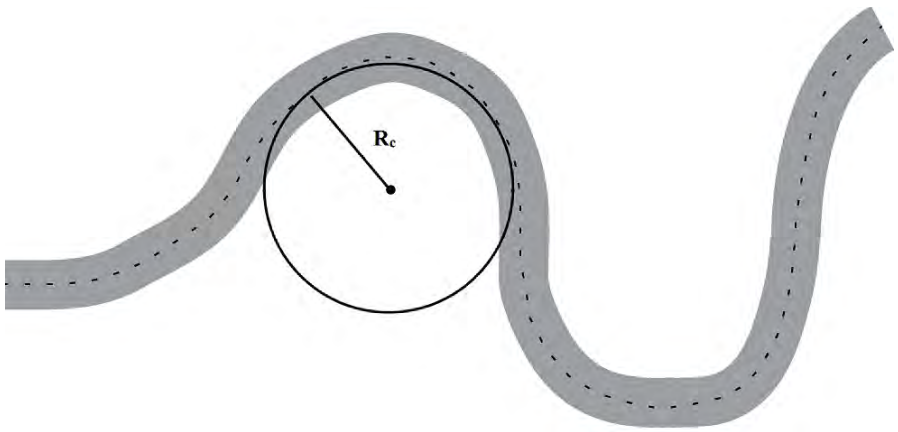

Figure 2.3. Radius of curvature of channel centerline.

Various important past attempts have been made to describe the behaviour of river meanders [*Ikeda et al. 1981, Olesen 1984, Struiksma et al. 1985*]. In alluvial rivers sediment is transported but also deposited mostly in the inner side of bends, forming the so called *point bars*. Their presence, together with erosion on the outer bend, dictates the shape of cross-sections. In greater detail, in a straight reach the cross-section tends to keep a more or less rectangular shape [Figure 2.4, section B]. On the other hand, in a bend, deeper pools are formed close to the outer bank and the shallower parts are by the inner bank due to the point bars effectively shaping the cross-section into an almost triangular form [Figure 2.4, sections A and C]. Depending on the meandering river's consecutive bends and their sharpness, the line of maximum depth called the *thalweg* goes from bank to bank and in the straight reaches through their middle area, changing sides when the curvature changes sign. Therefore, computation of the curvature can dictate on which side the pools may form.

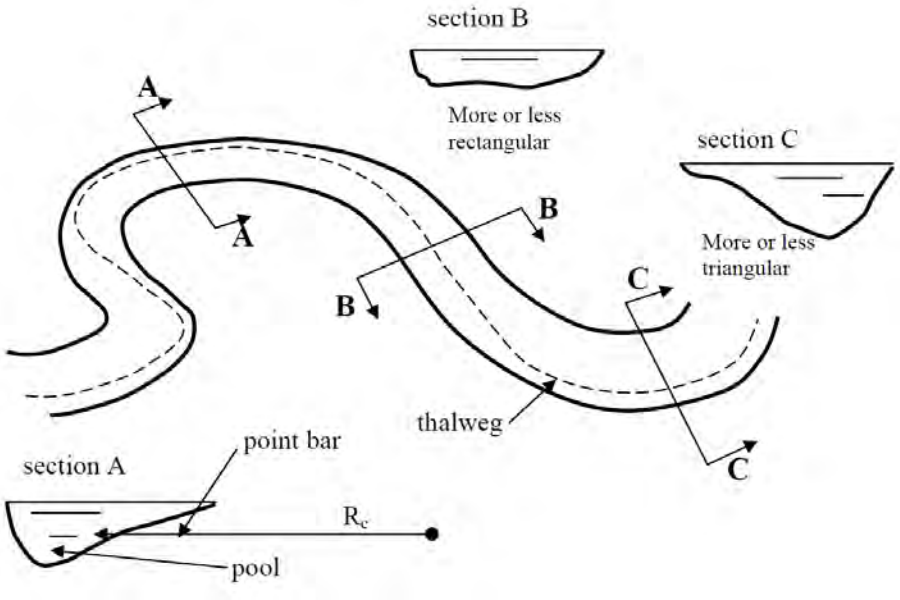

Figure 2.4. Typical river cross-sections along the longitudinal direction [*Crosato 2008*].

To support these cross-sectional profiles, a number of analytical equations have been derived by the deeper examination and breakdown of the physical effects taking place. Primarily, morphological changes need to take into account the sediment balance equation, based on the Exner principle of mass conservation [*Crosato 2012*]. Assuming a time interval infinitely small, the law of mass conservation for sediment dictates that the amount of transported sediment increases when the flow velocity increases. Thus, the Exner principle states that erosion occurs in areas of accelerating flow and sedimentation in areas of decelerating flow [Figure 2.5]. However, the flow velocities are difficult to be measured and usually data regarding them are inexistent. Assuming a constant discharge, the same effect can be attributed to areas of widening and narrowing parts of the river, where flows are respectively decreasing and increasing.

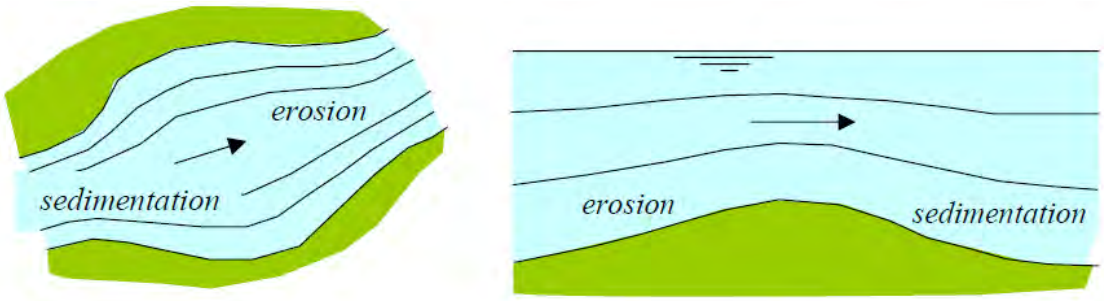

Figure 2.5. Erosion and sedimentation according to Exner's principle [*Crosato 2012*].

The difficulty in defining the velocities also yields from the nature of the water flow. In its full description, the water flow within a channel is three-dimensional. Modelling of the flow field has been attempted in [*Kalkwijk & De Vriend 1980*], but for wide open channel bends of mild curvature. For such assumptions, the shallow water approximations hold, derived from the Navier-Stokes equations [*Navier 1822*] and depth-averaged over a steady flow for a curvilinear system in *s* (streamwise), *n* (transverse) and *z* (vertical) directions [*Olesen 1987, Mosselman 1992*] [Figure 2.6].

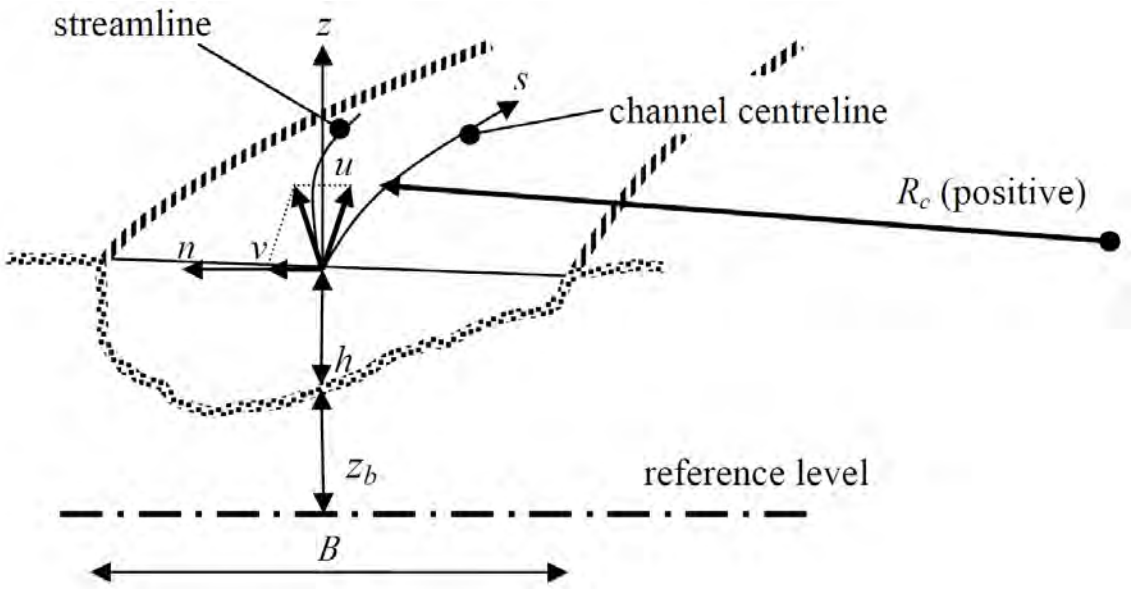

Figure 2.6. Cross-section of river bend in front, with 3D perspective behind. Coordinate system with s longitudinal coordinate as curvilinear and cross-stream and vertical coordinates n and z orthogonal [*Crosato 2008*].

As described in [*Ottevanger 2013*], a streamwise (v_s) and a spanwise (v_n) velocity govern the 3D (real) water flow [Figure 2.7]. The streamwise velocity can be approximated by its depth-averaged longitudinal components (U_s). The spanwise velocity is subdivided to the depth-averaged *cross flow* and the vertical deviations from it, which form the *secondary* flow (v^*_n,v_z) [*De Vriend 1981*].

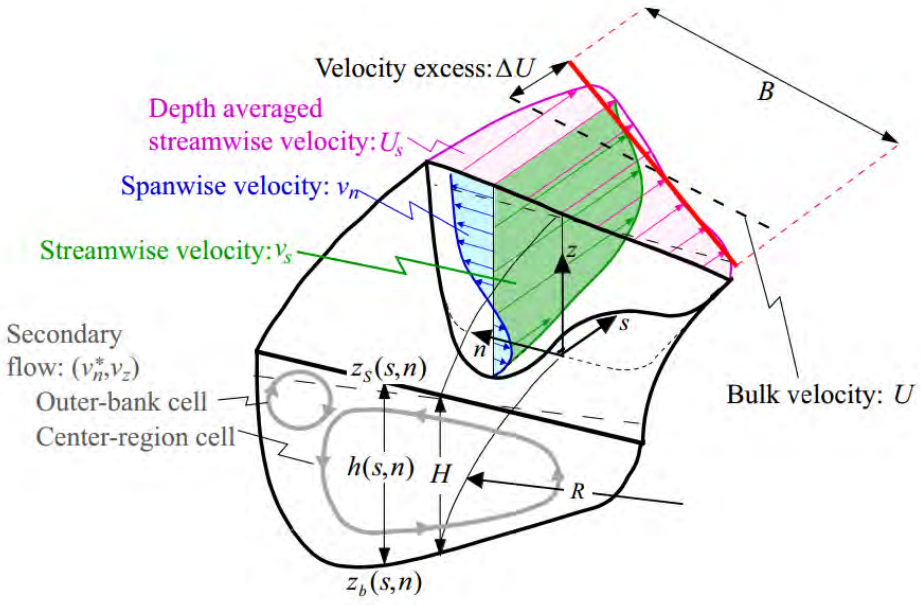

Figure 2.7. Schematized bend flow [*Ottevanger, 2013*].

In a river bend, higher velocity chutes direct towards the outside of the meander bend. Additionally, the surface of the water there is slightly higher (*superelevation*) because of the momentum and acceleration of the flow, similarly to the centrifugal acceleration [*Einstein 1926*]. Subsequently, the flow is forced down and returns towards the inside of the meander bend resulting in the center-region cell of the secondary flow. The outer-bank cell is of lesser influence, born due to instability and turbulence anisotropy, slightly amplified by the center-region cell's motion [*Blanckaert & De Vriend 2004*].

The intensity of the secondary flow increases with larger curvature in river bends. The resulting *helical* flow [Figure 2.8] affects the bed shear stress [*Koch & Flokstra 1980*] and is therefore taken under consideration in the simplified form of a weight coefficient A [*Jansen et al. 1979*]. This coefficient is usually either set empirically or needs to be calibrated for use in the physics-based bathymetry model.

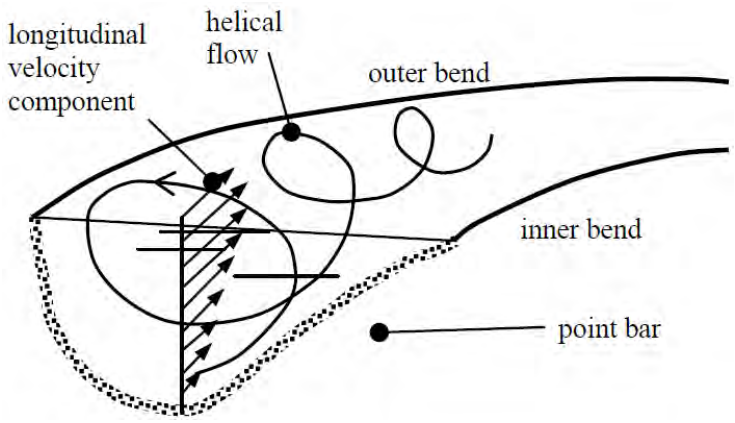

Figure 2.8. Helical flow in a mildly-curved river bend and small width-to-depth ratio [*Crosato 2008*].

The flow field can be derived by assuming depth-averaged steady-state continuity and momentum equations for shallow water. Bed shear stress in a curved channel relates to the depth-averaged flow velocity through the Chézy relation [*Struiksma & Crosato 1989*]. By linearization of the governing equations, a **zero-order solution** to the momentum and continuity equations provides the bed topography for a uniform flow in a straight and infinitely long channel, as follows:

$$h_c = \left(\frac{Q}{B\,C\,\sqrt{i}}\right)^{\frac{2}{3}} \qquad \text{(Eq. 2.2)}$$

where:

h_c - water depth at the centerline [m]
Q - the river discharge [m^3/s]
B - the width [m]
C - the Chézy roughness [$m^{1/2}/s$]
i - the river (longitudinal) slope [-]

Equation 2.2 describes a reference condition, which defines the "tendency" of the system. In this case, the tendency relates to a first water depth level, which is assumed along the centreline. Non-linear effects, like the change in curvature, can form further adjustments from this approximation. The way

river bends can affect the bed level, which can also be estimated by an **axi-symmetric solution** of the equations. In infinitely long bends with constant radius of curvature and discharge, the water flow is constant on the longitudinal. For impermeable banks, the sediment transport on the transverse is zero. Similarly, the depth-averaged transverse velocity is also zero. Assuming mildly-curved channels, the water depth variations by the axi-symmetric solution are given by:

$$h_{(n)} = h_c \, e^{A \, f(\theta) \, n \, / \, R_c} \qquad \text{(Eq. 2.3)}$$

where:

h - water depth along n [m]
A - coefficient weighing the influence of the helical flow
f(θ) - weighing function
n - coordinate orthogonal to the streamline [m]
R_c - radius of curvature [m]

Further defined:

$$A = \frac{2\,a}{\kappa^2}\left(1 - \frac{\sqrt{g}}{\kappa\, C}\right) \qquad \text{(Eq. 2.4, from } \textit{Jansen et al. 1979}\text{)}$$

and

$$f(\theta) = \frac{0.85}{E}\sqrt{\theta} \qquad \text{(Eq. 2.5, from } \textit{Zimmerman \& Kennedy 1978}\text{)}$$

where:

a - calibration coefficient [-]
κ - von Karman constant (≈0.44)
g - gravitational acceleration [m/s^2]
θ - shields parameter [-]
E - calibration coefficient

The last two parameters are as such:

$$\theta = \frac{u^2 + v^2}{C^2\,\Delta\, D_{50}} \qquad \text{(Eq. 2.6, derived from } \textit{Shields 1936}\text{)}$$

and

$$E = 0.0944\left(\frac{h}{D_{50}}\right)^{0.3} \qquad \text{(Eq. 2.7, empirical from } \textit{Talmon et al. 1995}\text{)}$$

where:

u, v - velocity in streamwise and transverse directions [m/s]
D_{50} - mean grain size diameter [m]
$\Delta = \frac{\rho_s - \rho_w}{\rho_w}$ - relative density (ρ_s, ρ_w- sediment and water densities, kg/m^3)

The above equations form the theoretical basis for the model used to compute the bathymetry without making use of any collected data. The full analysis of the equations and derivations can be found in [*Crosato 2008*]. In contrast to the assumptions mentioned above, in the implementation part the variations of the width and curvature in the chosen river parts are still considered, violating some of the theoretical aspects. However, this choice allows for more accurate local depictions of the bed topography. The hydrographical parameters required are also difficult to be exact and in a practical scenario they should be varying along both directions of the flow. In that sense, the geometry of the river bends can be more precise and help acquire these variations.

2.2 Spatial Interpolation Methods and Considerations

For computational geometry as well as maths, interpolation has been a common field of active research. With the advance of earth sciences further knowledge has been brought forth to deal with the need for predicting data such as elevation, temperature, precipitation and soil data. A better adjective to refer to those interpolation methods dealing with geographic information is spatial interpolation methods. Assuming a discretised area, spatial interpolation is the process of estimating values of properties at unsampled sites within the area covered by existing observations by using them as a weighted measure. In most cases, the unsampled locations greatly outnumber the sampled ones.

The main divide between spatial interpolation techniques in two dimensions categorizes them to *deterministic* and *geostatistical* methods. Deterministic interpolation techniques can approximate a surface based on a given smaller set of point values. The method is driven by either the extent of similarity or the degree of smoothing. Geostatistical techniques on the other side calculate the spatial autocorrelation of the given points, accounting for the way they are configured around the area that needs to be interpolated.

In the field of river research, a number of spatial interpolation techniques are already extensively explored like Inverse Distance Weighting (IDW) [*Philip & Watson 1982*], Kriging [*Oliver 1990*], Natural Neighbour [*Watson & Philip 1987*] and Spline methods [*Franke 1982, Wahba 1990*]. Digital Elevation Models (DEMs) in hydrology (raster or Triangulated Irregular Network - TIN) often use them where topographic variations are small, like for example for watershed delineation, but fail in river channel bed topography. In simpler cases where the need for accuracy is not great, Linear interpolation on the longitudinal direction can be substantive for covering specific unknown areas with full values.

To narrow down the interest that can lie on each of these methods, some spatial considerations need to be taken into account related to the thesis scope. Firstly, the known data points are given in “clusters” of data, having a pattern structure of either cross-sections or ship tracklines. Furthermore, the data sampled are considered scarce, thus the areas of uncovered data may be vast in comparison to the data collected. Consequently, a geostatistical method will be severely compromised by data unavailability, its predictions being influenced by too far apart measured points that seem to have a greater correlation than closer ones because of the shape of the riverbed.

As an example, a Kriging system is bound to yield a high covariance around the clustered areas and low further from them. Constructing a semivariogram from scarced data to guide the process is considered of little use, as it will mainly display a periodic pattern due to the similarity of points in the same longitudinal. As such, the results are governed by noise and most unknown values will result around the expected mean [Figure 2.9].

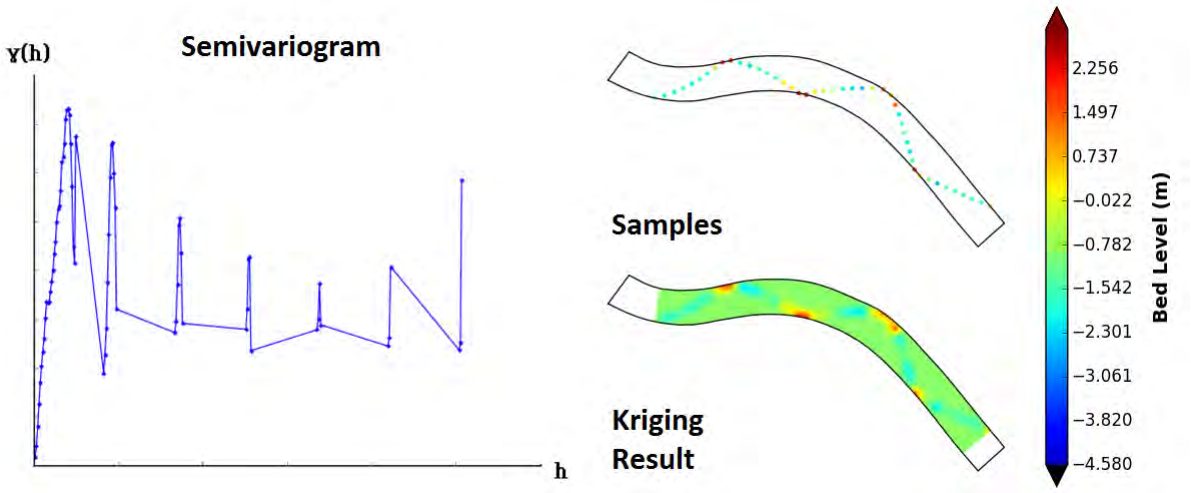

Figure 2.9. Kriging example with limited result for scarce data (*Python*). The periodic effect on the semivariogram relates to the fact that some locations that are far apart display much higher similarity in bed topography than locations that are close (i.e. points close river banks).

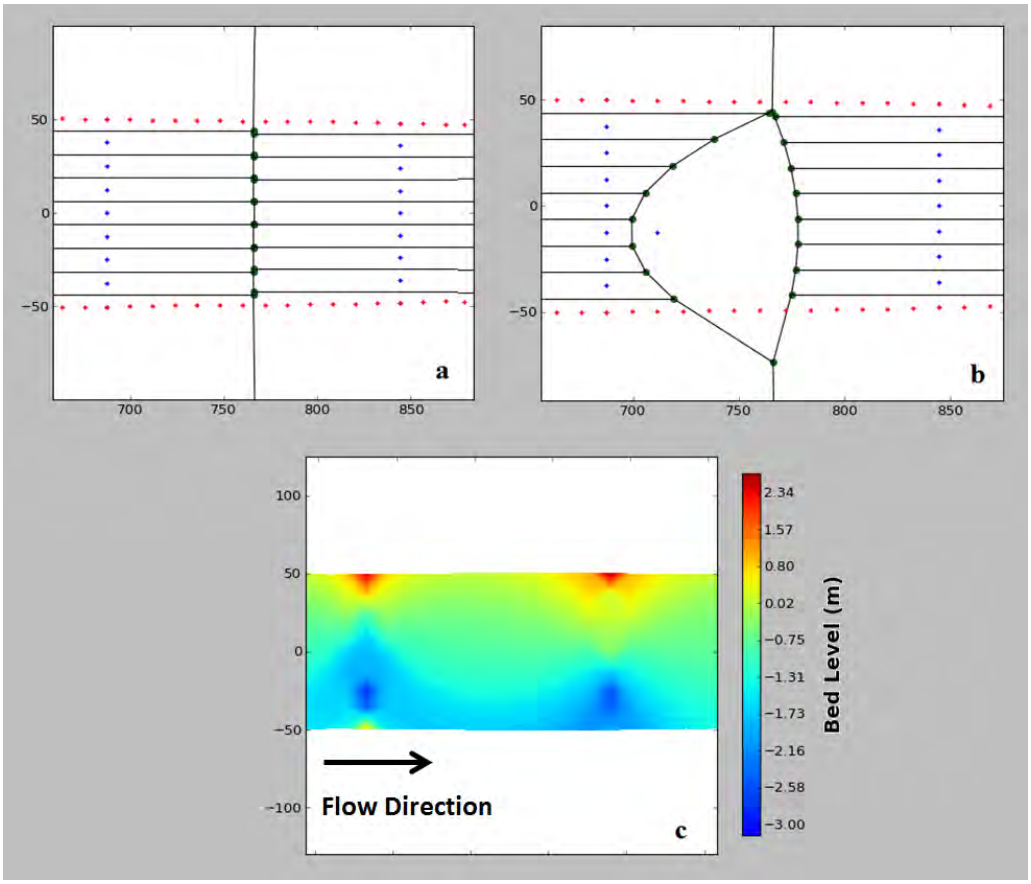

Figure 2.10. Natural Neighbour example on a cross-section (detail, flow-oriented coordinate system, *Python*). Red dots signify river polygon vertices, blue dots are the sampled point locations. (a) Original Voronoi tessellation, (b) Single unsampled point inserted and change in Voronoi tessellation, (c) Overall local interpolated result.

For different reasons, deterministic methods may also fail. In the case of Natural Neighbour [*Sibson 1981*] a Voronoi tessellation dictates the neighbours in between the sampled points. Each unsampled point is inserted in the set and it receives a weight based on the area it "steals away" from each sampled point of the original tessellation. The overall result in a case where there are scarce data can be disappointing. The problem can be displayed easier when cross-sectional data are present [Figure 2.10]. The inserted points receive weights from all the sampled points in between two cross-sections resulting in a big averaging of values further away from them. This "smudging" effect fails to grasp the riverbed topography shape, even more so than a simple linear interpolation. A similar display also appears when the available data are in trackline shape.

On the other hand, Thin Plate Splines (TPS) interpolation may overestimate depth values and assume wrong predictions. The name itself refers to the analogy of a thin sheet of metal bending to cover the interpolated area while passing exactly through the sampled points. A natural representation can be formed by a Radial Basis Function (RBF), which defines a spatial mapping for each location in space. However, in the special case of scarce datasets, such interpolation displays problems in the areas with poor sampling due to the 'warping' effect they pose [Figure 2.11].

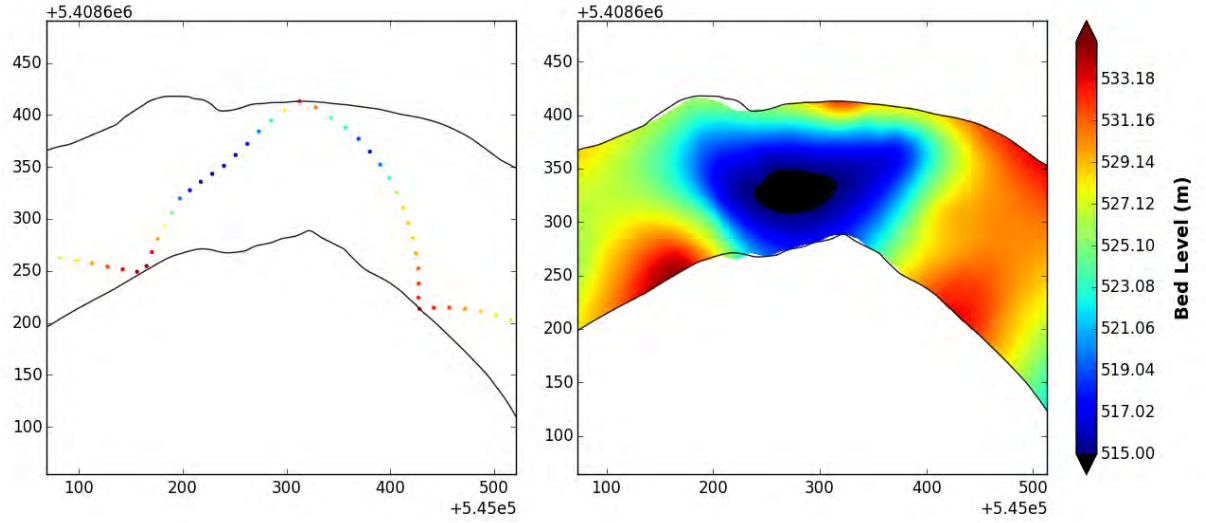

Figure 2.11. Thin plate spline (with Radial Basis Function) example (detail, *Python*). Left: trackline sampled points, Right: interpolated result. Great variations appear where data is not sampled.

Of higher importance is that the morphology of river channel beds is *anisotropic*, since the bathymetric variability is greater traverse to the flow than along it. Therefore, considering a flow-oriented coordinate system is a necessity to pursue a finer resulting interpolation. Towards this goal, in [*Merwade et al. 2006*] such a system is assumed and by evaluating different interpolation methods, it is shown to outperform the Cartesian coordinate system. Similar findings are portrayed in other researches [*Goff et al. 2004, Osting 2004*]. Partial consideration of this is taken also in [*Burroughes et al. 2001*], who developed a Zonal IDW (ZIDW) approach to deal with estuarine bathymetry. For these reasons, interpolation methods like Elliptical Inverse Distance Weighting (EIDW) have a higher interest to the covered topic.

EIDW is similar in sense with the IDW, taking advantage of the anisotropic nature of a river channel. IDW is based on the assumption that a point's whose depth value is unknown can be approximated by the weighted average of the values of the known points. If a global interpolator is used, all the known

points' values are taken into account. A local interpolator however uses only a subset of them within a circular neighbourhood [Figure 2.12(a)]. This neighbourhood's radius either is predefined or varies in order to include a specific number of closest known points. The equation governing the IDW method is as follows:

$$z_c = \sum_{i=1}^{N} w_i * z_i \qquad \text{(Eq. 2.8)}$$

where:

z_c : the value to estimate
N : number of points to average
z_i : the sampled points to take into account
w_i : the weights for each sampled point, which are given by:

$$w_i = \frac{\frac{1}{d_i^p}}{\sum_{i=1}^{N} \frac{1}{d_i^p}} \qquad \text{(Eq. 2.9)}$$

where:

d_i : distances between sampled – unsampled points
p: power exponent

The power exponent noted above denotes the significance of the surrounding points. A higher power is used when the further away points are of less importance and the closest points hold a greater significance. Typical values are 2 or 3, but they can be higher in special cases.

Instead of assigning circular neighbourhoods around the unsampled points, in EIDW the neighbourhoods are ellipses [Figure 2.12(b)]. Further apart points along a defined direction hold a greater importance, which applies in the case of rivers along the direction of the flow. To model this behaviour, the data points can be transformed to a curvilinear system of (s,n) coordinates [*Fukoka et al., 1973; Holley et al., 1986*] as described in the river physics framework (§2.1).

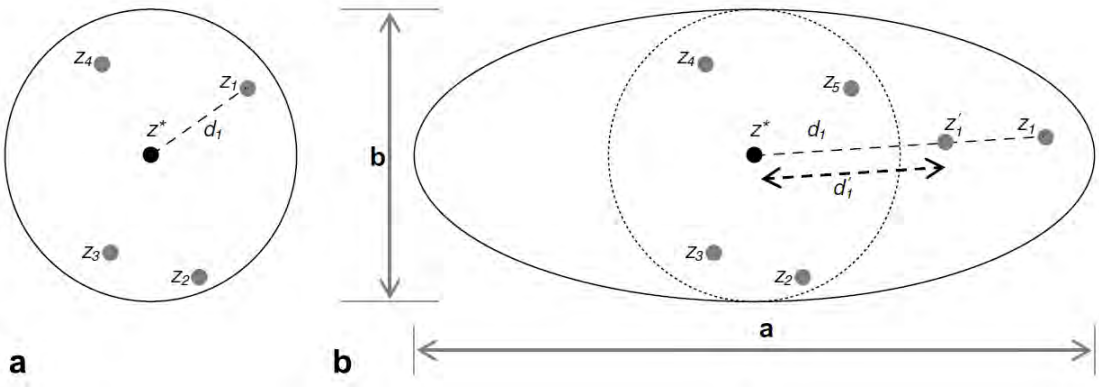

Figure 2.12. (a) IDW with circular neighbourhood, (b) EIDW with elliptical neighbourhood, with a as the major axis and b as the minor axis [*Merwade et al. 2006*].

After assuming such a system, the only difference with the IDW is that the EIDW replaces the calculated distances (d_i) with the following new distances:

$$d_i = \sqrt{\left(\frac{1}{a_r}(s_i - s_c)\right)^2 + (n_i - n_c)^2} \qquad \text{(Eq. 2.10)}$$

where:

(s_i,n_i): along-flow and transverse flow coordinates for the sampled points
(s_c,n_c): along-flow and transverse flow coordinates for the unsampled points
$a_r = a/b$: anisotropy ratio, with a the major axis and b the minor axis

The anisotropy ratio (a_r) describes the extent to which the further along the flow data points are taken into account than the transverse ones. Anisotropy here describes the directional dependence of the data point depths along the water flow, as opposed to isotropy, which implies identical properties in all directions. A high anisotropy ratio results in a system more influenced by the flow and should be treated as a variable to be fitted to the data.

Concerning further spatial considerations, extended research is performed in [*Merwade et al. 2008*] where GIS techniques have been incorporated to produce a coherent river terrain model using TINs. In addition, in [*Merwade 2009*] a method of locating and excluding spatial trends in river channels allows the use of isotropic interpolation methods, upon whose results the trends are back fitted to the calculated bathymetry points. However, the consideration of scarce input data is rarely accounted for. Some relevant research is conducted by [*Abebe 2011*] and [*Osting 2004*]. The first assumes a process of optimizing data using performance evaluation of the MIANDRAS model [*Crosato 1987 and 1989*] to derive the parameters for the prediction of bed topography. The latter compares a radial bounding interpolation method to the proposed method, which makes use of flow-oriented coordinate system upon a basis of a Finite Element Mesh. The proposed method does not use either of them, but findings in both are considered as useful information. Considering all of the above, anisotropy is an important factor in river channels and the chosen spatial interpolation techniques should account for it.

2.3 Additional Spatial Considerations and Evaluation

A number of additional processes, which do not form the core of the research, needed to be implemented. Related work is available on them, however their use in the project does not require a state of the art or "best" solution.

- **Grid and Centerline.** As stated in the previous paragraph (§2.2), a flow-oriented coordinate system would allow for a more suitable representation of data for applying the interpolation. In order to display, compute and store the data, a more ordered way of arranging them is required. For this purpose, a *curvilinear grid* is used, which follows the water flow. With the grid, continuous geographic space can be analytically characterized in both real and cognitive terms [*Berry 2013*] in order to structurally perform computations and comparisons on it. For constructing the grid and achieving its curvilinearity the *centerline* is constructed at first from the river polygon. There are multiple ways to create it, the most important ones are reviewed in Appendix A.

- **Aggregation of data**. After the raw data have been collected and cleaned, they are *aggregated* on the grid. This is effectively a process of rasterization; however, the output is still point data on the grid's intersection nodes. Extensive research has been performed on this topic both in image processing [*Foley 1995*] and data handling [*Wang et al. 2013*]. Depending on the desired grid resolution and the data spacing initially available, there are many ways of setting the data on the grid, like snapping, interpolating or averaging.

- **Smoothing**. Throughout the whole procedure of interpolating data and calculating parameter values like curvature, *smoothing* operations are applied. On the data, this is performed to acquire a more realistic and continuous result along the water flow. The smoothing can be attributed as a natural process to the advection and diffusion/dispersion of the riverbed [*Lecture notes ENV 208 Thayer School, Lecture notes EFM 1 University of Karlsruhe*]. Advection refers to transport with the mean water flow (longitudinal direction), whereas diffusion and its turbulent associate, dispersion, work to eliminate sharp discontinuities and result in smoother and flatter cross-sectional profiles. In this sense, smoothing is usually performed on one dimension to avoid the creation of boundary artefacts brought by 2D smoothing.

- **Evaluation.** As far as the *evaluation* process of the proposed method is concerned, three measures are taken under consideration for this thesis:
  1. The Root Mean Square Error (RMSE) is a frequently used measure for quantifying the differences between the actual values (ground-truth) and the ones predicted by a model or interpolation. This numerical measure is widely accepted [*Willmott et al. 1985, Hoehn et al. 1985, Kenney et al. 1962, Chai et al. 2014*] as a simple model evaluator when the data concerned cover a geographical area. For such area with known and predicted measurements at the same locations, RMSE can calculate a single number reflecting the overall error. The formula that describes it is as follows:

$$RMSE = \sqrt{\frac{\sum_{i=1}^{N}(\hat{v}_i - v_i)^2}{N}} \qquad \text{(Eq. 2.11)}$$

     where:

     N – number of predictions
     $\hat{v}_i$ – real value at i
     v_i – predicted value at i

     Its squared value is effectively equal to the sum of variance and squared bias. This means that the unbiased rooted estimator bears a strong penalty to both consistent bias and large errors making it a strict but unbiased estimator.

  2. Difference maps are a generally accepted form of depicting difference in values measured for an area [Figure 2.13]. In this thesis "error" maps are being used to visually evaluate the response of the method, analysing the errors displayed. The errors are the difference between the predicted bed topography values and the ground-truth ones. It is more of a qualitative depiction of the overall result, which allows to easily focus on problematic areas wrongly predicted.

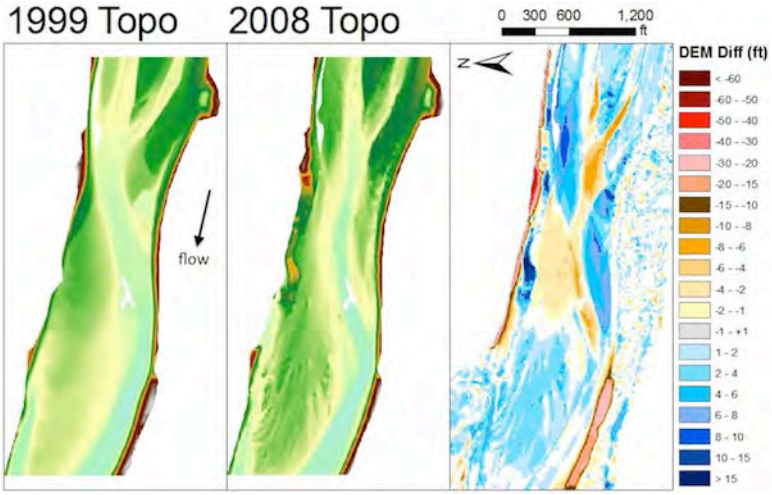

Figure 2.13. . Example of a difference map (right). [Credit: *Gregory B. Pasternack*]

3. Finally, the graphs of the normalized half-width of the transverse slope (NHWS) are being used as a last evaluator. This focuses on a centralized part of the river channel that bears a bigger interest for navigability. It has been chosen to cover the gap between the above two evaluators; however it has not been extensively used in other projects. The NHWS is used as a graphical representation of the bed level cross-sectional direction along the span of the river channel. It can resume some assessment not visible by the RMSE results and also cross-validate the error maps representations. Its basis forms from the mentions by [*Fargue 1868, van Bendegom 1947*] who report that the magnitude of the transverse bed slope in a river bend correlates well with the inverse radius of curvature (1/Rc) and the water depth (h). Related aspects can be found in [*Zimmermann et al. 1978, Odgaard 1981, Ottevanger 2013*].

2.4 Literature Review Conclusion

The theory related to the current project derives from various sources, but mainly the physics-based model's bathymetry approximations rely on the theory presented in [*Crosato 2008*]. Furthermore, the hypotheses made in [*Merwade et al. 2006*] for the anisotropic nature of rivers and the need to transform the data into a flow-oriented coordinate system prior to interpolation are also strongly supported here. The main aspects of the theory and literature consulted have been presented in §2.1 and they are used to construct the computed model bed topography of the study cases.

To the best of the author's knowledge, no mentions to scarce input data exist. In [*Abebe 2011, Osting 2004*], some insight is given on procedures that may be applied, but not enough information is given on how to couple successfully a spatial interpolation method to the physics of river morphology in order to achieve an acceptable result. It is therefore of importance to arrive to a solution that combines the two outputs of a physics-based model and an interpolation into a solution that gives better results.

Literature in general is a part that was constantly consulted throughout the progress of the project. Use of additional findings was made only when relevant in content to the topic.

3 Methodology

This chapter serves as an explanation to the research strategy followed, forming the methodology. In order to provide a clear overall perspective of the methodology, the research is broken down to the three abstract components it encompasses (§3.1). Furthermore, the methodological framework is presented and each of its components are described in §3.2. Finally, the proposed "Fusion" method is presented in concept form (§3.3) before all implementation steps are followed in Chapter 4.

3.1 Research Components

There are three main aspects of different importance and proportions surrounding this thesis: the physical, the spatial and the mathematical components [Figure 3.1].

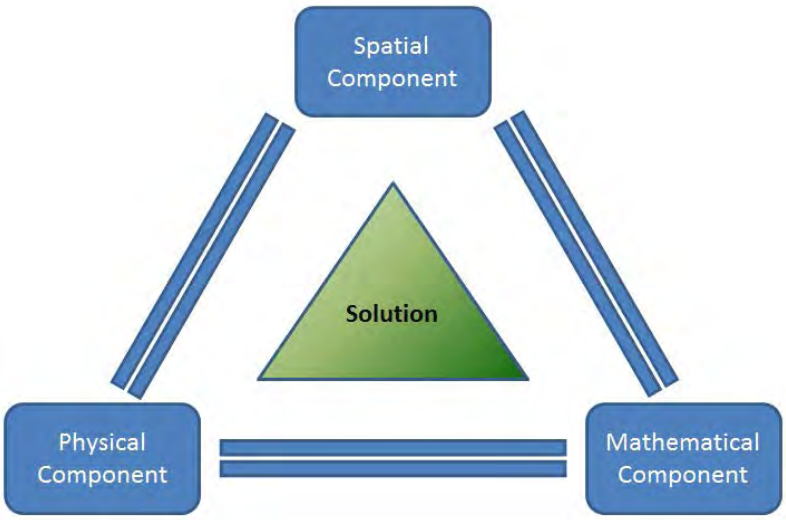

Figure 3.1. Components of the research conducted.

The *physical component* defines the physical descriptions of riverbed morphology along with the river effects that shape its bed form. The water flow and its behaviour in river bends with possible widening/narrowing parts, the hydrographical parameters, the physics-based models and relaxations of their assumed equations and the riverbed topography's predicted response describe the physics lens through which the research is viewed. Therefore, the greatest part of literature lies in this component, which constructs the computed riverbed topography by the model. Basically, this part contains what can be used to lead the method to a prediction of the riverbed topography where data is not available.

The *spatial component* is related to the "geometry" of the data, the regularization of input data (curvilinear grid, see §4.3.3), the parameters which define this, the correlations in space for the input datasets and the knowledge that can be derived from the way data has been gathered. Furthermore and more importantly, it includes the extra considerations made for applying an interpolation method in the correct 'spatial' context.

The *mathematical component* encompasses the algorithms and calculations behind the interpolation techniques to be considered, the numerical descriptions of the models and the computations that need to be performed upon the simplified equations.

With all three components mentioned above, the solution to the problem of data scarcity in rivers may be pursued. This solution is achieved within the frame of the proposed method and its validation.

3.2 Methodological Framework

The methodology followed in this thesis spawns from the problem as stated in §1.2. The diagram that describes it is presented in Figure 3.2 and broken down in parts below.

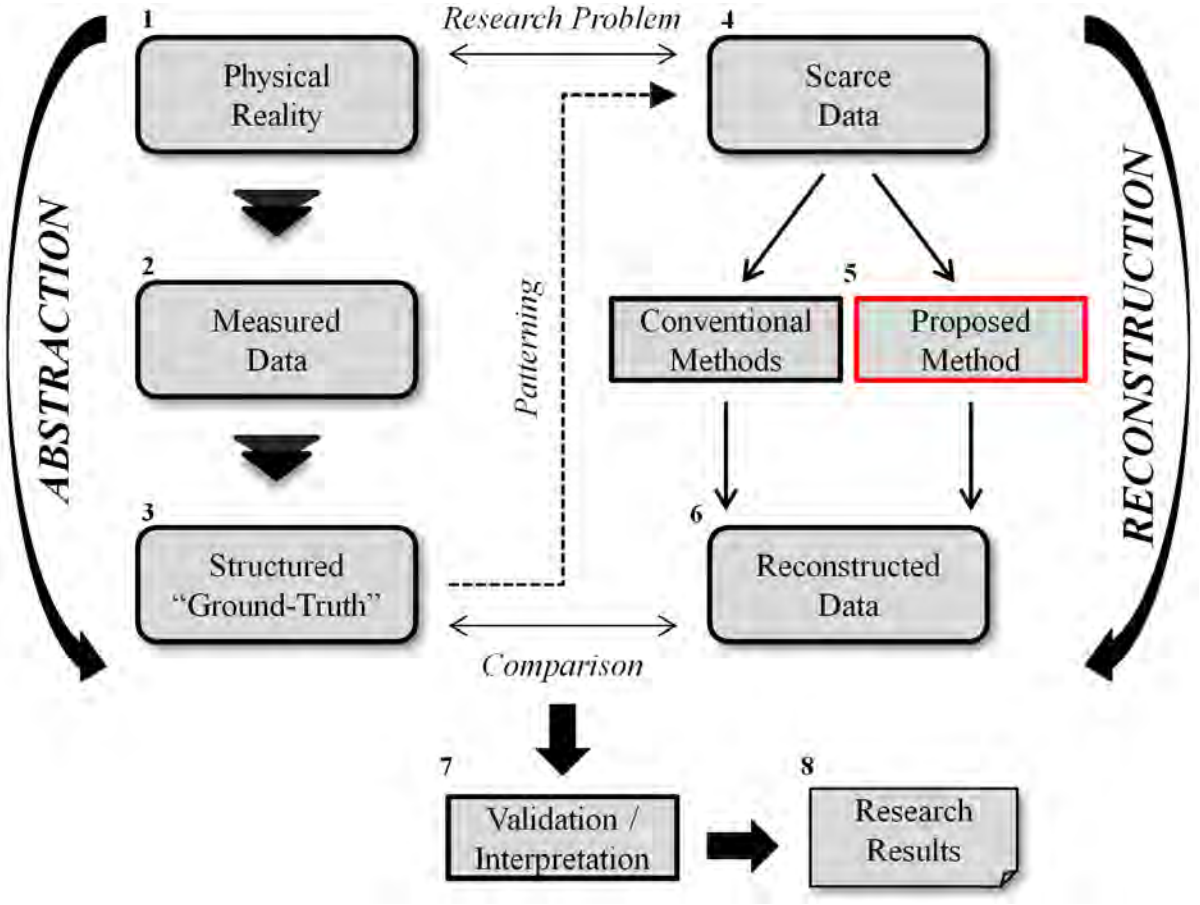

Figure 3.2. Methodology Diagram.

The first three blocks of the diagram reflect the levels of **abstraction** one can have in respect to the data available. The level of abstraction increases with every reformation. In particular:

1. The general prospect of the purpose behind any Geomatics project is to approximate as well as possible or dependently to the users' needs the real world. The *Physical Reality* therefore is in sense the real world, which in this case corresponds to the riverbed topography of the chosen study cases.
2. Using measuring devices, the Physical Reality transforms into what is sensed, what comprises the *Measured Data*. In the current context, these are riverbed topography or bathymetry data collected by multibeam or singlebeam echo-sounder devices. After they have been cleaned from any existing artefacts, the Measured Data provide the initial "raw" representation of reality.
3. In order to perform operations that require a specific structure from the data, they need to be formatted as such. Therefore, *Structured* data represent data that exist by a set of rules, applied to the initially sensed data. Here, the structure is defined by the shape of the river and the curvilinear grid that defines it. For all purposes towards a solution of the specified problem, these data form the *"Ground-Truth"*. They are essentially the last level of abstraction and the representation that is to be achieved by the method.

The next chain of blocks on the diagram displays the concept of **reconstruction**. From the problematic available data (scarce data), what is aimed for is to approximate in the best possible way the Ground-Truth as defined above. In detail:

4. The scope of the project responds to the problem, which is the scarcity of data. In context though, these data are collected on rivers and hold a pattern. They may be present in singlebeam tracklines or cross-sections. To have this kind of representation certain *patterning* assumptions are made up on the Ground-Truth data, from which the *Scarce Data* are extracted. In brief, scarce data are a patternized subset of the Ground-Truth data.
5. In the process of reconstructing the Ground-Truth, a number of methods may be followed. *Conventional Methods* relate to existing methods that can make use of the scarce data to reach a result. These include the spatial interpolation methods and the physics-based model considered in the thesis. However, in the core of the research lies the development of the *Proposed Method*. The latter is providing a result by combining spatial aspects, interpolation and the physics-based model in a complete solution that relates well to the scarcity of data.
6. The prior mentioned methods provide each a solution in the form of *Reconstructed Data*. These data are the approximation achieved by each method's rules and they need to be checked to see how well they represent the Ground-Truth.

The last parts of the diagram relate to the assessment of a retrieved result. This is performed by comparing the Reconstructed Data results with the Structured Ground-Truth and evaluating the performance of each method. Therefore:

7. The final step that follows in the research is the *Validation/Interpretation* of the results. In order to assess each method's performance, a goodness-of-fit can be chosen. In the current thesis, it is also part of the research to find one that can assess the results in an objective manner.
8. In the end, from the overall procedure performed, the *Research Results* are retrieved. Conclusions can be drawn from them, proposals of use for the proposed method as well as directions towards how research on the particular field can be extended.

3.3 Proposed Method

The proposed method mentioned in §3.2, incorporates a number of considerations and it tries to answer the main research question stated in §1.6. Breaking the method down to the parts that lead to it, one arrives to the diagram shown in Figure 3.3.

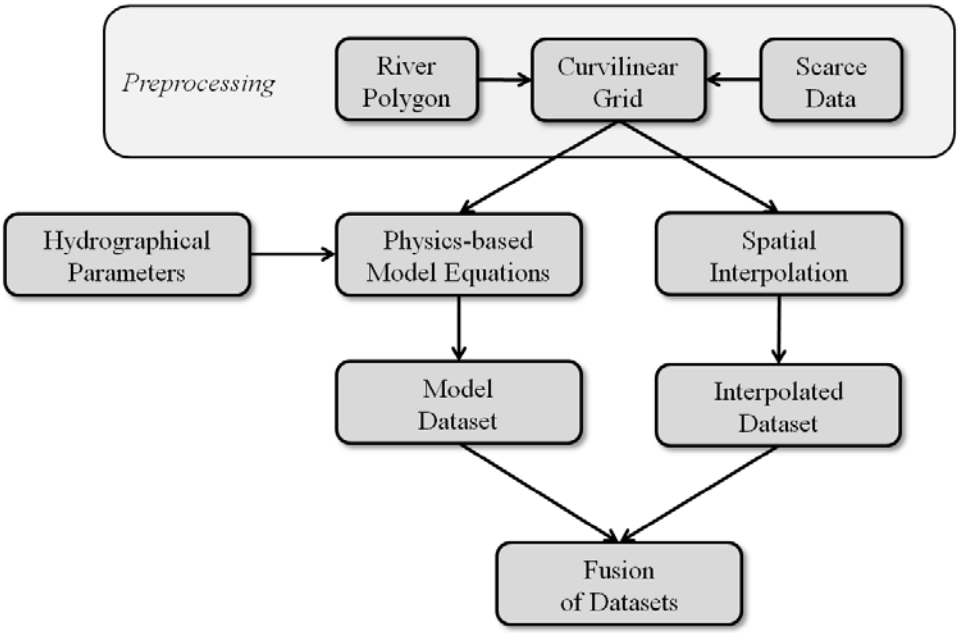

Figure 3.3. Fusion Method Process.

At first, a pre-processing step sets up the basis for performing computations, by defining a curvilinear grid that follows the water flow direction. The grid is constructed from a given river polygon and its implementation is covered in §4.3. The scarce data are also fitted on the grid in order to perform computations with them. The aggregation process and the creation of such datasets are presented in §4.4.

Using the grid, the equations behind the river physics framework of §2.1 can be solved, using a set of hydrographical parameters. That results in a dataset that has been computed totally by a physics-based model. The grid is also used by spatial interpolation methods together with the scarce data, resulting in an interpolated dataset.

The proposed method is based on a basic assumption: that the two aforementioned datasets can be merged in order to create a new dataset that holds a better prediction of the ground-truth. The two datasets both hold information that are useful and can basically complement each other. Because of the above idea, the proposed method is called the "*Fusion*" method.

However, the Fusion method is not a simple averaging of the two datasets, but it takes into account a number of spatial considerations. The two datasets acquire varying weights based on the distances from the sampled data and the resulting fused dataset has properties of both. The overall implementation of the method is presented in §4.7.

4 Implementation

In this chapter, the methods and procedures followed are presented and analysed towards implementation of all aspects of the project. In order to aim for a successful solution, a large portion of the process relied in literature research. A considerable amount of time was also spent on manipulating the data and exploring the possibilities in a spatial context. The main focus though lies with developing the Fusion method in question and arriving to acceptable, valid results.

This field of study is quite extensive with multiple assumptions to be made and simplifications to govern the progress in the limited period of completing the thesis. Therefore, cases where the state-of-the-art is questionable are not extensively explored or even considered out of scope. Solutions are provided however as needed, as long as they set a common backend over which the final evaluation procedure can be objective and the research goals are fulfilled. These cases include the centerline, the grid construction and the fitting of the real data on the grid. There are numerous studies that deal with these frequently rising problems, but a best result is not to be evaluated here.

To display in whole the procedure followed, a bend from the Kootenai River is chosen as a preliminary depiction of the processes and to show what are the expected results. More results and concluding images are shown in Chapter 5, in which all chosen cases are evaluated.

From a practical perspective, the Deltares RAT-IN tool has been entirely written in Python 2.7. Therefore, the coding process followed the same direction with any new libraries and extension packages used as new instalments wherever needed. GIS functions serve a practical aim, providing already established processes or being a means of representation of data and results. As such, open-source products like QGIS, SAGA, GRASS, PostGIS but also Delft3D can be listed in the project's utilities.

The chapter opens with a diagram that displays the workflow of the main steps followed, but also the extra considerations throughout the process (§4.1). Then, an analysis of the data is made (§4.2). The construction of the centerline and the curvilinear grid are covered in §4.3, followed by the creation of the ground-truth and test datasets (§4.4). Afterwards, the physics-based model is presented (§4.5) and the spatial interpolations considered are analysed (§4.6). The subsequent proposed Fusion method is explained in §4.7 and the chapter closes with the considerations for validation (§4.8).

4.1 Overview of Implementation

The general workflow assumed is presented in the Implementation diagram of [Figure 4.1]. Following an initial literature research (A, Chapter 2), the study cases are chosen based on the topic's requirements. From them choices of specific channel bends are made that abide to the project's scope (B, §4.2).

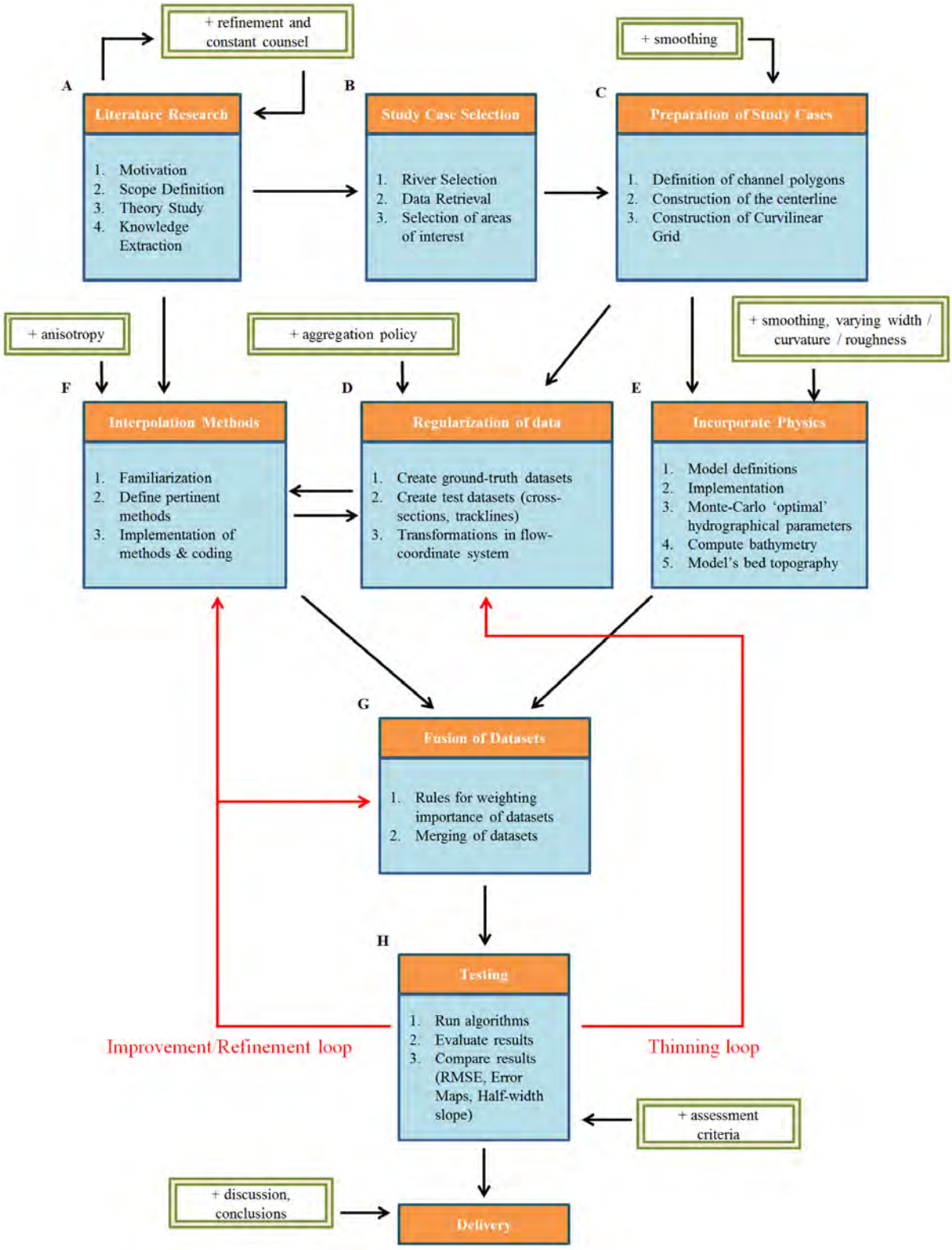

Figure 4.1. . Implementation diagram.

To have a structured representation and be able to perform computations and transformations on the data, a curvilinear grid can be constructed from the study case geometry. In order to do so, the river banks should be defined, effectively describing the river as a polygon geometry. Then, the centerline of the river is computed and from that, a curvilinear grid is constructed (C, §4.3).

As such, the required preparation has been performed and the basis representation is set in gridded data points. Based on that grid, the input data are mapped onto the locations of its intersection nodes (D, §4.4). Each such point acquires an elevation value. The edge points of the cell polygons now define the ground truth dataset, which will be used for the assessment of the interpolation method. Test datasets are extracted from the ground truth in form of either supposed tracklines or cross-sections.

The theory of the physics-based model was covered in §2.1. Eq. 2.2 and 2.3 are used to compute the bathymetry and assume a modelled riverbed topography (E, §4.5). A number of hydrographical parameters are collected for each study case and a Monte Carlo approach is followed to optimize them based on the equifinality principle. Given or extracting the water levels from the data, the bed topography according to the model is outputted.

A number of spatial interpolation methods are tried out on test datasets to minimize the scope of interest relevant to the topic (F, §4.6). Together with the considerations made in literature, the most notable ones are chosen to be implemented and used for comparisons.

After the above, the proposed Fusion method is implemented (G, §4.7). The model's computed bed topography together with the best-performing interpolation results are merged in a fused dataset that is calculated by following a distance-based rule of proximity between unknown and known data.

For inspecting how well the interpolation method works with scarce datasets, the Test datasets can be iteratively made thinner, or the samples' distances vary greater in space. Validation ensues with multiple runs of the process and critical evaluation of the results (H, §4.8). If possible, the methods are re-assessed and refined to achieve better results.

By delivery at the tool's completion, a discussion reflects upon the method's strengths and weaknesses along with the general process (Chapter 6).

4.2 Data

The first step towards applying a theory, testing a hypothesis or evaluating the results of a method is the collection of data. The selection of study cases was made based upon the data available that matched the profile of meandering alluvial rivers with mild curvature and few widening/narrowing parts. Another factor was that the rivers should be of a varying degree of human influence but at the same time important to the human ecology and navigability of ships. Finally but not least importantly, datasets of the cases had to be available and fit for use in due time.

To this extent, three rivers were chosen: the Kootenai River in Idaho (US), the IJssel branch of the Rhine (Netherlands) and the Borcea branch of the Danube (Romania). For each river, two channel bends were selected fitting the description made above. The data that was finally used for all cases needed to be further polished, in order for the method in the end to work uniformly and without biased complications. All of the rivers mentioned are further inspected in detail in Chapter 5.

4.2.1 Collection and Analysis

Collection of data is performed in terms of gaining the riverbed topography datasets of the study cases in the best resolution possible, which is as dense as possible after cleaning. Furthermore, additional hydrographical data are desirable to be received, within the correct timestamp if possible. In absence of hydrographical data, assumptions and approximations can be made, without deviating from the validity of the method and its results. These include the bed slope, flow velocity, sediment grain size, water levels and bankfull discharge.

Data sources are provided by both the Deltares institute and online free data. Specifically, data for the Danube River are given by Deltares in the form of dense single-beam tracks, which cover parts of the overall riverbed. Hydrographical data are also available of the form of reports from prior projects. For the IJssel and Kootenai cases, the datasets are in multi-beam collected points. For the first, the Deltares data is formed onto a regular grid (1x1 m), whereas the latter is distributed by the U.S. Geological Survey (USGS) science organization in an irregular but dense form. The IJssel is provided with sufficient hydrographical data retrieved from Deltares reports, but for the Kootenai case they are missing. Some like bankfull discharge can be extracted from an online web service and USGS reports.

Upon inspection, all the datasets have been cleaned beforehand from outliers, so no cleaning step is required. The depth data are defined by regional vertical datums relative to local sea levels, which means that depth values may have great differences in between the three rivers. In particular, the Ijssel bed topography is referenced by NAP (Normaal Amsterdams Peil) and the Danube uses the mean sea level at Constanta, whereas the Kootenai has the normal NAVD 88 (North American Vertical Datum 1988). Therefore, the Danube and IJssel data are in meters, whereas the Kootenai depth is measured in feet. In addition, some may have both positive and negative values, depending on the referenced sea level [Figure 4.2]. The Coordinate Reference Systems (CRS) for each of the rivers are as follows: IJssel – Amersfoort / RD New (EPSG:28992), Danube – Pulkovo 1942(58) / Stereo 70 (EPSG:3844) and Kootenai – NAD83 / UTM Zone 11N (EPSG:26911).

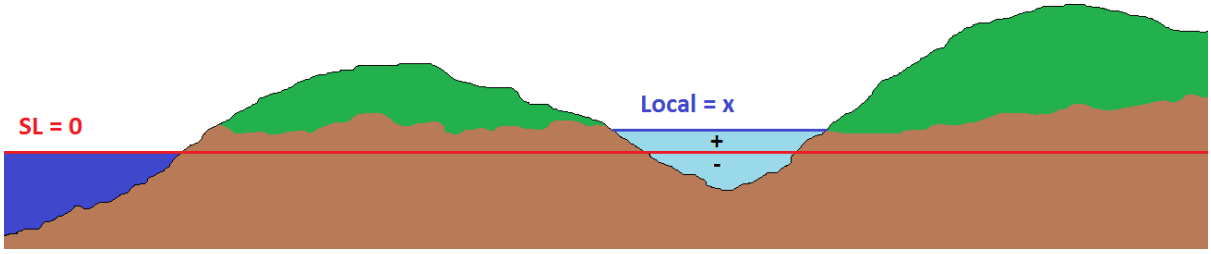

Figure 4.2. Local riverbed topography, if referenced by sea level.

4.2.2 Selection and Manipulation of data

The study case datasets cover vast areas of the rivers. However, for testing the developed method, only sub-parts of those rivers are selected. These include river bends of mild curvature with few widening and narrowing parts. This selection relies mainly on visual inspection of the areas, since the scope of the research does not include partitioning or applying semantics. Therefore, a selection is made based on where physical features appear to be of interest for testing the developed method. Such selection might have a small influence on the method's development in cases where there is definite

physical impact (ie floods, local scours) or human input (i.e. groynes). To the best of the author's ability, areas including such cases were avoided. Also, within the context of the project, data is viewed as a 'snapshot' of the study cases. Therefore, the time element is not considered.

Data manipulation is performed in terms of constructing the ground-truth and test datasets including any functions for extracting, merging or reordering data. Depth values measured in feet (i.e. Kootenai River) are transformed to meters in order for the physics-based model's functions to be applied. The input river channel polygons are also simplified in cases where banks were considered In order to create a "common grounds" depiction of what is perceived as the real world case, what is available as input and what the method outputs, all the data are fitted on a constructed curvilinear grid, whose creation is covered on the next paragraph (§ 4.3.3). As such, the resolution is variable and totally dependent on the grid's spacing. However, the evaluation does not suffer from this, because of basing the comparison on the ground-truth dataset, which is also subject to the grid's formation.

4.2.3 Model and Structure

All study cases original datasets are in point format of Northing-Easting topography data (xyz text data) in their local Coordinate Reference System (CRS), whereas the hydrographical data come in terms of either universal parameters ready to be used (ie bankfull discharge) or parameters to be computed for each point (ie distance from centerline). In this study lies no interest concerned to the semantics or classifications of river data. Therefore, the data model is not approached from either a conceptual or logical level. From a physical perspective, all input data are stored as files in a Comma-Separated Value (CSV) float data type with the following form:

X (local CRS)	Y (local CRS)	Z (elevation relative to sea level)

After the initial data have been fitted onto the grid and the ground truth datasets have been formed, the data could be perceived as an "irregular" raster. Because all ground truth points lie on the cells' intersection nodes of the curvilinear grid, the data hold the topological properties of a raster but not its rectangular shape structure. The representation is extending the raster base with a continuous colour gradient visualization showing the depth. Furthermore, in order to achieve a better interpolation result, all grid cell point data are transformed from their local world coordinates to a flow-oriented coordinate system (s,n,z) as described in §2.1. After interpolation, they return to their initial form for representation. Additionally, also during interpolation, the methods that make use of the anisotropy factor transform by a fraction the s-coordinates of the flow-coordinate model (m,n,z).

The input river polygons are represented as an ordered dictionary in x,y with an additional indexing for the polygon's parts including any holes also as a part. For acquiring the river's local widths, the minimum distances of the centerline points to the polygon's edges need to be computed. Therefore, the polygons are translated into lines and a closest line segment to point computation ensues.

A loose data model is viewed below [Figure 4.3]. Grid_Trans() relates to the procedure followed for transforming data from one coordinate system to the other and Aniso() when the anisotropy factor is applied.

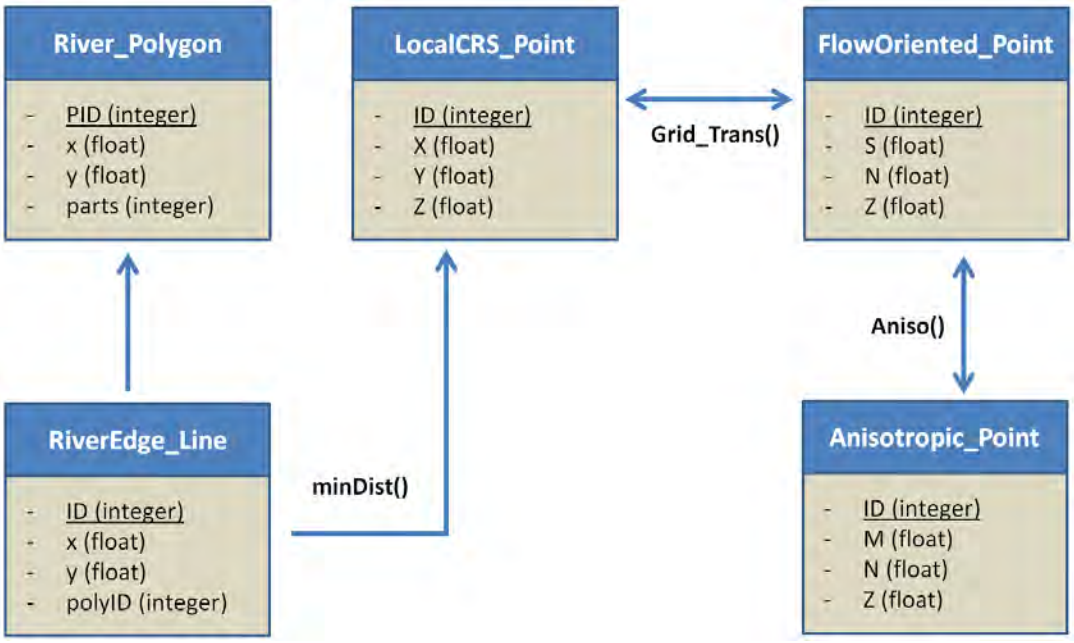

Figure 4.3. Loose data model.

Concerning the spatial data structure, no necessity for a specialized data structure was detected for this project. Data are handled on the fly from text to arrays and associated arrays (dictionaries) with floating data types for points and depths. In only one case a data structure is required for efficient and faster use. That is during the aggregation of the original data on the grid and the creation of the ground-truth datasets. For this purpose, a kd-tree is used so that the nearest neighbour search is efficient and relatively fast. The kd-tree structure partitions the 2D space based on the input points of X and Y values assuming that the depths are of minimal influence. During aggregation, when an intersection node of the grid needs to acquire a value, the nearest neighbours within a specified radius can be easily found [Figure 4.4]. This is the only operation performed and since the data are only points and kd-trees are easier to implement in memory, other spatial trees were not considered further.

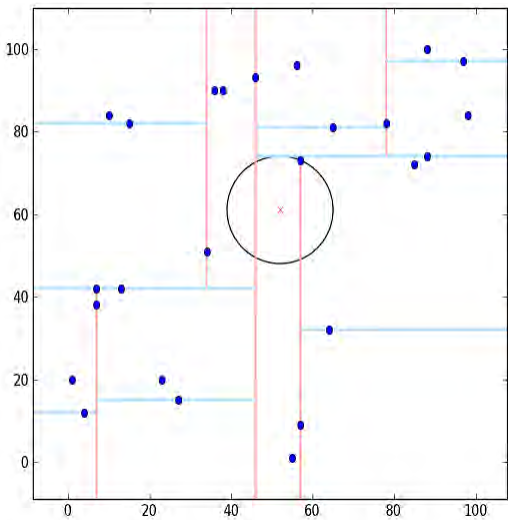

Figure 4.4. KD-tree concept for nearest neighbour search.

4.3 Construction of the Centerline and Curvilinear Grid

The centerline (or centreline) of each river channel polygon is a crucial part of the process because it defines the construction of the grid upon which the data is fitted, as well as the direction of the flow relevant for the curvature, an important parameter used in the physics-based bathymetry model. As such, a prior important step is the definition of the river banklines, which essentially define the river channel polygon. Although an analysis of the most efficient solution for both of these issues is not considered a hard requirement for this research, options were nevertheless explored and a definite choice was made to fit the purposes of the thesis direction.

In the next few parts, the steps taken to form the curvilinear grid are presented. First what constitutes a river polygon is defined (§4.3.1), followed by the extraction of the centerline from it (§4.3.2). Then the curvilinear grid can be constructed (§4.3.3) which forms the basis for representation and computations. Finally the curvilinearity of the grid is displayed (§4.3.4) which assumes the water flow.

4.3.1 River Polygon Definition

A clear description of where the river banks lie can be highly inaccurate both due to the variations in water levels and the river's nature of migration and erosion. The interface between a river and land is called a riparian zone. Riparian zones in the real world usually form a fuzzy boundary and are extensively studied for understanding bank erosion and bank accretion, processes with which the river is thought to migrate. The meander migration process however is not lying within the scope of this research and is therefore not hard-stated. The river polygon representation and the related data are considered to be a "snapshot" of reality without any time-relevant changes taking place. Nevertheless, the river polygons of the bends need to be defined for efficient use.

These polygons can be either given together with the matching point dataset (IJssel, Danube cases) or described through visual inspection based on the data and a map of the same temporal coverage (Kootenai case). The latter can be either automatically extracted, for example by acquiring the concave hull of the point dataset or manually be visually defining the polygon. The first option can be extremely inefficient in terms of computations and still the final output would require further manual inspection and refinement. Therefore, the latter was used where the polygon description was missing.

A final approximation is the simplification of the river polygon. Quite often, the polygons are described in higher detail than necessary including groynes and bank extensions to the inland, especially considering the migrating nature of meandering rivers. In the current thesis, the river banks have been simplified where needed to avoid extreme sudden changes in curvature due to an acute local centerline curve.

As a first step, to reduce the number of local minor bifurcations a buffering and de-buffering process is followed [Figure 4.5]. By buffering and dissolving to a certain extent, all the sharp edges and bank variations are extinguished. Then, by de-buffering by the same extent, the resulting river polygon already is presented simplified. Afterwards, if needed, a smoothening algorithm can be run to further reduce any remaining hard edges and have a better continuous depiction of the polygon [Figure 4.6].

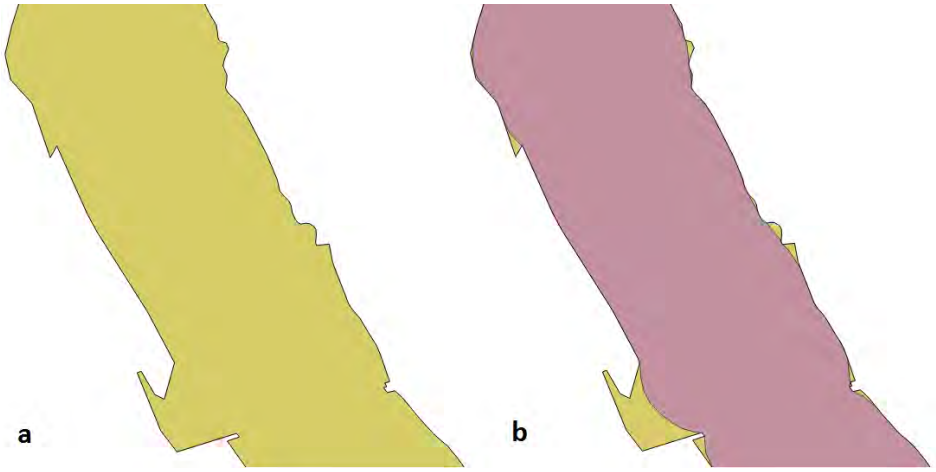

Figure 4.5. Simplification of polygon: (a) Original polygon, (b) Resulting polygon in purple after buffering-debuffering. Danube channel (detail, *QGIS*).

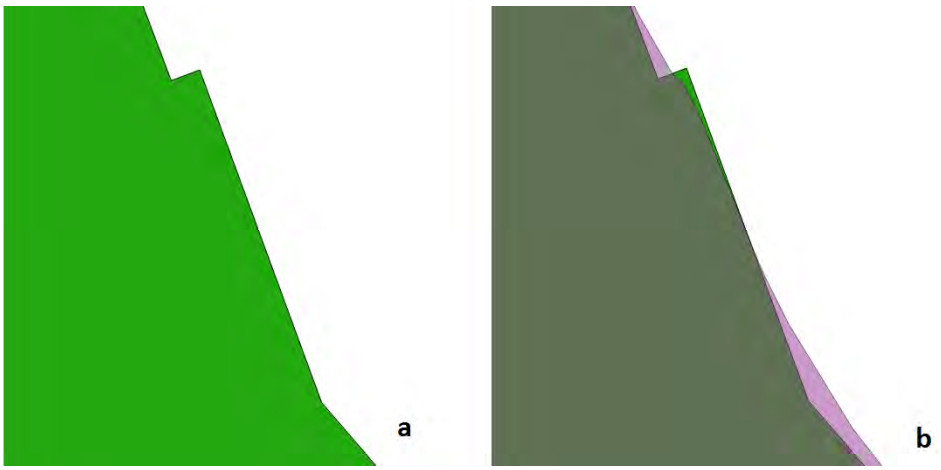

Figure 4.6. Simplification of polygon: (a) Sharpe dge, (b) Edge after smoothing in purple. Danube channel (fine detail, *QGIS*).

4.3.2 Centerline

The simplified polygon of the previous subsection describes the river area to be approximated by the grid. In order however to have a curvilinear grid the centerline first needs to be extracted from the polygon. This is still an open problem in the field of mathematics, but for practical purposes, an approximation is possible. There are a number of different ways to implement the centerline extraction and they are covered in Appendix A. For this project, the chosen method involved the Voronoi method.

First, the points of the outer boundary of the simplified polygon define the points for the Voronoi tessellation. Then, by defining the tessellation as lines, an intersection process allows to keep only the lines that reside within the polygon, which creates a skeleton for the polygon. The skeleton is cleaned from any unwanted branching lines and only the one that spans the whole polygon extent is kept. Finally, points are chosen at regular distances and that formulates the final centerline [Figure 4.7].

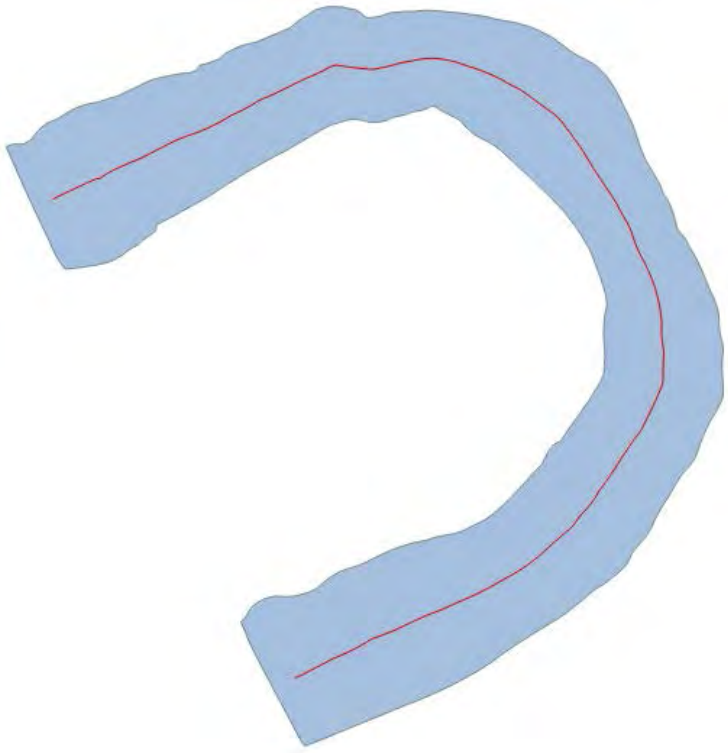

Figure 4.7. Voronoi-defined centerline (*Python*, representation in *QGIS*).

4.3.3 Construction of the Curvilinear Grid

After the centerline has been acquired and the points along it have been selected to have a regular spacing, the construction of the grid may commence. The centerline is assumed that it follows naturally the water flow due to the river polygon's banklines, which have been shaped by the mean water flow. As such, the grid can be constructed by using the centerline and extruding perpendicular lines on each cross-sectional point [Figure 4.8].

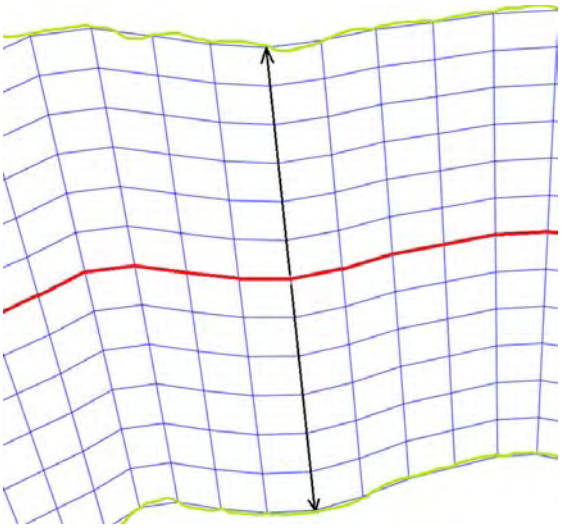

Figure 4.8. Construction of the curvilinear grid. Centerline in red, cross-sectional perpendicular line in black, river banks in green.

However, the widths of each cross-section vary slightly based on the edges of the polygon. The distances of each point on the centerline to the closest polygon's edge are computed first and then an equal number of lines parallel to the centerline are interweaved on both sides to form the final curvilinear grid. Depending on how fine/coarse the grid is, the more/less smoothing is required on the channel centerline in order to avoid cases where the perpendicular lines of the grid cross each other. An example of how different a grid can be is shown in [Figure 4.9] and [Figure 4.10].

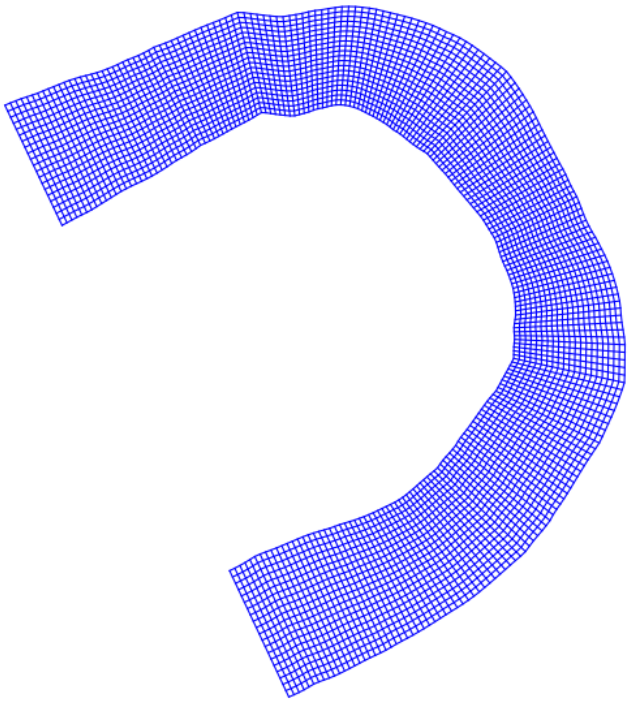

Figure 4.9. Fine Grid (*Python*).

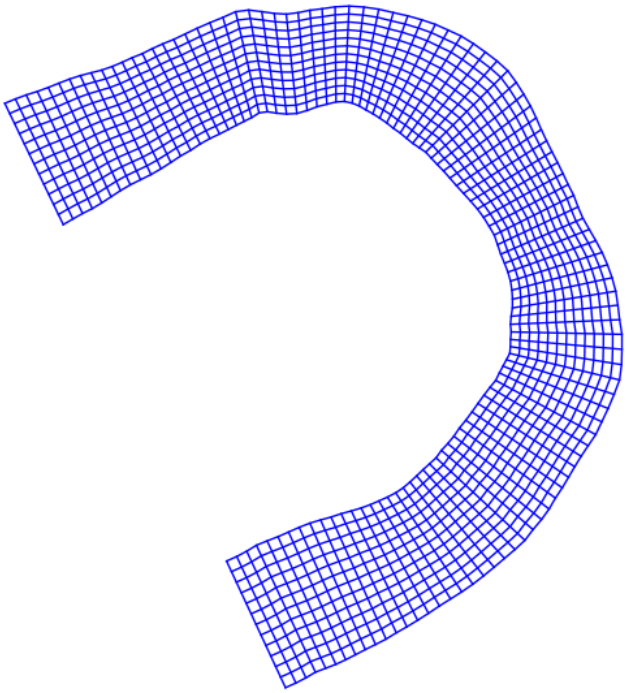

Figure 4.10. Coarse Grid (*Python*).

The grid's "resolution" and cells are irregular and mainly dictated by the curvature of the centerline. The cells cannot have a uniform size because of the varying curvature. That violates some of the assumptions present in the theoretical physics-based model for computing the bathymetry (§2.1). To mitigate the effect of gridlines' convergence or divergence, mild curvature channels of small width variations should be chosen.

The initial choices made by the user for the centerline points' spacing and number of longitudinal lines define the number of cells present. From a general perspective, the grid's resolution should try to maintain the original data resolution. An automatic calculation of the suitable grid cell size has been researched [*Valenzuela et al. 1990, Borkowski et al. 1994, Hengl 2006*], however in the current thesis the scalability and the flexibility was put in favour to abide to the RAT-IN tool's requirements. The user is able to define the spacing of the centreline points and the number of longitudinal lines, effectively defining the grid. Upon visual inspection or by an automated check for intersecting grid lines, the user can assess the suitability of the resulting grid for every individual purpose. As a conclusive remark, a nested grid output could have been taken into account, however due to its complexity in implementation and the fact that such grid would violate the theoretical assumptions for the physics-based model equations, the simpler case was eventually chosen.

4.3.4 Flow-oriented coordinate system

The "curvilinearity" of the grid is more evident if the grid is displayed in the flow-oriented coordinate system [Figure 4.11]. This system follows the main water flow as described in §2.1. It is simply translates each point on the curvilinear grid to a point that has an *s* coordinate based on the centreline chainage and an *n* coordinate above or below (or on) the centreline. This transformation assumes the first point of the longitudinal and the middle of the first transverse cross-section to be the origin point with *(s,n)=(0,0)*. The rest of the points along the *s*-direction follow the almost regular spacing of the centreline and the ones on the *n*-direction are varying based on the distances calculated at each cross-section.

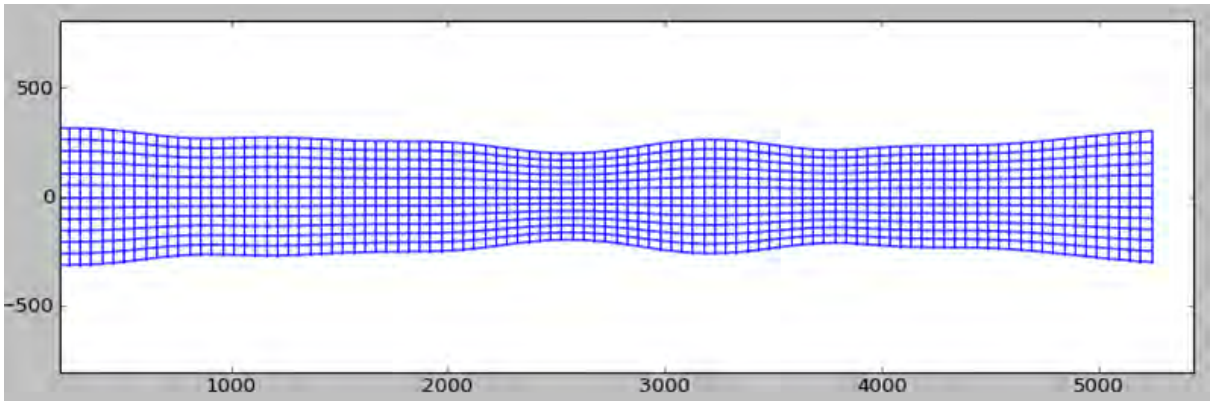

Figure 4.11. Coarse Grid of Figure 4.10 in flow-oriented coordinates (s,n).

The immediate advantages of such coordinate system are not evident until the data have been fitted on the grid and projected in such a way. By preforming this procedure, the points attain their real spatial distances as described by the river boundaries and direction of flow. This has a great influence to the results of the spatial interpolation methods applied.

4.4 Creation of Datasets

The data provided in each of the three rivers explored are of different collection methods (singlebeam/multibeam) and have different density of samples. The raw data have been cleaned and any artefacts have been removed, however, they are still in irregular form, without a specific structure that would suit the proposed method's practical need. In order to have a more regularized way to compare any of the results, the initial data are fitted on the grid. The outputted data are defined as the "Ground-Truth" datasets and are considered to be the real representation of the world. The options considered for this process are reviewed in Appendix B: Data Aggregation.

The Test datasets are a subset of the Ground-Truth datasets. As such, they are extracted from them. To have a "scarce" data representation that abides to the way of collecting such data, some further processing is required. If the initial datasets are in multibeam collection format, cross-sections or tracklines are automatically extracted from the Ground-Truth datasets to create the Test datasets. If they are in singlebeam, parts of the Ground-Truth datasets are manually chosen for the Test datasets.

In the following two subsections, the two types of datasets created to test the method are presented. In §4.4.1 the real world representation is created by defining the Ground-Truth and in §4.4.2 it is shown how Test datasets are extracted from them.

4.4.1 Ground-Truth Datasets

The Ground Truth datasets derive from the aggregation of the initial datasets on the grid. In the current thesis, for the IJssel and the Kootenai rivers the initial data are given in full multibeam coverage. As such, they may be much denser than any of the grids constructed to be effectively used. Therefore, a nearest point snapping practice is followed, through which the nearest point to each grid's intersection node point is assumed to approximate the best that point's value following the first rule of geography: *"Everything is related to everything else, but near things are more related than distant things."* [*Tobler, 1970*]. An example is shown in [Figure 4.12].

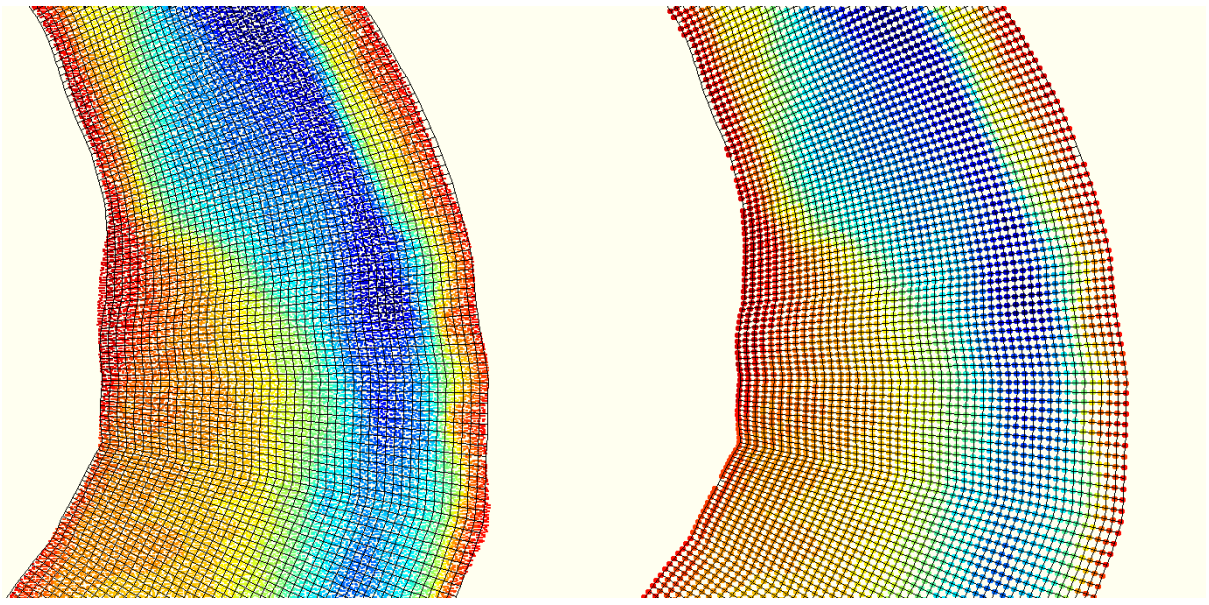

Figure 4.12. Averaging multibeam data on grid (detail). Left: Provided dataset. Right: Averaged dataset. Grid is in black colour (implementation in *Python*, representation in *Delft3D*).

In the case of Danube where the data is in singlebeam form, the values on the grid intersection points are approximated by IDW interpolation with a calculated threshold for the circular neighbourhood. If the grid is not defined to have almost square cells, issues may arise if a small value is given as the threshold radius [Figure 4.13]. In order to mitigate that and provide an automatic radius value calculation for the IDW, the threshold radius is defined as equal to the distance from the grid's intersection node point to the furthest away cell center of the surrounding grid cells [Figure 4.14]. Although the resulting dataset is not in its sense covering the whole extent of the grid, since it is the only data available, it is considered to be a "Ground-Truth" dataset.

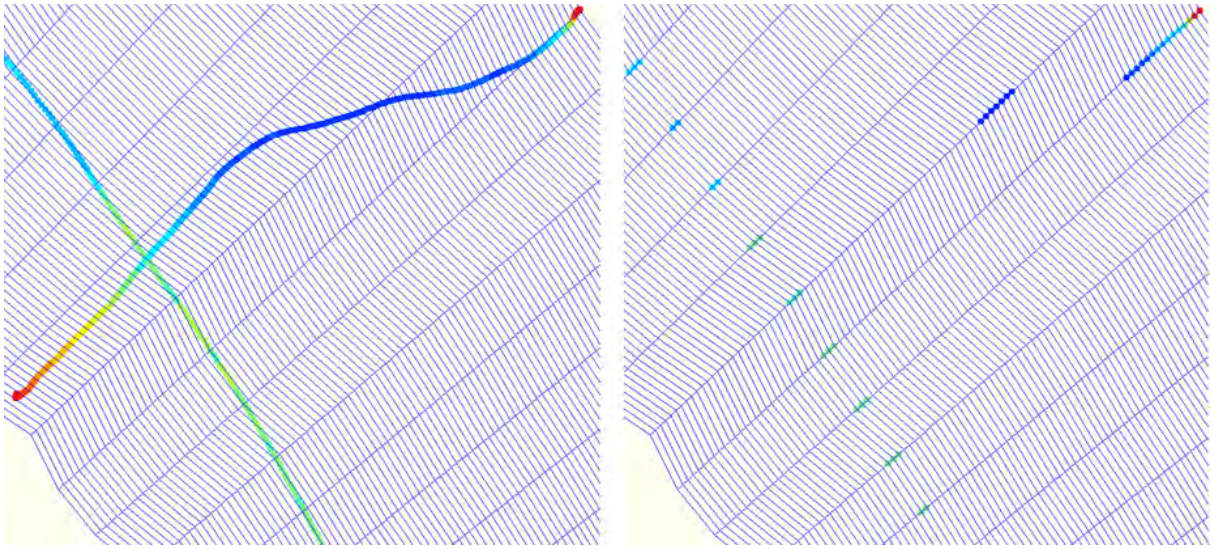

Figure 4.13. Averaging singlebeam data on grid (fine detail). Left: Provided dataset. Right: Averaged dataset. If the grid is not well-defined, there is great loss of data (implementation in *Python*, representation in *Delft3D*).

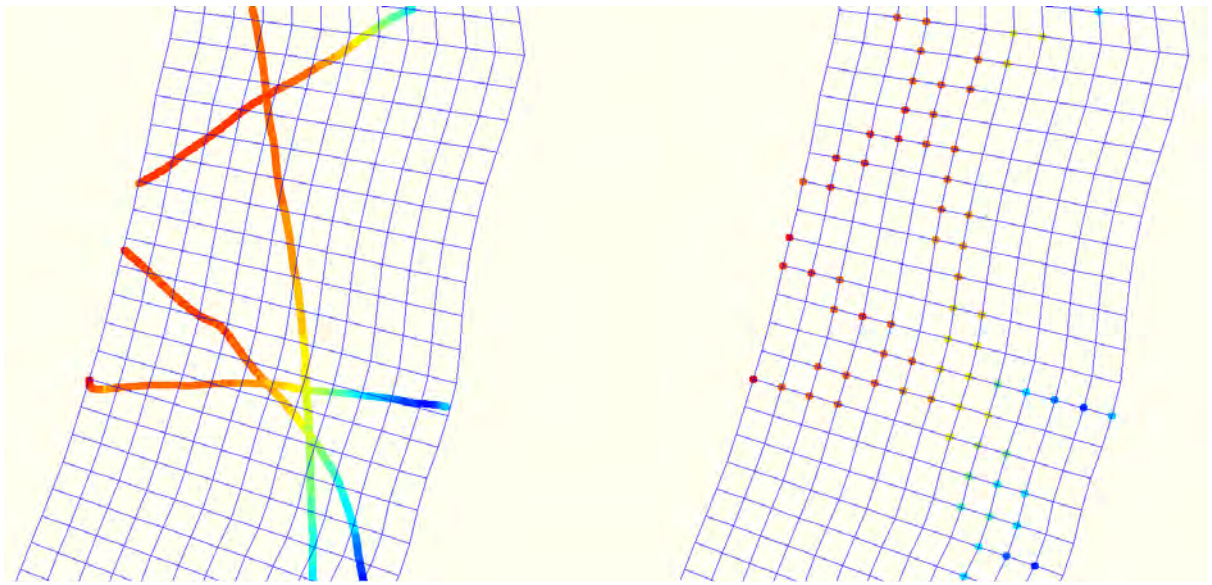

Figure 4.14. Averaging singlebeam data on grid - fine detail (implementation in *Python*, representation in *Delft3D*).

For displaying the differences that may be apparent by using different grid resolutions, [Figure 4.15] and [Figure 4.16] show a Kootenai bend's multibeam data fitted onto a fine and a coarse grid (as per [Figure 4.9] and [Figure 4.10]). The fine gird has as expected a more detailed representation closer to the initial data and the coarse one represents them smoothed-out.

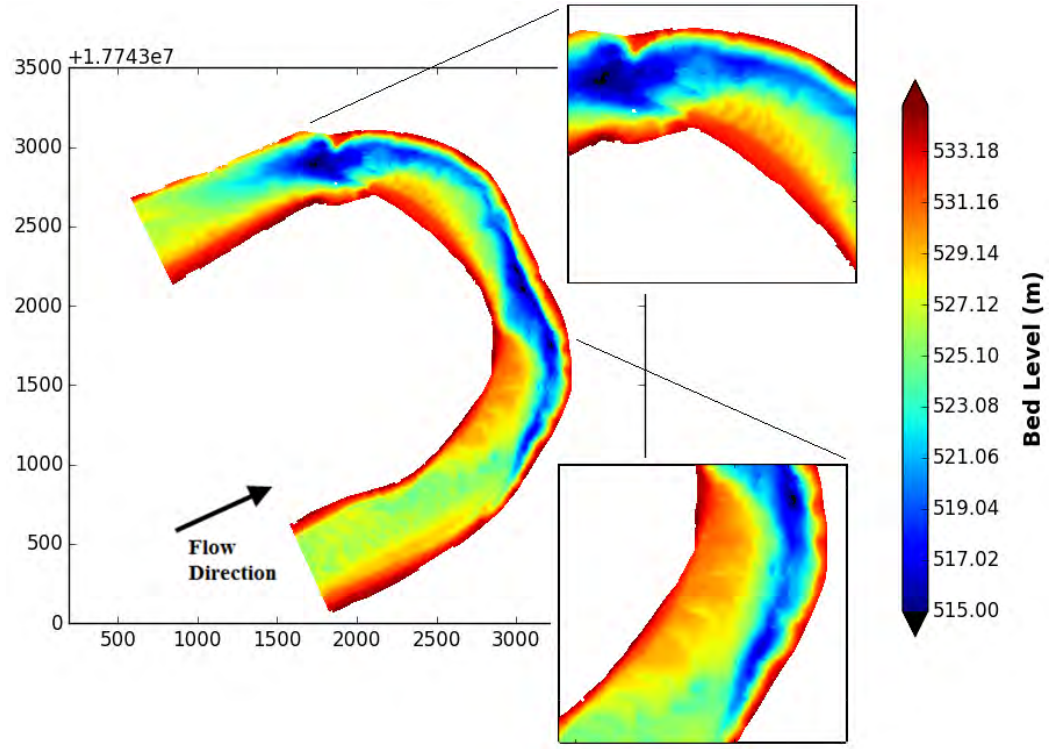

Figure 4.15. Fine grid Ground-Truth Dataset with detail (Python).

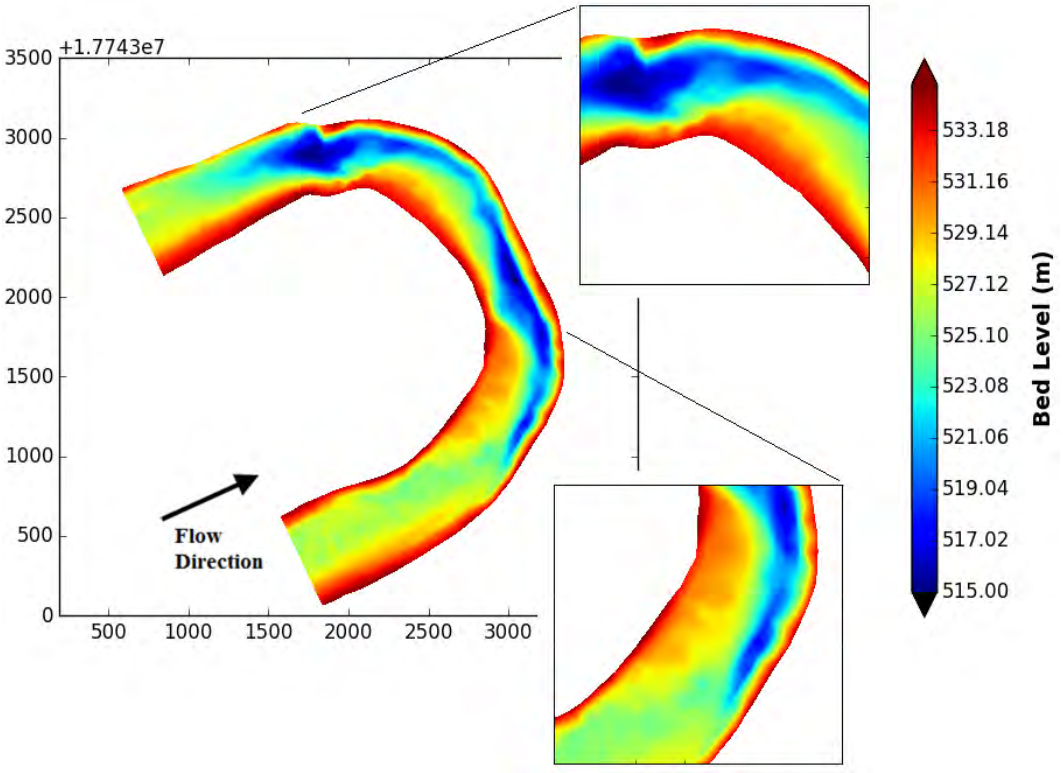

Figure 4.16. Coarse grid Ground-Truth Dataset with detail (*Python*).

4.4.2 Test Datasets

The Test datasets are extracted from the Ground-Truth datasets created as per above. In the cases where a full multibeam coverage of the river bend is available, the extraction is made by an automated procedure that can create cross-sections or trackline data. Since the Ground-Truth data are described on a grid, points can be chosen on regular specified gaps by defining the line and column sampling on the grid. Furthermore, the spacing between the sampled points can be adjusted. The two collection methods are shown in [Figure 4.17] and [Figure 4.18]. On the other hand, particularly for Danube where the ground truth data are in singlebeam format, the Test datasets were manually extracted by choosing the sampled data [Figure 4.19]. That is because the structure of such "Ground-Truth" datasets would not allow for an automated extraction.

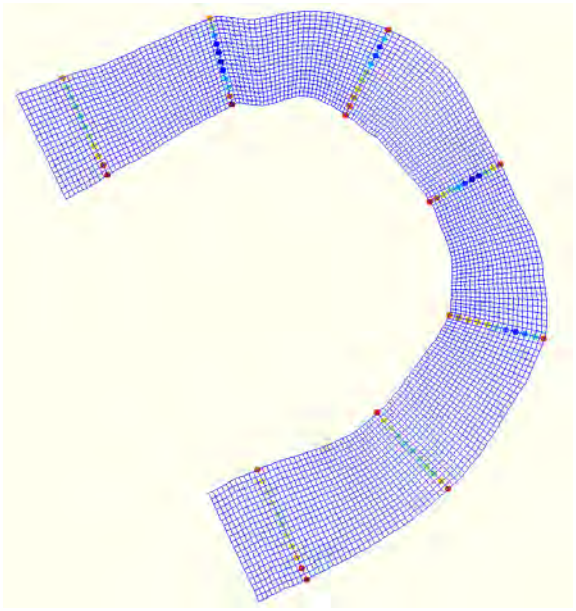

Figure 4.17. Cross-sectional Test dataset example (implementation in *Python*, representation in *Delft3D*).

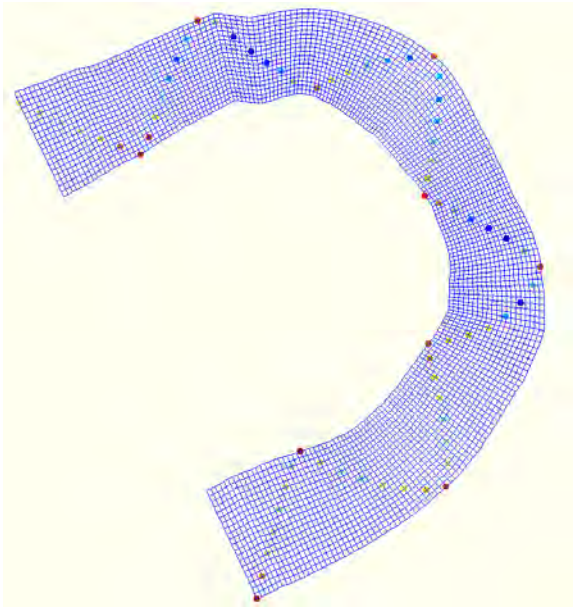

Figure 4.18. "Trackline" Test dataset example (implementation in *Python*, representation in *Delft3D*).

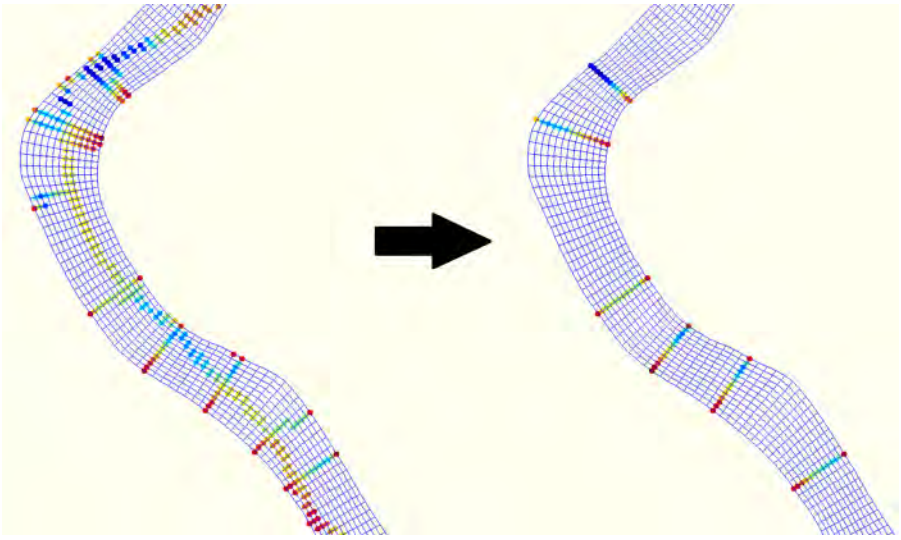

Figure 4.19. . Manual cross-sectional Test dataset example (implementation in *Python*, representation in *Delft3D*).

In a real-world scenario, the cross-sectional data would ideally be collected on areas of expected morphological interest. However, this analysis is both beyond the scope of the research and unnecessary to validate the method's results. Sometimes in real-case situations, the collection of cross-sectional data would be made at a regular sampling on a river stretch. The automated process as described above allows such Test datasets to be created by regular spacing.

From a similar perspective, the trackline data would follow the ship trajectory along the survey conducted. However, unless dictated by a prior morphology survey, this way of collecting data is usually either dependent on past practices or can even be relatively random. Therefore, the assumption of trackline data following a regular "zig-zag" pattern with cross-sections in between is viable for the scope of this research.

For testing the proposed method, a thinning of the Test datasets is required. The reduction of the Test datasets size is mainly dictated by either the number of cross-sections in a bend or the percentage of data available in a trackline scheme. In the cases of manual extraction, an initial Test dataset is created as dense as possible for both schemes of cross-sectional and trackline data. Then, that dataset is also manually decreased in size wherever possible. This is usually possible with cross-sectional data where the number of cross-sections is clearer.

4.5 Physics-based Model

The bathymetry model used in this research is a simplified geometrical and physics-based model based on the work by [*Crosato, 2008*]. The underlying equations have already been presented in detail in §2.1 (Eq. 2.2, 2.3) and are mentioned here for ease of reading:

$$h_c = \left(\frac{Q}{B\,C\,\sqrt{i}}\right)^{\frac{2}{3}} \qquad \text{(Eq. 4.1)}$$

$$h_{(n)} = h_c\, e^{A\, f(\theta)\, n\, /\, R_c} \qquad \text{(Eq. 4.2)}$$

Equation 4.1 describes the *zero-order solution*, calculating the reach-averaged values of depth assuming an infinitely long straight channel with constant discharge. In this thesis however, the averaged widths denoted by parameter B are assumed to be varying, based on the provided river polygon. Although this violates the theoretical assumptions, it ensures a justified difference in the topographic depths where the river is widening or narrowing, respectively related to the sedimentation and erosion of the riverbed by Exner's principle.

Furthermore, the Chézy roughness coefficient (C) is a value that physically relates to the water flow velocity and should be varying. Even if the hydrographical values are fully described, it is usually difficult to acquire a varying roughness coefficient. Instead, usually a single expected or calculated value is given. In lieu of information about flow velocities and assuming a steady discharge value, it is proposed to allow for a variation of a given Chézy value based on the widths calculated at each cross-section:

$$C_{(s)} = C \frac{B_{(s)}}{\bar{B}} \qquad \text{(Eq. 4.3)}$$

where:

$B_{(s)}$ – width at s point along the centerline
$\bar{B}$ – averaged widths along a (short) river bend

This means that the given value of roughness increases with a width higher than the average of the river bend and decreases if the width is smaller than the average. This assumption can allow for mild variations in the value when a relatively short river bend is considered without large differences in widths.

Equation 4.2 calculates the *axi-symmetric solution*, which provides the riverbed cross-sectional variations from the reach-averaged depths, effectively fitting an exponential profile based on the hydrographical parameters. These hydrographical parameter values can either be collected through survey or approximated by calibration. The extent of the variations is defined by n which holds values between $[-B_{(s)}/2, B_{(s)}/2]$.

The value of h_c practically represents the depth on the centreline of the river and the values of h the transverse variations from it using an exponential equation. That ensures that the calculated depths will always be below water level (after assigning a negative sign to them). Given from reports or extracting the water levels from the data, the riverbed topography according to the model is outputted.

In the next subsections the curvature and hydrographical parameters of the equations are reviewed, along with any assumptions made (§4.5.1, §4.5.2). Also, the optional additional bankline profiles are selected (§4.5.3) forming the final description for the representation of the riverbed by the model (§4.5.4).

4.5.1 Curvature

In Eq. 4.2, R_c denotes the radius of curvature. However, since a practical calculation of it is difficult, the inverse of it is computed. This is the reciprocal to *curvature* which is the amount by which the river geometry or centreline deviates from being straight. It is described as:

$$\frac{1}{R_c} = k = \frac{d\alpha}{ds} \qquad \text{(Eq. 4.4)}$$

where:

dα – change between signed directions
ds – distance between two consecutive points

Direction is defined as the angle formed between the previous and next points to the current one for which the curvature is calculated. In Figure 4.20 these values are depicted. The points on a cross-section will hold the same dθ value because they have the same change of α angles due to the grid's curvilinearity. However, minor changes appear on the ds distances. For that reason, a local curvature vector is calculated for each longitudinal line's point on the grid.

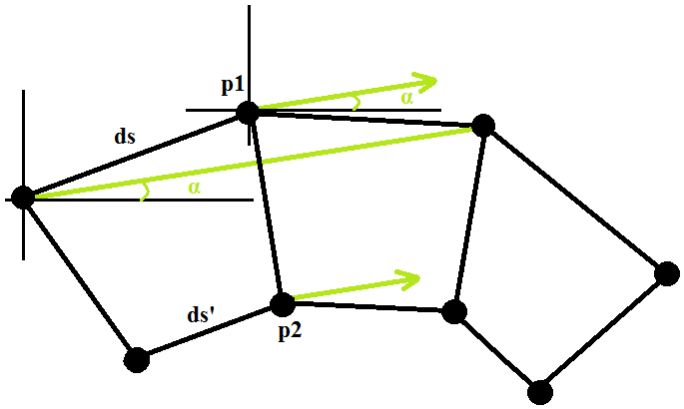

Figure 4.20. Part of grid structure, direction in green. α is the angle of direction for a point on the grid. ds and ds' are distances. Point p1 and point p2 are on the same cross-section. They have the same directions but bear different curvature due to the different distances.

Geometrically, the curvature measures how fast the unit tangent vector to a curve rotates. However, the grid representation of the centerline and its parallels is discrete. That means that there might be steep changes in between the intermediate points of the grid. For this reason, initially a 1D Gaussian window smoothing is used to allow for mild changes in curvature and then further a Savitzky–Golay filter is applied to assure noise reduction.

After this change, the equation 4.2 can be rewritten as:

$$h_{(n)} = h_c \, e^{A \, f(\theta) \, n \, k_{(n)}} \qquad \text{(Eq. 4.5)}$$

4.5.2 Hydrographical Parameters

In order to solve the two equations of Eq. 4.1 and Eq. 4.5, a number of parameters need to be known a priori. These parameters should describe the river area in study by its physical and morphological perspective. The parameters are:

Q – bankfull discharge [m^3/s]

C – Chézy roughness [$m^{1/2}/s$]

i – longitudinal slope [-]

u, v – velocity in streamwise and transverse directions [m/s]

D_{50} – mean grain size diameter [m]

$\Delta = \frac{\rho_s - \rho_w}{\rho_w}$ – relative density (ρ_s, ρ_w- sediment and water densities, kg/m^3)

The velocity in the transverse direction is assumed to be negligible and on the longitudinal close to an order of 1. The relative density receives values depending on the density of the sediment, but in alluvial rivers the relative density is assumed to be close to 1.025 kg/m^3.

The remaining values may vary greatly and are distinct for each river. For the three cases visited, most of the parameters were attained by expedition reports or some educated guesses have been made. In detail, for Kootenai, all values but the roughness were retrieved from reports by USGS [*Barton 2004, Fosness 2013*]. The IJssel data were retrieved both from a sedimentation report and by the online database of the Ministry of Infrastructure and the Environment of Netherlands [*Ministry; Rijkswaterstaat*]. Danube values were assumed from prior project reports made by Deltares.

These values are however not precise unless given together with the initial data collected. Some generalizations may be assumed, but also a more rigorous calibration procedure can be of significance. The physics-based model itself is sensitive to incorrect values, however the correct collection of such information and sensitivity analysis of the model were not part of the thesis. For these reasons, the *Monte Carlo simulation* is used. With this method, models of possible bathymetry values are built by substituting a range of values for each hydrographical parameter. This is performed using a Gaussian normal distribution, with a mean based on either the documented value as stated in reports above or an educated guess.

The models are run a large number of times, with each time a different set of hydrographical values formed. At the end of the specified number of runs, the best performing set in terms of RMSE is assumed to be the correct one. This method would not be necessary if the real values of these parameters were known. However, since the precise numbers are almost never available, an equifinality approach is a promising direction that practically resolves the issue [*Beven 2006*] in contrast to an exact optimality approach.

4.5.3 Bankline Profiles

The physics-based bathymetry model assumes coverage of the main riverbed topology. That means that it is excluding the river banks which may form in different places. Using the model without consideration for them runs the model for the full coverage of the specified grid. The results can be incorrect and unfair to the method used, because of the big differences formed between an exponential computed for an outer bend and a slope of a bank. Therefore, in cases where the river banks are covered in the data, the grid's extent needs to be altered to include them. To do so, areas on both outer sides of the grid need to assume a rising slope. This can either be calculated and approximated by the input cross-sectional data or specified by the user and then smoothened with the computed bathymetry data.

The different slopes that may be assumed are presented in Figure 4.21. In general, there is no clear choice between them other than assuming the most natural representation. This can either be Figure 4.21 b or c. Together with the subsequent cross-sectional smoothing performed, the shape of the slope will change to fit the data depths [Figure 4.22].

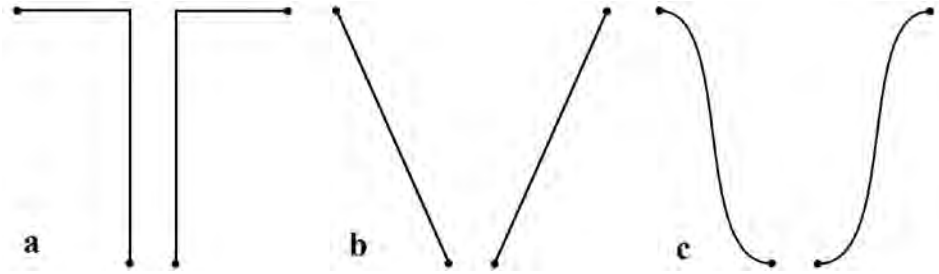

Figure 4.21. Possible left and right bank profiles: (a) No slope, (b) Linear Slope, (c) Sigmoid slope.

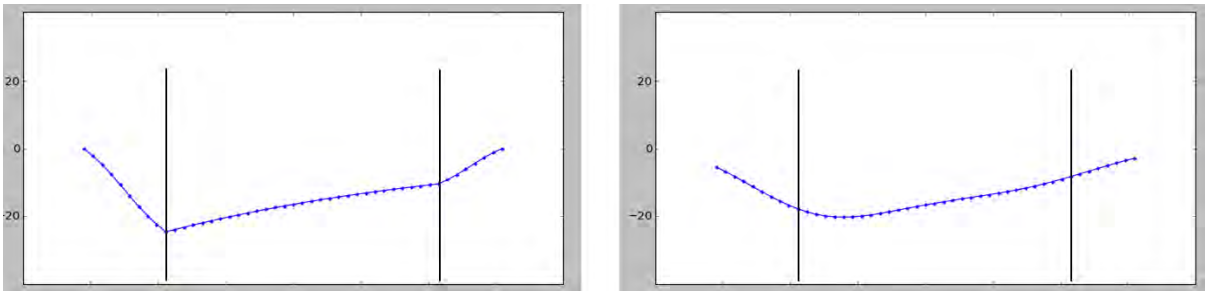

Figure 4.22. Example cross-section with sigmoid banks included. Left: Before smoothing, Right: After smoothing. Depth values are in feet. Vertical lines denote left and right banks.

In a real-world scenario, the banks are unknown unless there is data close to the edges of the river polygon where the bankfull limits are assumed. If there is some data that extend to these limits, a spatial analysis of them may convene a general bank's profile. If there is either no data reaching the edges, either an educated guess must be made, or it is better to diminish the polygon's limits to the computable grid area and assume no banks.

4.5.4 Model Profile

Together with the banklines profile consideration, the representation of the cross-sections for the physics-based bathymetry model has been set. The local water level elevation may vary between areas. That is either available by the reports stated previously (§4.5.2) or needs to be extracted from online databases like Google Maps or available elevation data like AHN2 (for Netherlands).

Firstly, the local elevation needs to be considered. The data points usually do not reach the bankfull extent. Therefore, a small height difference might exist between the bankfull point and the first available data point. This additional height needs to be subtracted from the local elevation level to assume a water level elevation above the sea level.

Banks may exist left and right of the grid and be of varying length. After defining them, the resulting diminished part of the channel is the active alluvial channel. Its width is a fraction of the full grid extents and this is considered in the calculations. The remaining area is the extent for which the physics-based bathymetry model runs. The resulting riverbed approximation is further smoothened to simulate the diffusion and advection physical processes and have a better overall representation. The full cross-sectional profile described is shown in Figure 4.23.

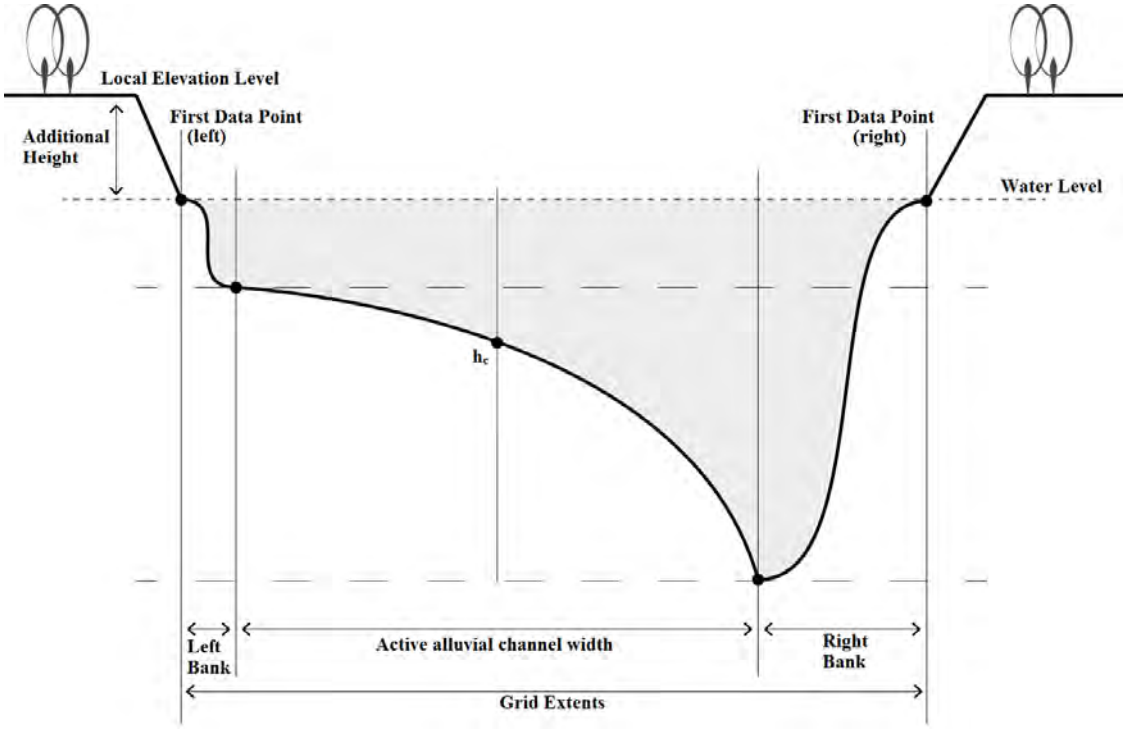

Figure 4.23. Physics-based bathymetry model cross-section with all assumptions included.

An example of the computed physics-based model riverbed topography is shown in Figure 4.24 using the example polygon of Kootenai bend #2 with the following hydrographical parameters:

Discharge	Q = 1200.0 m^3/sec
Roughness coefficient	C = 60 $m^{1/2}$/s
Slope	i = 2.0x10^{-5}
Mean Sediment Size	D_{50} = 800.0x10^{-6} m
Calibration coefficient	a = 3.0

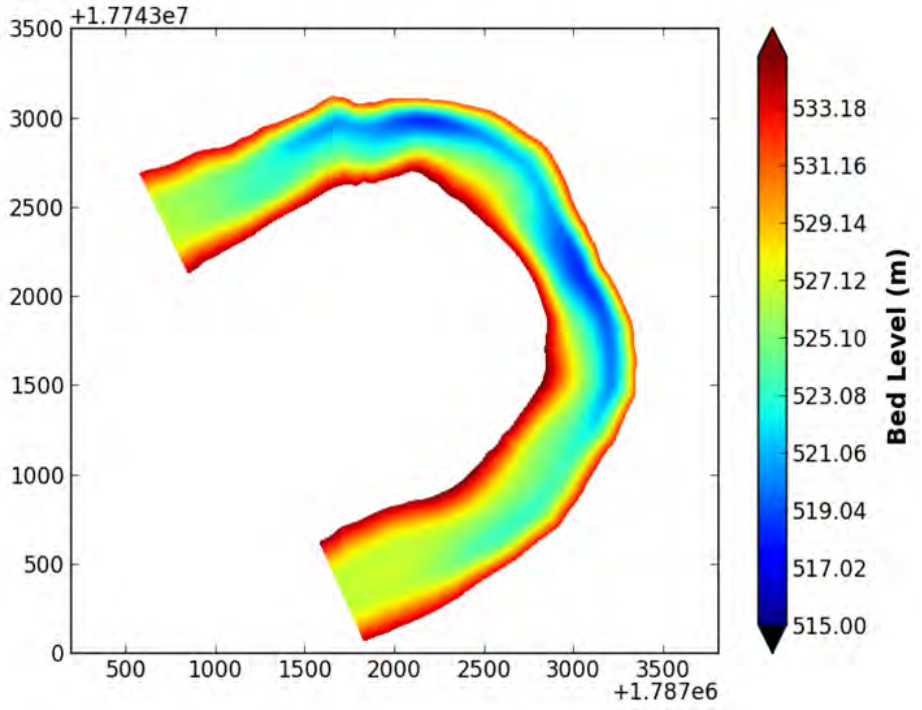

Figure 4.24. Physics-based model's computed bed topography example.

4.6 Spatial Interpolation Methods

A number of interpolation methods were mentioned in §2.2. As described in that part, in the special case of scarce datasets in rivers geostatistical methods like Kriging do not manage to approximate the riverbed correctly, because the covariance between the data is directionally correlated and the samples are too little to allow for a good estimation. Also, Natural Neighbour interpolation also fails due to the extreme averaging during the weight assigning. The Thin-plate splines by RBF may have an acceptable result when data is not very limited, but extra data at the river's boundaries or if too far away are required; otherwise, there are great derogations from reality. Therefore, these classes of interpolation are not considered.

One main point to be made is that anisotropy should be accounted for and implemented in the spatial interpolation method. Based on that but also for comparison's sake, profiles of Linear (Barycentric) Interpolation (§4.6.1), Nearest Neighbour (§4.6.2), IDW (§4.6.3) and EIDW (§4.6.4) were explored. In the cases of IDW and Nearest Neighbour, some smoothing is required to mitigate for their lack of directional considerations during the interpolation of the values.

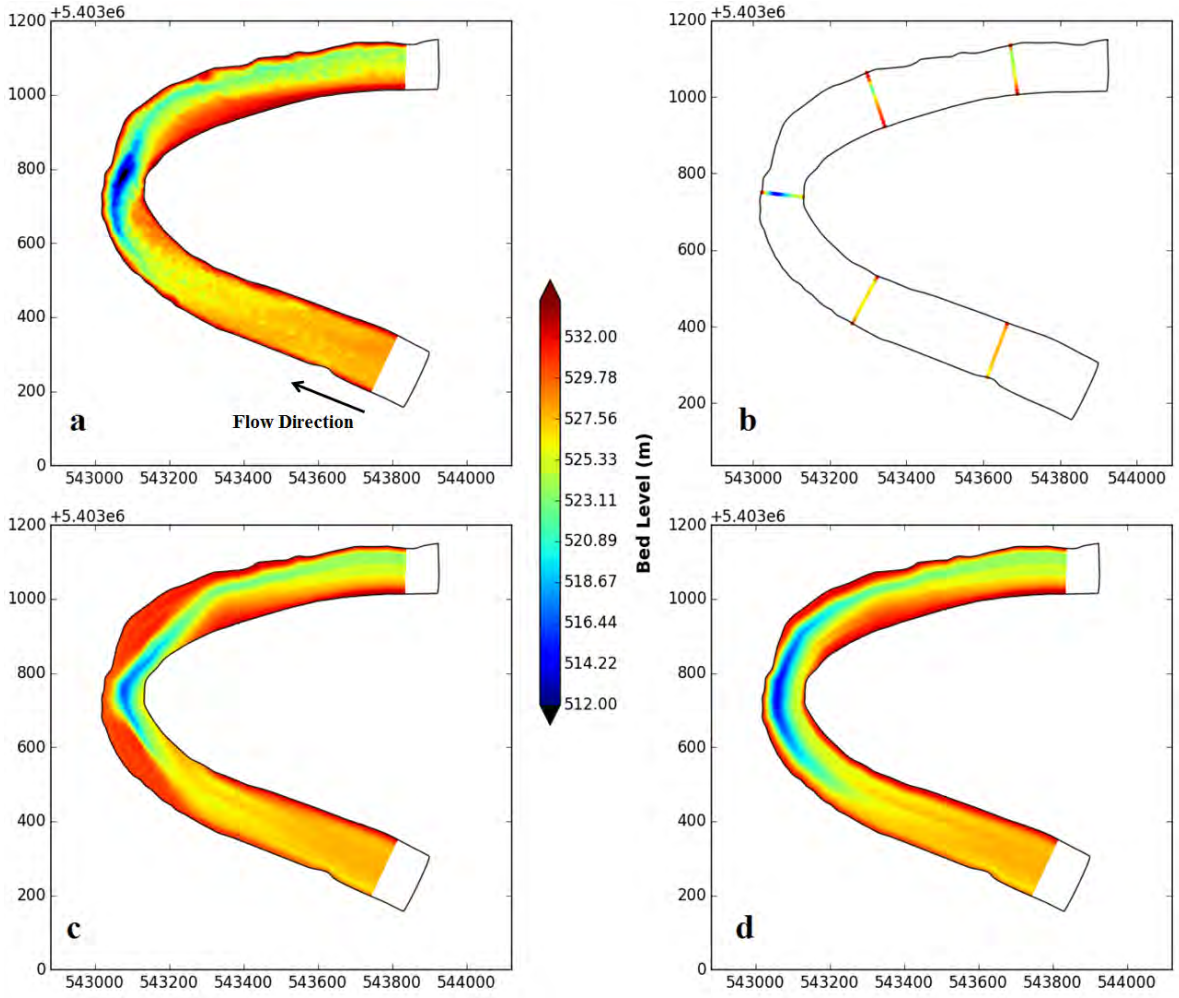

Figure 4.25. Linear Interpolation in two coordinate systems. (a) Ground-truth dataset, (b) Test dataset, (c) Linear Interpolation in Cartesian, (d) Linear Interpolation in Flow-oriented system.

Additionally, of importance is to note that the flow-oriented coordinate system is supported in all of the interpolations performed, as stated in §2.2 and presented in §4.3.4. As shown in [*Merwade et al. 2006*] it results in a better outcome, because it defines space in the correct manner, which follows the natural course of the rivers. Were it not to be taken into account, the values of the non-transformed sampled points would have a greater influence to the unsampled points due to their topological proximity, especially in the areas of bends. This problem is even more evident in the case of scarce data as the influential locations hold a greater weight. Figure 4.25 displays such example in the case of Linear interpolation for the second Kootenai River bend chosen. Interpolation in the Cartesian results in a skewed prediction, whereas the flow-oriented corrected direction has a smoother depiction.

For any interpolation method used, based on the associated grid, the transformation is performed following the centerline's direction, as described in §4.3.4. The resulting grid has its intersection nodes on the flow-oriented coordinate system, as shown in Figure 4.11. Since the sampled data lie on some of the grid's intersection nodes, they transform similarly into the described system. To make things clearer, a display of the ground truth and the Test datasets is shown in Figure 4.26. For all of the following examples, Kootenai bend #1 was sampled for seven cross-sections extracted from the ground truth data shown in the figure.

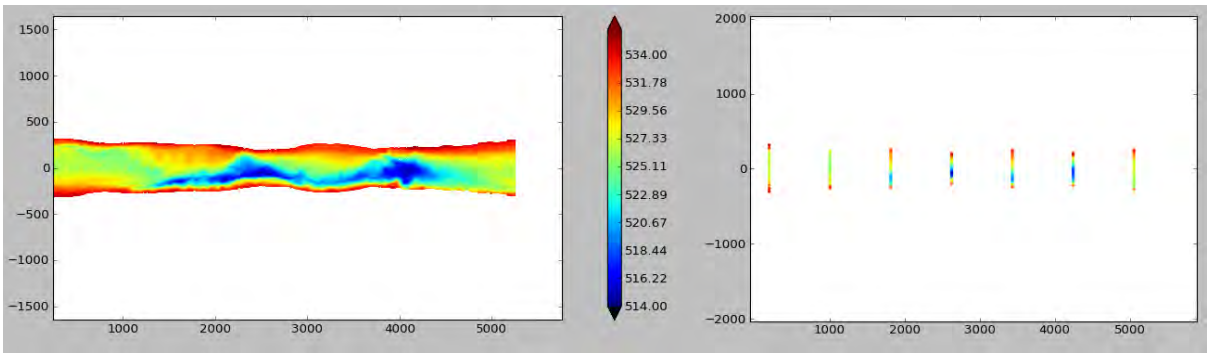

Figure 4.26. Flow-oriented Coordinate system transformation. Left: Ground-truth dataset, Right: Test dataset (7 cross-sections, 0.15% data).

4.6.1 Linear Interpolation

Linear Interpolation as used in this thesis initially triangulates the sampled data and then performs linear barycentric interpolation on the triangle each unsampled point lies on. The underlying concept is shown in Figure 4.27. The method suffers from the positions the sampled data may have, which usually does not cover the edges so that triangulation can cover as much of the grid extent as possible. Such missing areas from the final result are linearly filled in per longitudinal line of the grid. Furthermore, the interpolated areas close to the sampled points may display sudden sharp artefacts as the described triangulated areas change, especially in the case of trackline data. The interpolation is performed in the flow-oriented coordinate system. An example result is seen in Figure 4.28.

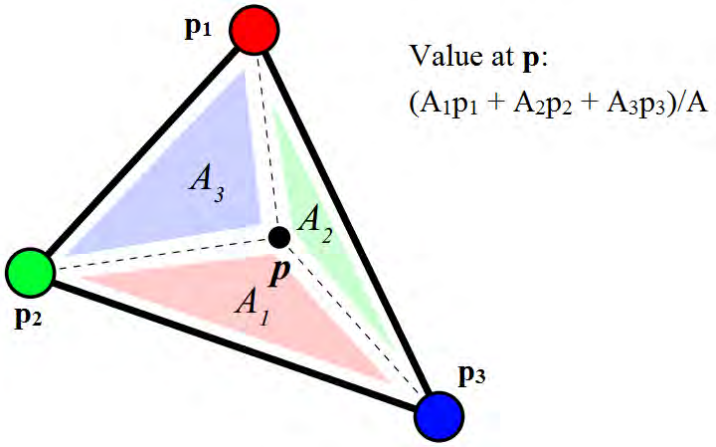

Figure 4.27. Linear Barycentric Interpolation. Each point inscribed by a triangle of sampled points acquires a value based on the percentage of the triangle area on the opposite of the sampled point to the whole area of the triangle.

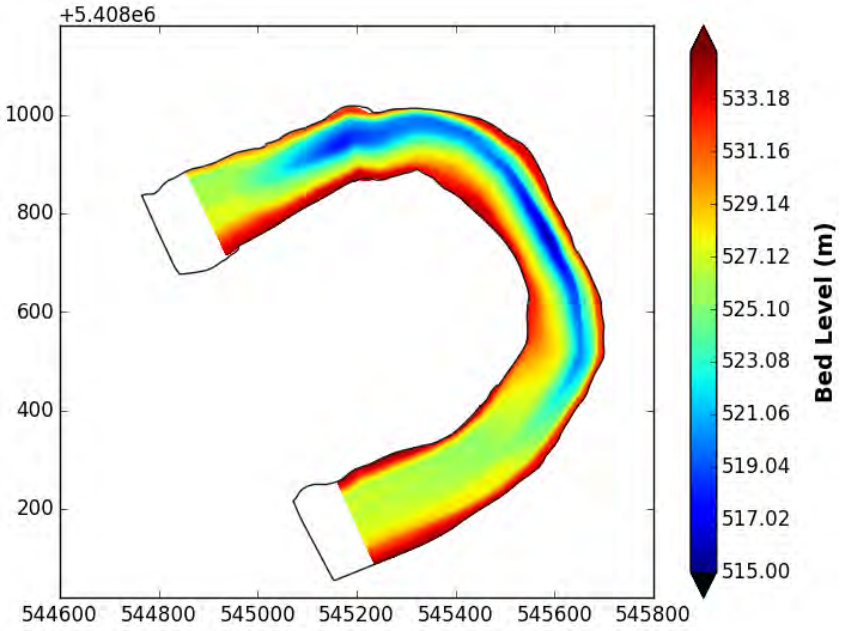

Figure 4.28. Linear interpolation of 7 regularly spaced cross-sections, no smoothing.

4.6.2 Nearest Neighbour

This method does not qualify as an interpolation method but more of a rule-based value assignment. It bears however an interest because of its simplicity and its capability to come close to Linear and IDW interpolation results when smoothing is applied, especially when dealing with scarce data. In particular, the value of an unsampled point is forced equal to the value of the one closest sampled point. As with the rest, this method is performed in the flow-oriented coordinate system. To be able to have viable results, extensive smoothing is required along the water flow, which however spreads out the values and results in an overall averaged outcome with crisp artefacts [Figure 4.29]. Additionally, the value assignment is highly dependent on the sampled data locations.

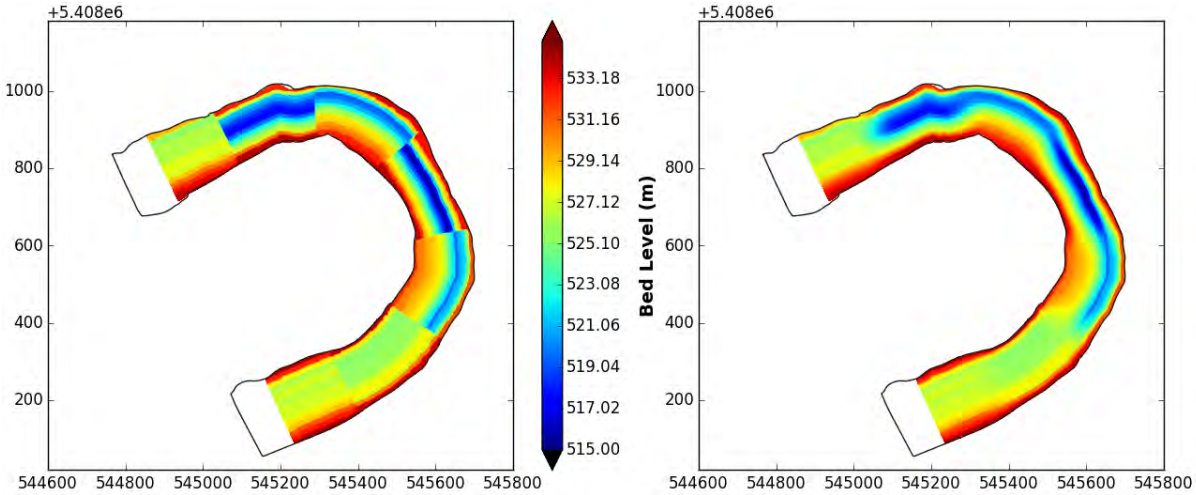

Figure 4.29. Nearest Neighbour interpolation for 7 cross-sections. Left: No smoothing. Right: Gaussian window smoothing.

4.6.3 IDW

The distance weighing factor perspective for IDW was given in §2.2, Eq. 2.8, 2.9. With IDW however, the anisotropy factor is not taken into account. Therefore, given a meandering river, a global interpolator for IDW can have relatively bad results, especially in parts where the meander river banks are close to each other. To avoid this, the transformation to the flow-oriented coordinate system of the sampled data is a necessity.

Another problem of the IDW is that it is sensitive to clustering and spacing between the sampled data, something significant in the case of cross-sections. The power factor in Eq. 2.9 needs to be relatively large depending on the distances between sampled data. Regular values for it are 2 or 3; however, when dealing with scarce data, it is necessary to have much larger values, otherwise the interpolation results in an over-generalized output. In the experiments, values between 4 to 25 were used. Applying this large power exponent for the inverse distances, together with smoothing along the water flow, a satisfactory result may be retrieved. However, it is usually difficult to scale the power factor to the sampled data sampling distances. An example is shown in Figure 4.30 below.

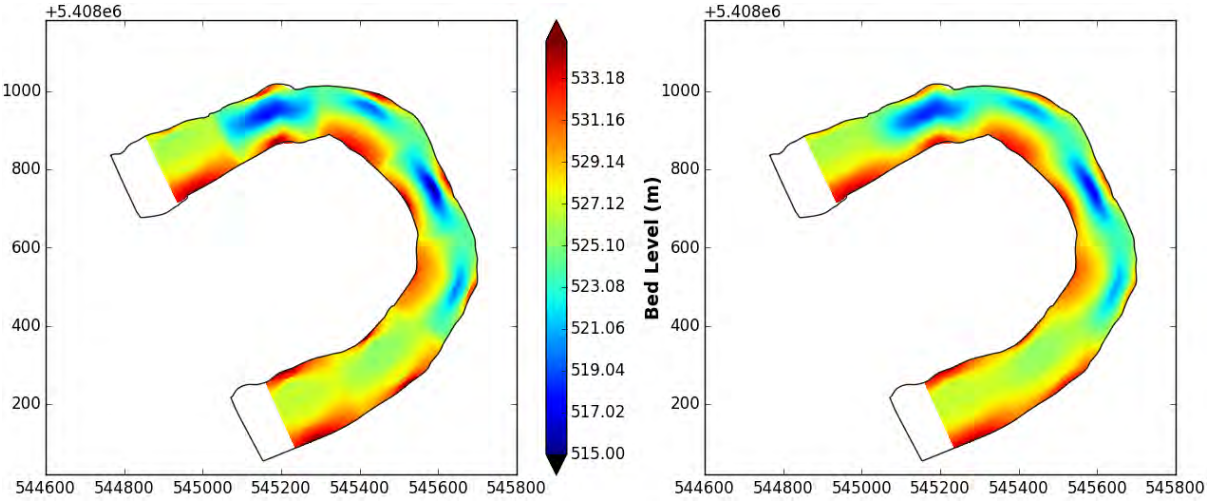

Figure 4.30. IDW with power exponent = 10, 7 cross-sections. Left: No smoothing. Right: Gaussian window smoothing.

4.6.4 EIDW

This method is similar to the IDW, applying a weighted distance factor. It also profits from transforming the data into the flow-oriented coordinate system, which is necessary for a correct weighting of the distances. That is because this method accounts for the anisotropy in the data specified. This is introduced by the anisotropy factor as explained in §2.2 (Eq. 2.10), which brings closer the data points on the longitudinal direction of the water flow (s-direction). Therefore, sampled data first need to be described in that system and then anisotropically weighted for each unknown point.

The effect of the power exponent here can be made less severe and brought closer to normal values without need to adjust much. Furthermore, smoothing can be of less influence, mainly because the underlying process is already performed in part by the anisotropy consideration. The anisotropy ratio itself can be either arbitrarily defined or ascertained by computing the variance ratio of the sampled data. The example of this method lies below [Figure 4.31].

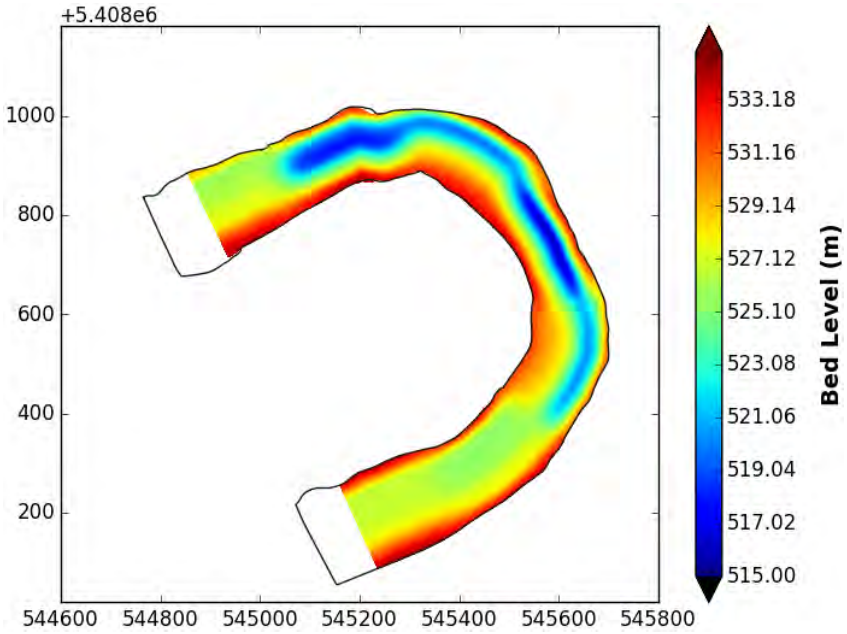

Figure 4.31. EIDW with power exponent = 5, ar = 8, 7 cross-sections, no smoothing.

4.7 Fusion of Datasets

The interpolation methods can provide an output depending on the input data received. The more the data, the better the output is approximated to the ground truth dataset. However, in the current thesis the data available are scarce, which complicates the results of the aforementioned spatial interpolation methods. The bed topography computed by the physics-based model can provide the extra feedback on areas of missing values.

In order to make the best use of the two datasets, a straightforward assumption is made to apply a number of weights to the interpolated dataset and the model's dataset. These weights gain values depending on how close each unsampled point lies to a sampled point or a cluster of known data. The closer it is, the more the interpolated result should be accounted for its value, whereas points further

away from sampled points consider the computed model topography to be the most valuable estimator.

Applying these weights to the two datasets a third "fused" dataset is acquired. Any type of interpolation can be used in this process, however taking into consideration all the theoretical assumptions and perspectives that guided this thesis until here, the EIDW in a flow-oriented coordinate system is the one used for the fusion. The two types of scarce datasets described (cross-sectional or trackline data), presented in [Figure 4.17] and [Figure 4.18]) also assumed different weights based on the assumptions of their structure in space.

The two weights of the interpolation and the model add up to one, so that when multiplied with the respecting computed values on the specific location they result in a fused value to assign to the unknown point. Therefore, the weights have values in the range of [0,1]. Taking that into consideration, a simple equation of a masked result is as follows:

$$F_{(s,n)} = w_{(s,n)}\, B_{(s,n)} + (1 - w_{(s,n)})\, I_{(s,n)} \qquad \text{(Eq. 4.6)}$$

where:

$F_{(s,n)}$: fusion result at (s,n)

$B_{(s,n)}$: model result at (s,n)

$I_{(s,n)}$: interpolation result at (s,n)

$w_{(s,n)}$: model weight at (s,n)

4.7.1 Cross-sectional Scarce Data

To model the weighting behaviour mentioned in the previous paragraph, each of the cross-sections that has known data is perceived as a cluster of data. Under this assumption, any unsampled point that lies in between two sampled cross-sections receives two weights: one in respect to the physics-based model computed topography and one of the interpolated dataset. On a conceptual level, a gradient weighting is formed between each couple of cross-sections, with the weights closer to the cross-sections having values close to 1.0 for the interpolated result and 0.0 for the model's result, and vice versa in the middle between the cross-sections [Figure 4.32].

Figure 4.32. Gradient concept of weights applied in fusion method for cross-sectional scarce data. Black colour corresponds to the interpolated result, whilst white to the model computed topography.

The procedure to achieve this is as follows. Initially the locations of the cross-sections on the grid are computed. Then, the distances of an unsampled point to the two (different) closest cross-sections is calculated. Afterwards, the weight of the model is calculated based on the distances a point has to the in between cross-sections, according to the following equation:

$$w_{(s,n)} = \begin{cases} 0 & , \quad d = 0 \\ \dfrac{1}{1 + \left(\dfrac{D-d}{2d}\right)^2}, & otherwise \end{cases} \qquad \text{(Eq. 4.7)}$$

D is the largest distance of the two and d the smallest. This ratio ($w_{(s,n)}$) acquires values between [0,1] and is the weight applied to the physics-based model result. The weight for the interpolation is the result of subtracting the aforementioned ratio from 1, as per Eq. 4.6.

Assuming two cross-sections at a certain distance, the above weights gain values according to the diagram shown in Figure 4.33 below, based on Eq. 4.7. To make a connection to the conceptual representation of these weights, Figure 4.34 shows how the model's weights are distributed as a gradient function between the cross-sections. An example result follows in Figure 4.35.

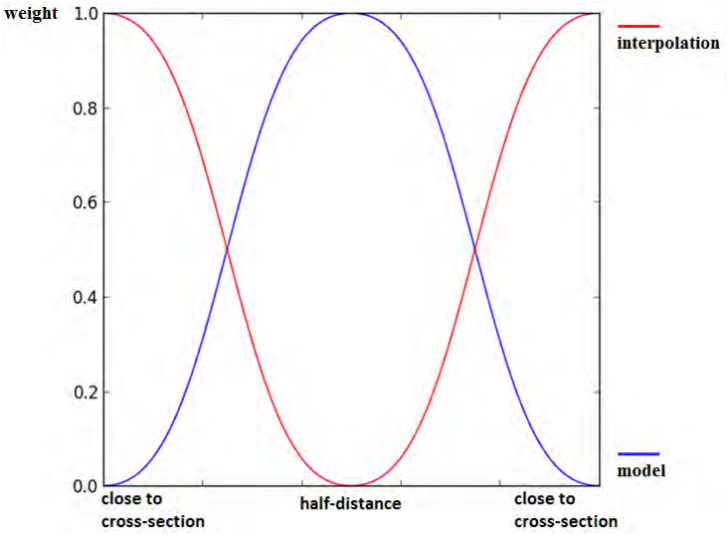

Figure 4.33. Weights applied to unsampled points based on their distances from sampled areas. For each dataset: blue colour for the model, red for the interpolation.

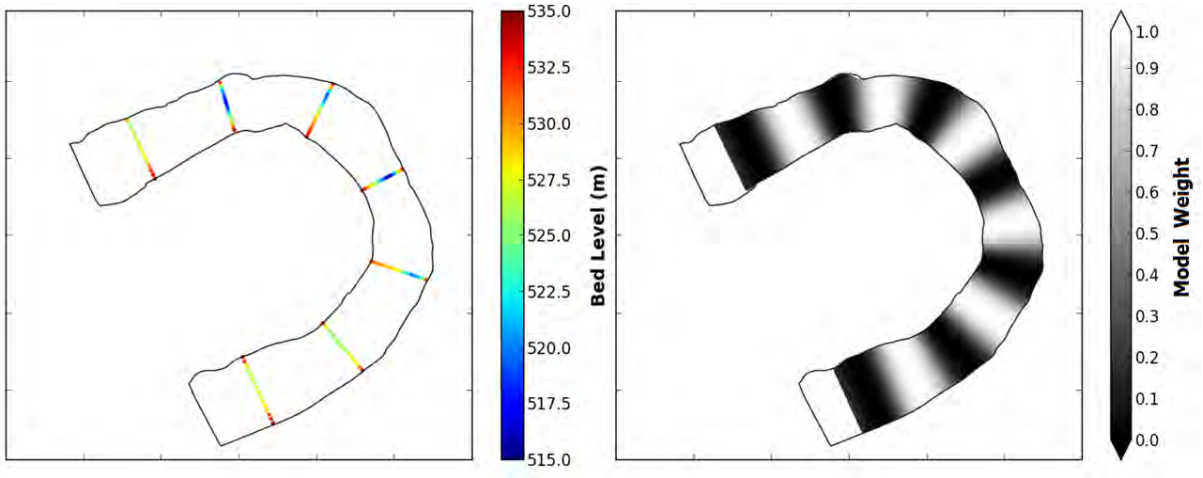

Figure 4.34. Physics-based model weights as dispersed in between cross-sectional data. The inverse of these colours would respond to the weights of the interpolated dataset.

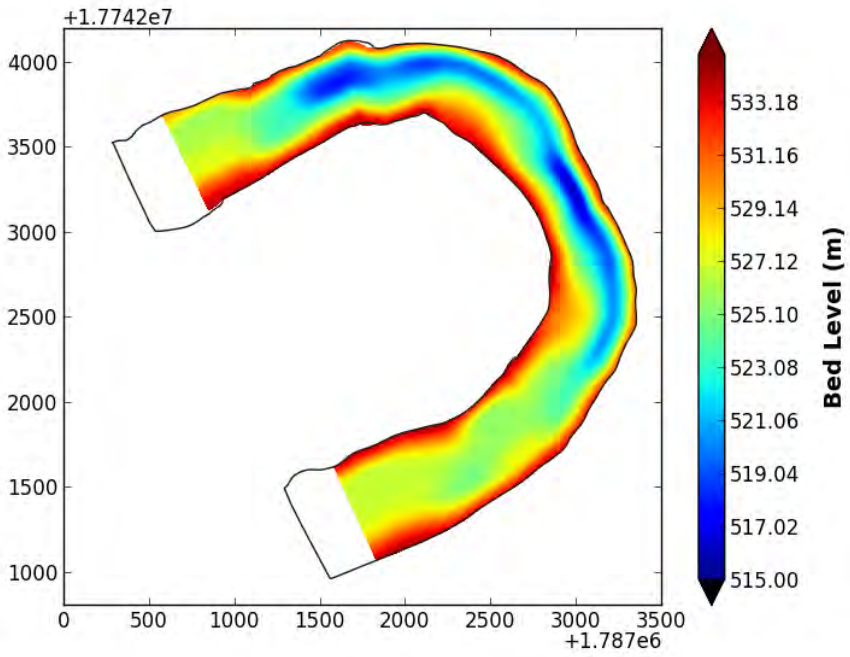

Figure 4.35. Fusion dataset result for cross-sectional scarce data, using EIDW (7 cross-sections) and the physics-based model.

4.7.2 Trackline Scarce Data

When only trackline data is available, the distances between the sampled points have no specific relation, especially if the way of collection is unorderly. There is not a certain rule for the weights to be applied in this case to each of the model and interpolated results. A way of dealing with disorderly data is to assign a threshold distance value.

For each unsampled point, the distance to the closest sampled point is calculated (d). If it is above the given threshold (D_{thres}), the computed model result receives a weight of 1.0 and the interpolated value a 0.0. If it is less than the threshold, a fraction of the two distances can give a value between [0,1]. Therefore, the conditional is formed as:

$$\begin{aligned} &\boldsymbol{if}\ \boldsymbol{d \geq D_{thres}}\boldsymbol{:} \\ &\quad w_{(s,n)} = 1 \\ &\boldsymbol{else}\boldsymbol{:} \\ &\quad w_{(s,n)} = \frac{d}{D_{thres}} \end{aligned} \qquad \text{(Eq. 4.8)}$$

This calculation can be extended by additional requirements like the unsampled point needing to be to at least k other sampled points below the threshold, or assume an averaged resulting distance to at least k other closest sampled points. A simple suggestion for a relatively straight river would be to use the smallest cross-sectional width as this threshold distance.

In the current context, for the cases where the Test datasets have been extracted in a structured way (IJssel, Kootenai) the threshold distance can also be calculated. In the Danube case, an educated guess is assumed close to each channel's average width (about 300 m). The conceptual depiction of such trackline data weighting of the model's values can be seen in Figure 4.36. Below that is an example of the resulting fused dataset for the Kootenai River bend [Figure 4.37].

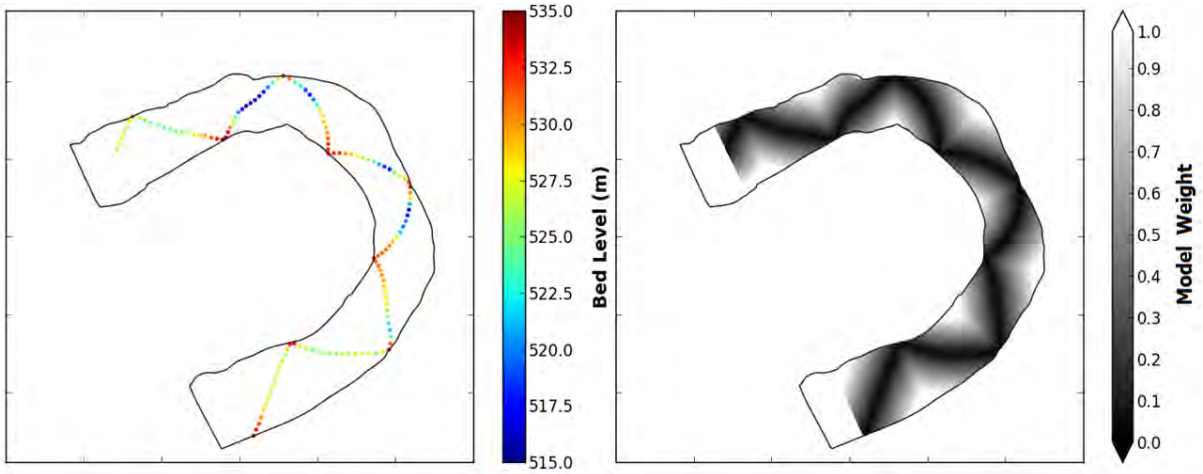

Figure 4.36. Physics-based model weights as dispersed in between trackline data. The inverse of these colours would respond to the weights of the interpolated dataset.

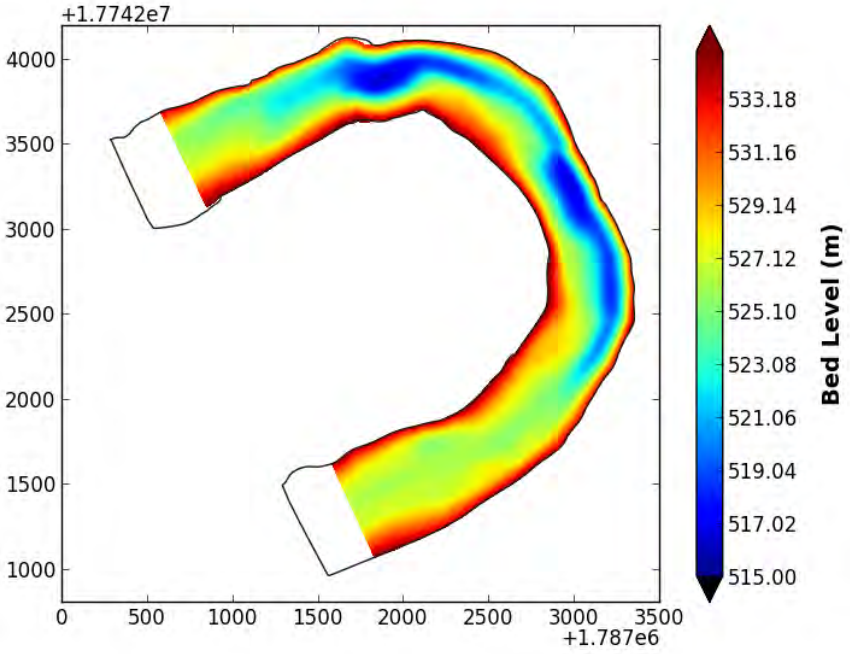

Figure 4.37. Fusion dataset result for trackline scarce data, using EIDW and physics-based model results.

4.8 Validation

Validation of the devised method is made possible by providing evidence that the requirements and goals set are fulfilled. This can be in terms of presenting the results, comparing with other methods or proving the solution's correctness.

For evaluating the results of the Fusion method, comparisons between the ground-truth data and the resulting datasets are made for the proposed method, the physics-based model and the spatial interpolations. The stricter output is in the form of the numerical evaluator of Root Mean Square Error (RMSE) values, which is a commonly addressed model evaluator. It can be a harsh measurement because it punishes both consistent bias and large error variance, as mentioned in §2.3.

A single numerical value cannot always display all features captured by a method. Therefore, a visual qualitative depiction with error maps is presented to address a more intuitive evaluation. The error maps show a distinct view of the signed difference between the ground truth and the predicted fused results. With them, areas of wrong predictions are more highlighted by overestimated or underestimated values. An example is shown in Figure 4.38.

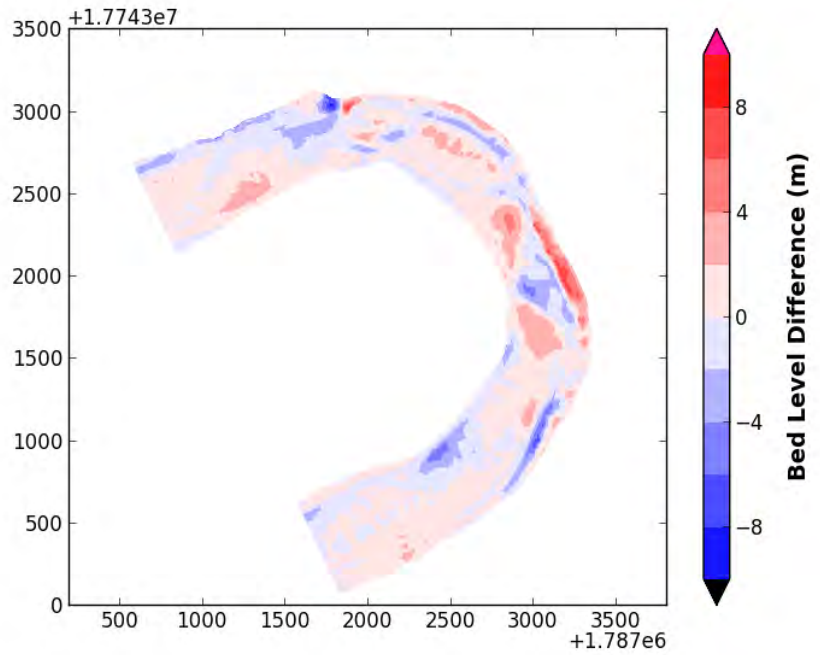

Figure 4.38. Error map of Fusion method, trackline dataset of Figure 4.35.

One step further is considering the application use of the results, which is aimed for the RAT-IN tool for ship navigability. Therefore, a final estimator can be the normalized half-width cross-sectional slope (NHWS), which focuses on the centralized area of interest. Here, the slope is assumed as the angle formed by the first-degree polynomial (linear) fit to the points in the centralized half-width for each cross-section of a dataset [Figure 4.39].

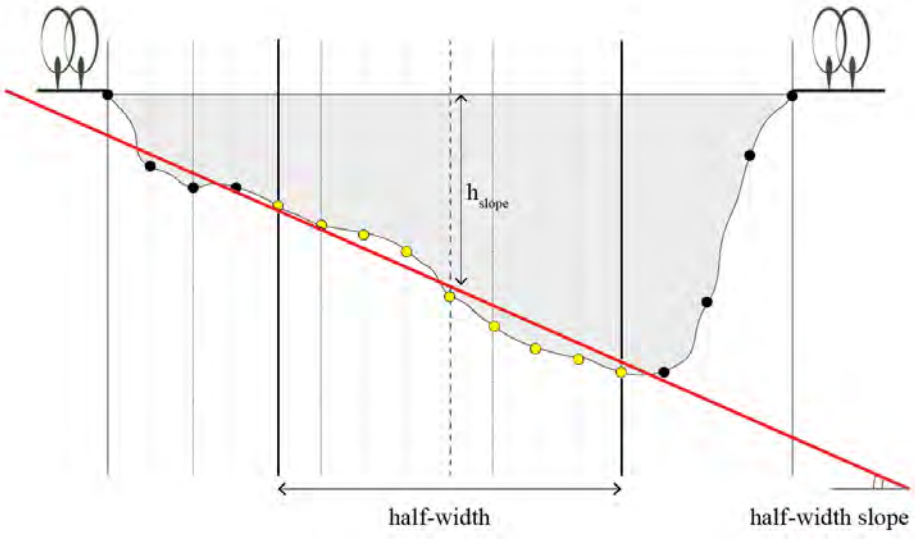

Figure 4.39. Depiction of half-width slope in a cross-section. Only the middle yellow points are used for the 1st degree polynomial fit (red line).

The slope is normalized by the water depth calculated at the central point of the slope so that the depth factor of the curve fit is also considered. By popular notation:

assuming the cross-sectional curve fit as:

$$z_{(n)} = a\,n + b, \qquad \text{with } \frac{B}{4} \leq n \leq \frac{3B}{4}$$

where B is the width at the given cross-section, the NHWS is given by:

$$NHWS = \frac{1}{h_{slope}} \frac{\partial z_b}{\partial n} = \frac{1}{a\frac{B}{2} + b}\, a \qquad \text{(Eq. 4.9)}$$

The comparison and critical evaluation is made by graphical representation [Figure 4.40] in the sense of how much the predicted data follow the cross-sectional slopes defined by the centralized half-width points of a channel as shown in §2.3.

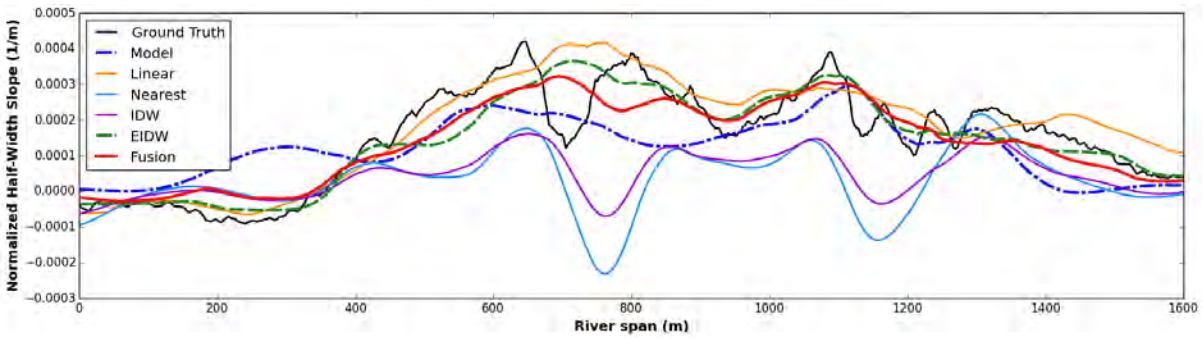

Figure 4.40. Normalized Half-Width Slope for all interpolation methods, model and Fusion method of trackline dataset of Figure 4.18.

5 Results and Evaluation

In the previous two chapters, the overall procedure of the methodology and implementation were presented. In this chapter, the steps presented are applied on all study cases and results are acquired for each river channel. The evaluation procedure commences with the use of RMSE as numerical estimator and error maps for analysis and critical reflection. NHWS is also used to bring more insight to the evaluation. It is to be noted that RMSE values are relative to each case and especially subjective to the local riverbed elevation order.

Six river bends from three rivers have been chosen, two from each river. To validate that the bends chosen hold a mild curvature, the curvature ratio (γ) is used as described on §2.1. The constructed grids were made to hold cells as close as possible to the data's resolution or to an extent that would allow for an accurate representation of the results. All data are presented relative to sea level and all depth values are in meters.

"Scarce" data were considered depth data that are located only on a few of the curvilinear grid's intersection node points. In particular, the overall number of these grid's points is considered to hold the full possible represented data, however if known depth values are below a certain number of them, they are labelled as scarce. This is referred as percentage of data coverage, where 100% responds to all such grid points having a depth value. The data thinning for the Test datasets was made in terms of number of cross-sections and trackline distances from each sinusoidal curve.

At first, all of the three rivers are presented with the parts chosen (§5.1). Then, for each river the results of the physics-based model, the spatial interpolations and the proposed Fusion method are presented (§5.2, §5.3, §5.4) and a summary is given in the end (§5.5). Only a few selected test cases and results are presented in this chapter. For further examples, refer to Appendix C: Test Results.

5.1 Study Cases

The river choices made for the extent of this research and the evaluation of the applied method involve three cases of varying interest. All three rivers are within close to very close range to populated areas, but serve different interests. Most importantly, the rivers should be of a meandering alluvial formation, in order for the physics-based model and theory to be applied without complications. Secondly, data needed to be available if possible in multibeam form. Finally, the selection was based upon the degree to which the human factor has been present and intervened to the natural formation of the river. Towards these goals, the cases of IJssel (Netherlands), Danube (Romania) and Kootenai (US Idaho) have been chosen, which in this order have a decreasing degree of human intervention.

Two channel parts per river have been chosen to cover various different cases and present more output for generality of results. These cases included features appearing at or near bends, therefore the

choices targeted such areas. For Danube, longer channel parts were chosen due to the limited data. Together with the ground-truth representation, the curvature ratio (γ, Eq. 2.1) maximum and mean values are given for each channel bend to validate their response to the mild curvature ($\gamma \approx 0.1$) expectancy.

What follows is a display of the three rivers and their ground-truth datasets (§5.1.1 to §5.1.3) after the initial data have been aggregated on the curvilinear grid, as well as the values relating to the hydrographical parameters used for the experiments (§5.1.4).

5.1.1 Kootenai (US)

Figure 5.1. Kootenai River, US (Credit: Alan Negrin).

The Kootenai (or Kootenay) River in Idaho of the United States is a mostly natural river extending its reach from Rocky, Salish, and Purcell Mountains to the Cabinet Mountains and north terminating at Kootenai Lake in British Columbia. Anthropogenic influence does exist in shape of small dikes and the Libby Dam constructed in 1972, which was hypothesized to have caused problems to the natural habitat of the river. In response, in 2009 the Kootenai Tribe of Idaho released and implemented the Kootenai River Habitat Restoration Master Plan, which with the support of the U.S. Geological Survey scientific agency (USGS) lead to the collection of the dataset at hand [*Fosness 2013*]. The dataset is available freely online [*USGS 2013*] and is in full multibeam xyz format in irregular form. The time frame in which it was collected was 3 months (May to July, 2011), but at the moment exact hydrographical data is not available. Nevertheless, in lieu of any further information, a provided web service allows for some approximations (http://nwis.waterdata.usgs.gov/nwis/uv?site_no=12310100) together with a sedimentation report [*Barton 2004*].

The chosen bends include parts of the river with interesting bed formations and some varying widths with natural erosion and sedimentation. These cases are presented in coming [Figure 5.2, Figure 5.3, Figure 5.4] below.

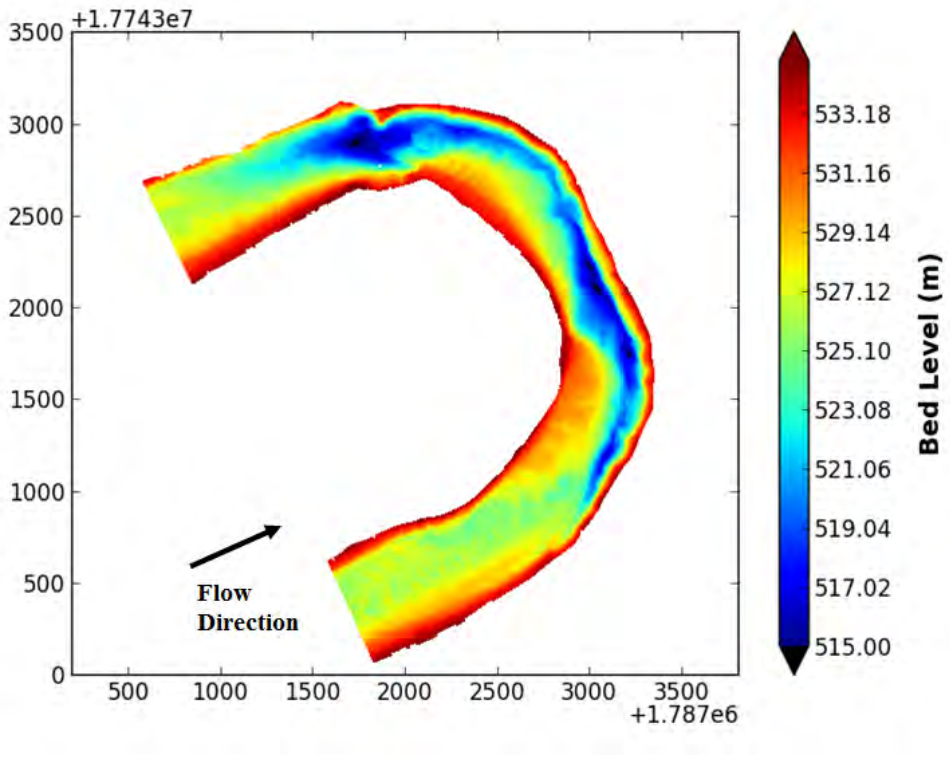

Figure 5.2. Kootenai River bend #1 (North, ~1.6 km). Curvature ratios: γ_{max} = 0.37, γ_{mean} = 0.11.

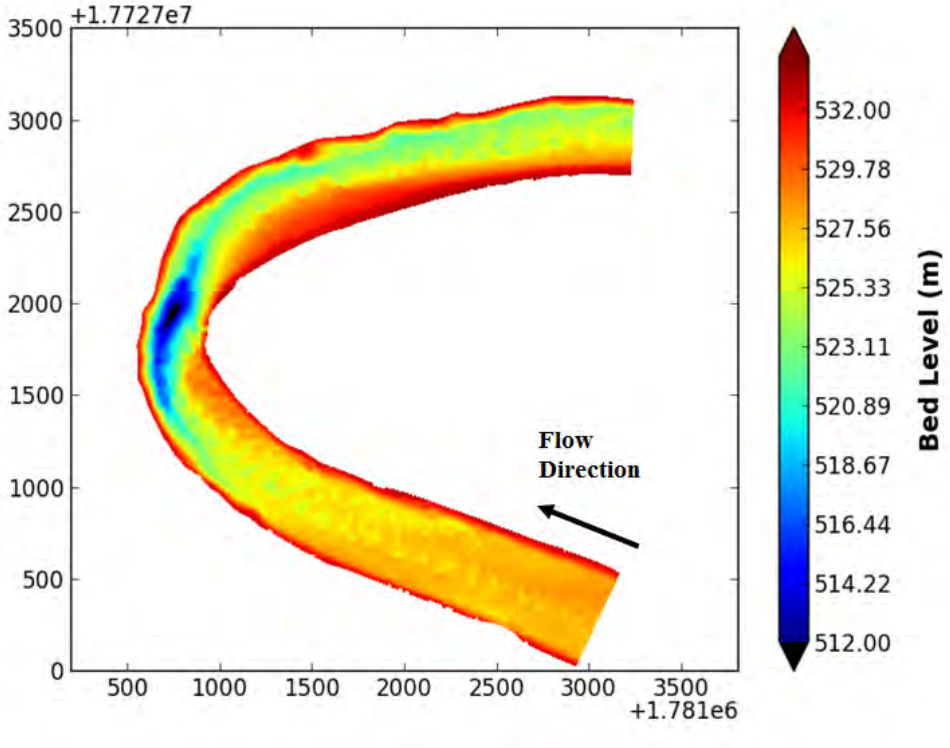

Figure 5.3. Kootenai River bend #2 (South, ~1.8 km). Curvature ratios: γ_{max} = 0.33, γ_{mean} = 0.08.

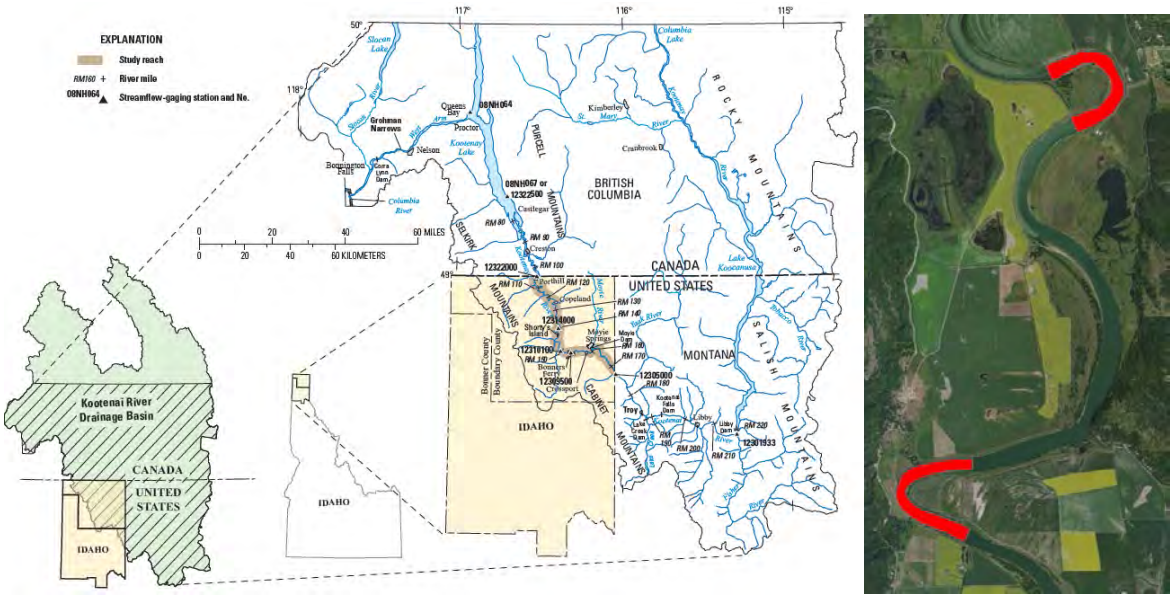

Figure 5.4. Kootenai River location and dataset. (Left: *Fosness 2013*, Right: *Bing maps*).

5.1.2 IJssel (Netherlands)

Figure 5.5. The IJssel River, the Netherlands (Commercial usage, all rights released).

The Rhine in Europe is a river that originates from the Swiss canton Graubünden and empties into the North Sea in the Netherlands. The Waal and IJssel rivers of the latter country have been commonly used for research purposes, given the high interest in protecting the land from floods. As such, a large number of hydrographical data is available, yet it is to be noted that there has been extensive human interference upon them, since include flumes, groynes, dikes and other artefacts. Out of the two, the IJssel section is chosen, as it holds an additional interest due to its almost uniform width and because it acts as a busy navigation route for ships Areas with bends, far apart from each other and (as much as possible) varying widths were chosen and are presented in [Figure 5.6, Figure 5.7, Figure 5.8] below. The datasets are of full multi-beam coverage on a regular spacing of 1 by 1 meters.

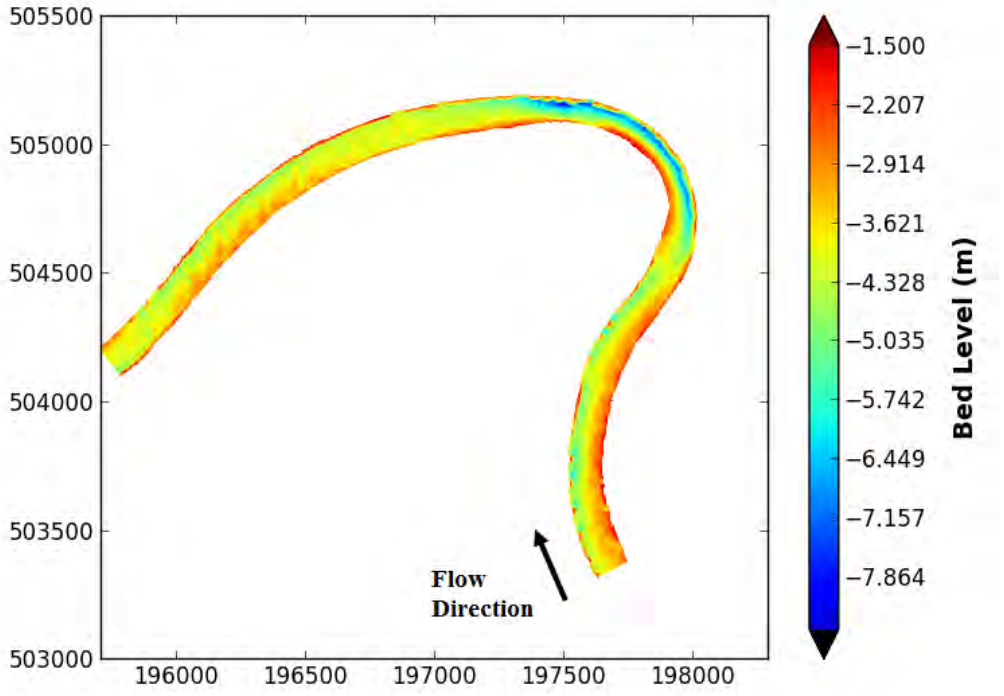

Figure 5.6. IJssel River bend #1 (North, ~4.25 km). Curvature ratios: γ_{max} = 0.47, γ_{mean} = 0.15.

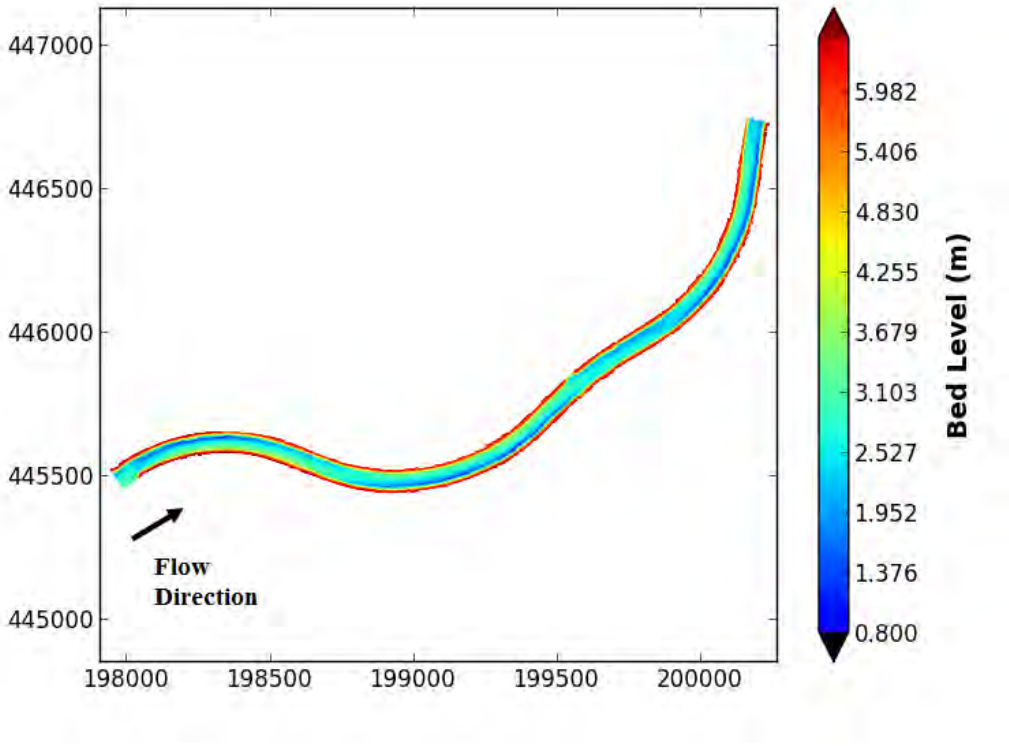

Figure 5.7. IJssel River bend #2 (South, ~3 km). Curvature ratios: γ_{max} = 0.15, γ_{mean} = 0.09.

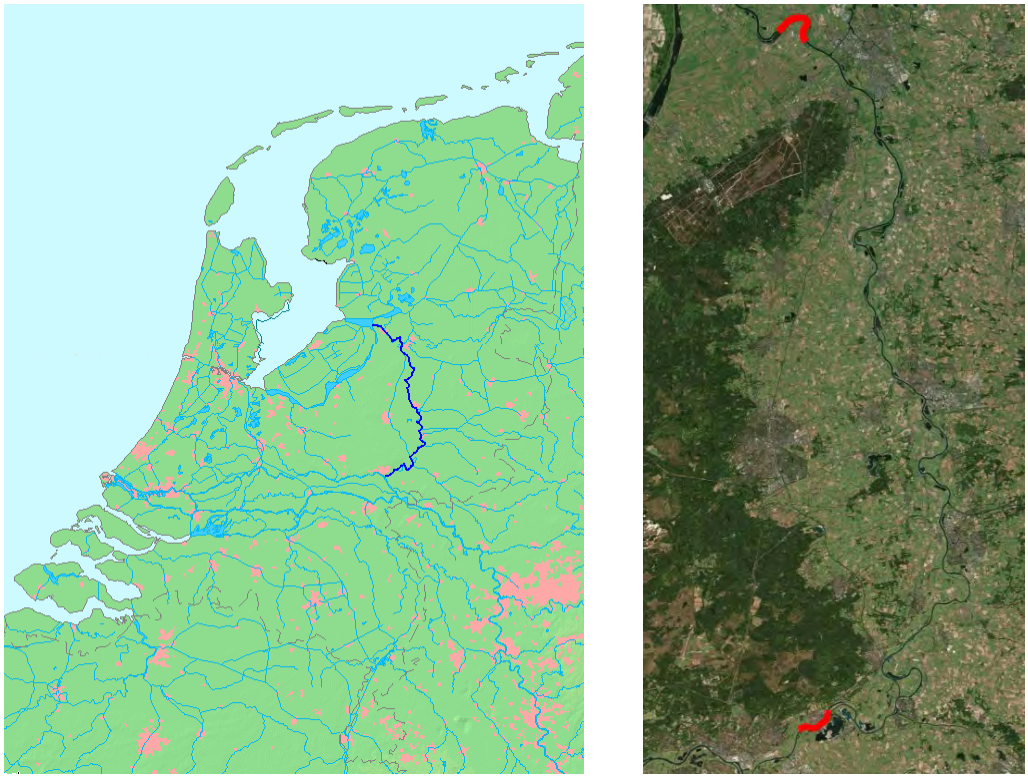

Figure 5.8. IJssel River (blue) in the Netherlands and dataset (Left: *Wikipedia*, Right: *Bing Maps*).

5.1.3 Danube (Romania)

Figure 5.9. Borcea Branch of Danube River, Romania (Credit: *Andi Schlangen*).

The Danube is a river used since ancient times for transport and trade. At 2800 km it is the second largest river in Europe, 2400 km of it being navigable. In Romania the Bala-Borcea part is nowadays the main navigational route, which however creates some bottlenecks due to the limited width of the fairway. The Romanian dataset for this project lies between Calarasi and Braila, close to the Black Sea where the Danube empties into. In the Borcea branch, interest lies in monitoring the western branch for navigational purposes. These parts have been expectedly influenced by the human element, which is heavier in these areas, but still the Danube holds some of its natural perspective.

The two cases chosen lie close to each other inside the west Borcea branch. The available data is in single-beam form and of varying density, changing from parts with only some ship tracklines to other much more densely collected profiles of close cross-sections. The width may be varying, but usually in a smooth fashion along the river flow, considering the generalized river banks. Some hydrographical data is available from past reports. [Figure 5.10, Figure 5.11, Figure 5.12] depict those bends. Their maximum curvature ratio, although relatively high locally (max), it does not exceed the mild curvature requirement.

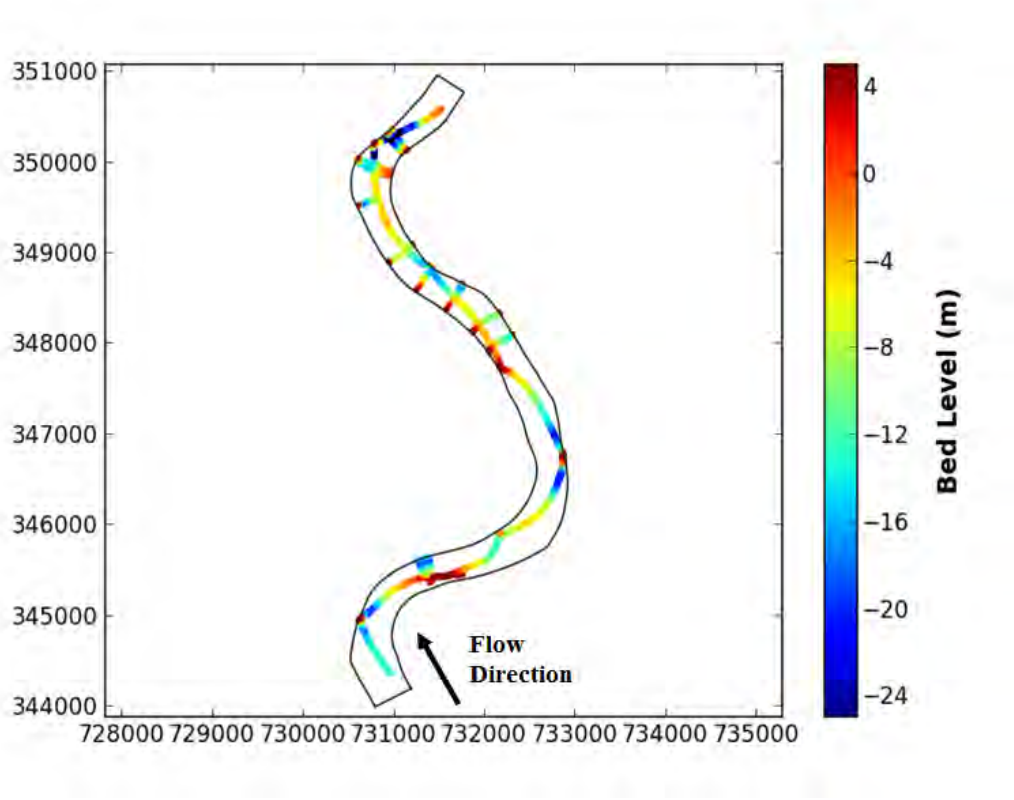

Figure 5.10. Danube River bend #1 (North, ~8.5 km). Curvature ratios: γ_{max} = 0.96, γ_{mean} = 0.29.

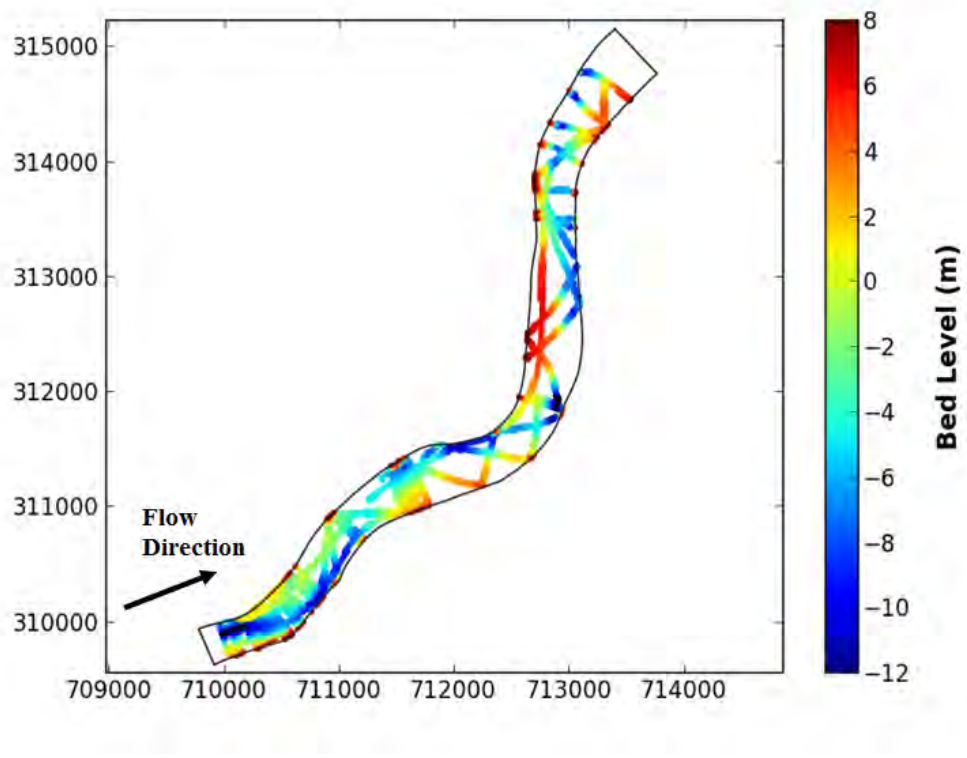

Figure 5.11. Danube River bend #2 (South, ~6.5 km). Curvature ratios: γ_{max} = 0.52, γ_{mean} = 0.21.

Figure 5.12. Danube in Romania and dataset (Left: *http://www.danube-river.com*, Right: *Bing maps*).

5.1.4 Additional Data

Additional data related to each river had to be also collected for the extent of the chosen channels, in order for the physics-based model to compute the bathymetric dataset. These are mainly the hydrographical parameters described in §4.5.2. They are assumed to be known or an educated guess

can be made about them. Because most of these parameters are not exact in nature, the Monte-Carlo simulation was used to assume the 'optimal' values, making use of the devised ground-truth datasets. Table 4.1 below summarizes the values collected from various sources used as the mean values of the Gaussian distribution and Table 4.2 the final calibrated values for input in the model.

Table 4.1. Collected and educated guesses of hydrographical parameter values. [Green: *Barton 2004*, *Fosness 2013*; Blue: *Sedimentation Report, Deltares*; Red: *Project Reports*, *Deltares*].

	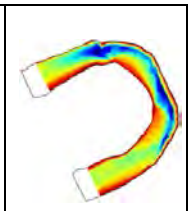	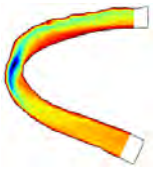			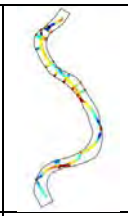	
	Kootenai #1	**Kootenai #2**	**IJssel #1**	**IJssel #2**	**Danube #1**	**Danube #2**
C[$m^{1/2}/s$]	57	70	65	65	40	60
i [-]	$2*10^{-5}$	$2*10^{-5}$	$9*10^{-5}$	$9*10^{-5}$	$4*10^{-5}$	$4*10^{-5}$
D_{50} [m]	$750*10^{-6}$	$500*10^{-6}$	$458*10^{-6}$	$4014*10^{-6}$	$200*10^{-6}$	$200*10^{-6}$
a [-]	2.0	3.5	1.5	2.5	1.2	0.85
Q [m^3/s]	1200	1200	650	650	4000	4000

Table 4.2. Calibrated hydrographical parameter values after 10,000 runs (Monte Carlo simulations).

	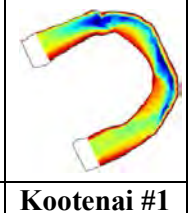	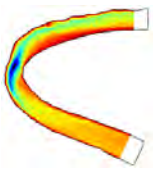			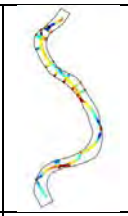	
	Kootenai #1	**Kootenai #2**	**IJssel #1**	**IJssel #2**	**Danube #1**	**Danube #2**
C[$m^{1/2}/s$]	59.26	66.88	63.66	65.77	45.57	64.05
i [-]	$1.99*10^{-5}$	$2.01*10^{-5}$	$9.11*10^{-5}$	$9.00*10^{-5}$	$4.04*10^{-5}$	$4.05*10^{-5}$
D_{50} [m]	$814.53*10^{-6}$	$520.59*10^{-6}$	$458.55*10^{-6}$	$4013.52*10^{-6}$	$182.18*10^{-6}$	$218.42*10^{-6}$
a [-]	3.11	2.91	1.17	1.44	1.20	1.04
Q [m^3/s]	1174.30	1200.16	644.77	656.22	4004.74	3983.65

5.2 Kootenai – Results

Throughout the implementation steps described in Chapter 4, the North bend of the Kootenai River was used to represent the intermediate results. Here the process is fully followed for a number of different cross-sectional and trackline Test datasets.

The general result in terms of RMSE values displays a clear trend for both datasets. In the case of cross-sectional data [Figure 5.13, Figure 5.14], the RMSE values are increasing in a similar manner for all interpolation methods while the data are thinned down from 9 cross-sections to 2 cross-sections. However, the method's results are displaying an interesting observation; although the data are thinned out, the overall RMSE result for the fusion method stays quite stable. This is probably to be attributed to a well-calibrated physics-based model result. It is to be noted that by having a

relatively stable RMSE level, the fusion method outperforms all spatial interpolation methods for any data below 8 cross-sections in the North bend and anything below 6 cross-sections in the South bend. That corresponds to any cross-sections' spacing larger than 200 m for Kootenai #1 and 225 m for Kootenai #2.

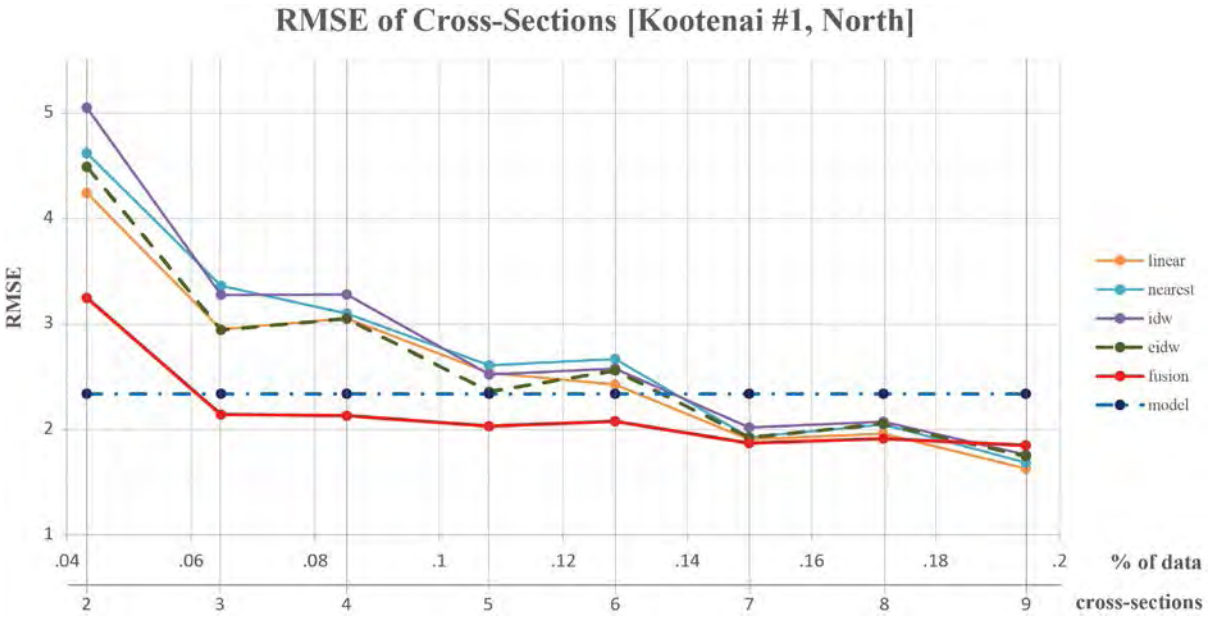

Figure 5.13. RMSE values for cross-sectional Test datasets for Kootenai #1.

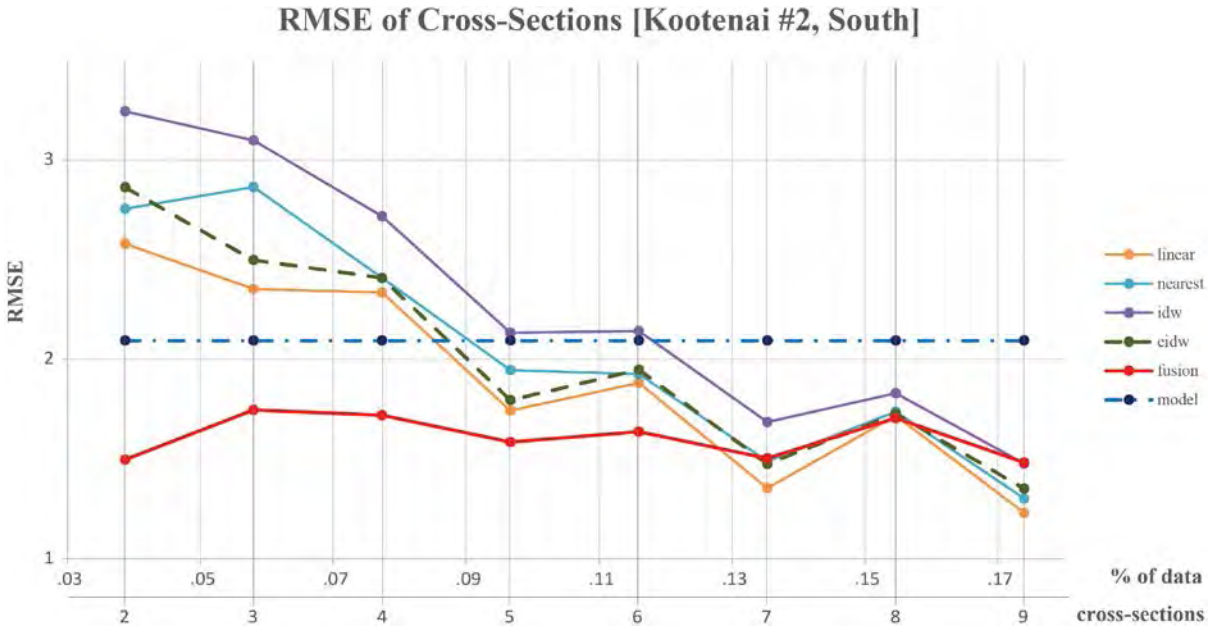

Figure 5.14. RMSE values for cross-sectional Test datasets for Kootenai #2.

With the trackline datasets, the intervals between the percentages of data are larger because of the sinusoidal shape of the data itself. With fewer curves, a much lesser number of points are sampled. Nevertheless, the RMSE values can in general be lower than in the cross-sectional datasets. It is obvious that the IDW and Nearest Neighbour methods are failing the most in this case. This is because of the way they interpolate points which are closer to the sampled data, without regard for anisotropy [Figure 5.15]. EIDW does take it into account and Linear interpolation is performing well because of its barycentric/gradient direction of interpolation in flow-oriented coordinates. In fact, when data is plenty, linear interpolation can outperform the rest, but below 0.25% the proposed fusion method is better [Figure 5.16, Figure 5.17]. The reason for the sudden jumps that appear more strikingly in these test cases is because of the samples failing to pass through an important riverbed feature like a local erosion or sedimentation part.

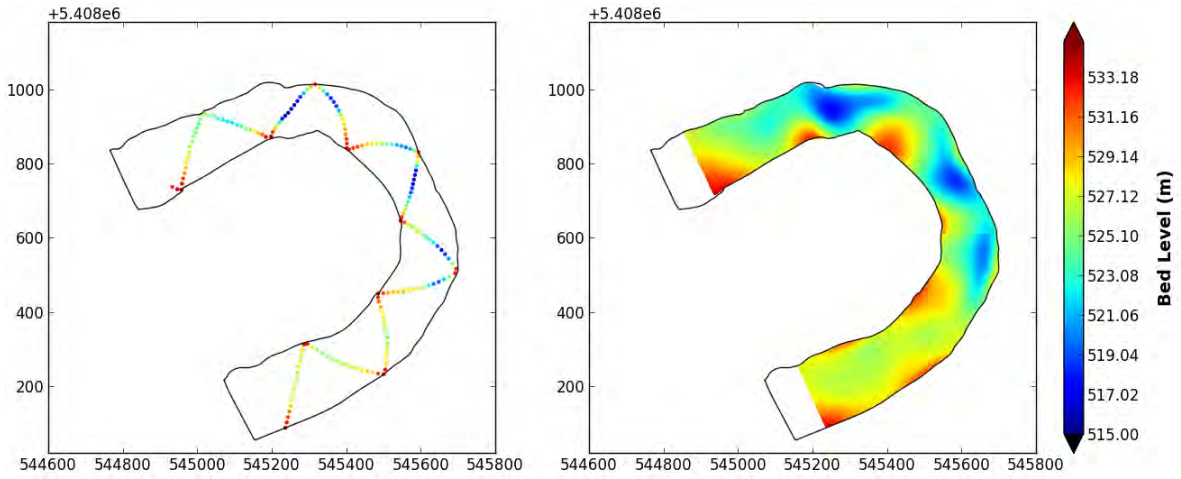

Figure 5.15. IDW failure in trackline datasets. Left: Trackline Test data (0.24% coverage), Right: IDW result, power exponent = 4, smoothing applied.

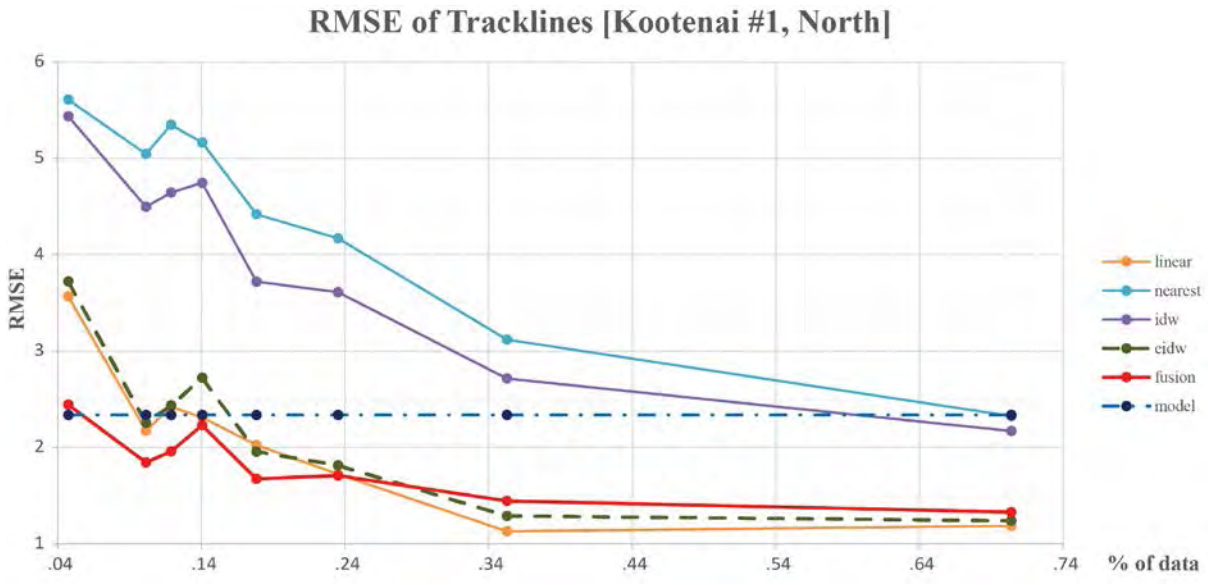

Figure 5.16. RMSE values for tracklines Test datasets for Kootenai #1.

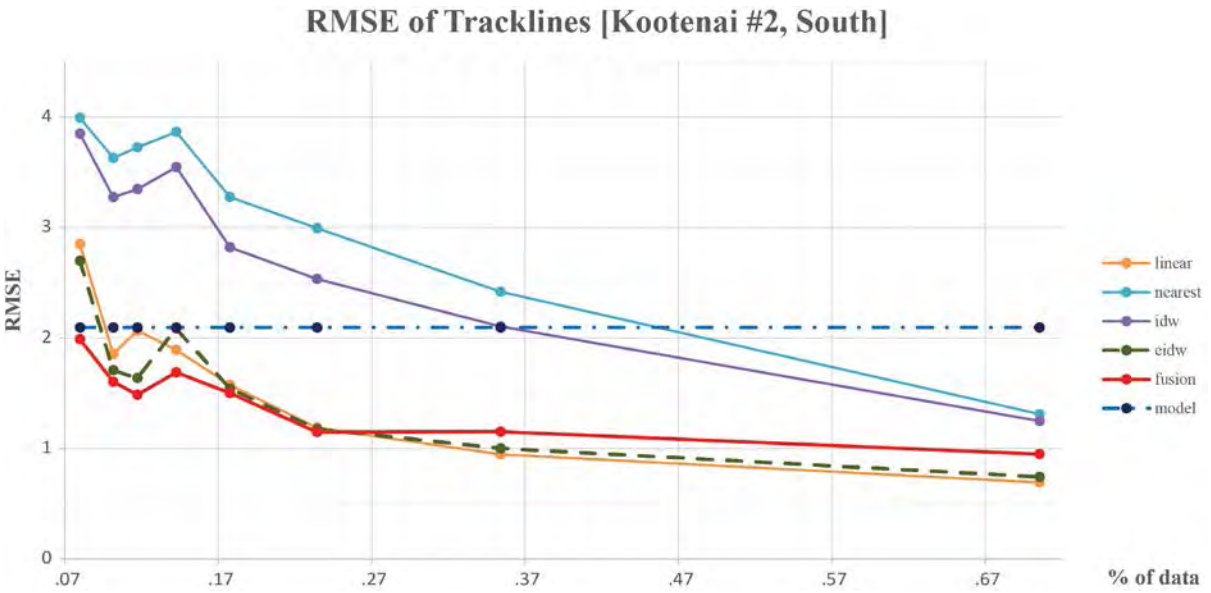

Figure 5.17. RMSE values for tracklines Test datasets for Kootenai #2.

The Kootenai River is mostly a natural river where various planform changes in its general structure may cause unexpected artefacts to appear. One of the most striking ones is the sudden erosion hole at the north of Kootenai bend #1 (North, Figure 5.3). This feature cannot be covered by the model's simplified equations, nor interpolated by any method. Therefore, if there is no data collected in the area, it is impossible to predict these cases. However, in areas where predictable erosion and sedimentation happens, the method can be very successful in achieving a much better reconstruction of the riverbed than an interpolated result. This is shown in Figure 5.18 for two different scenarios. For Kootenai bend #1 [Figure 5.18 a,c,e] the testing trackline does not pass through the bend's erosion pattern. For Kootenai #2 [Figure 5.18 b,d,f] an extreme case of only 2 cross-sections is portrayed, which although do not cover the middle of the bend, the fusion method manages to recreate the pattern.

In the latter case of Kootenai #2 bend, the success of merging the two datasets from EIDW and the model's computed riverbed topography is even more striking when the error maps of these cases are deployed. As seen in Figure 5.19, the model suffers partially in various areas over-estimating or under-estimating the depths. On the other hand, the EIDW interpolation result is obviously failing at the channel's most curved part since it was omitted from sampling. However, when combined, most of the differences are mitigated and only some depths are mostly underestimated (ground-truth depths are deeper than the fusion method's results). For navigation purposes, this is preferable to overestimating depths, because if a bend is considered deeper than it is, there might be problems with larger ships running aground.

These results are supported by the NHWS presented in Figure 5.20. The fusion method's slope follows closely the ground-truth values, whereas the other methods deviate greatly. In the graph, the fusion's curve is achieving the trough realized by the counter-clockwise erosion in the middle of the bend, due to the model's successful prediction. In the more stable parts before and after that, the EIDW interpolation's results help achieve the more static profile. Similar results appear for the two Kootenai bends cases when data is very scarce, but it must be noted that in most of the remaining results Linear interpolation performs better in the NHWS graphs.

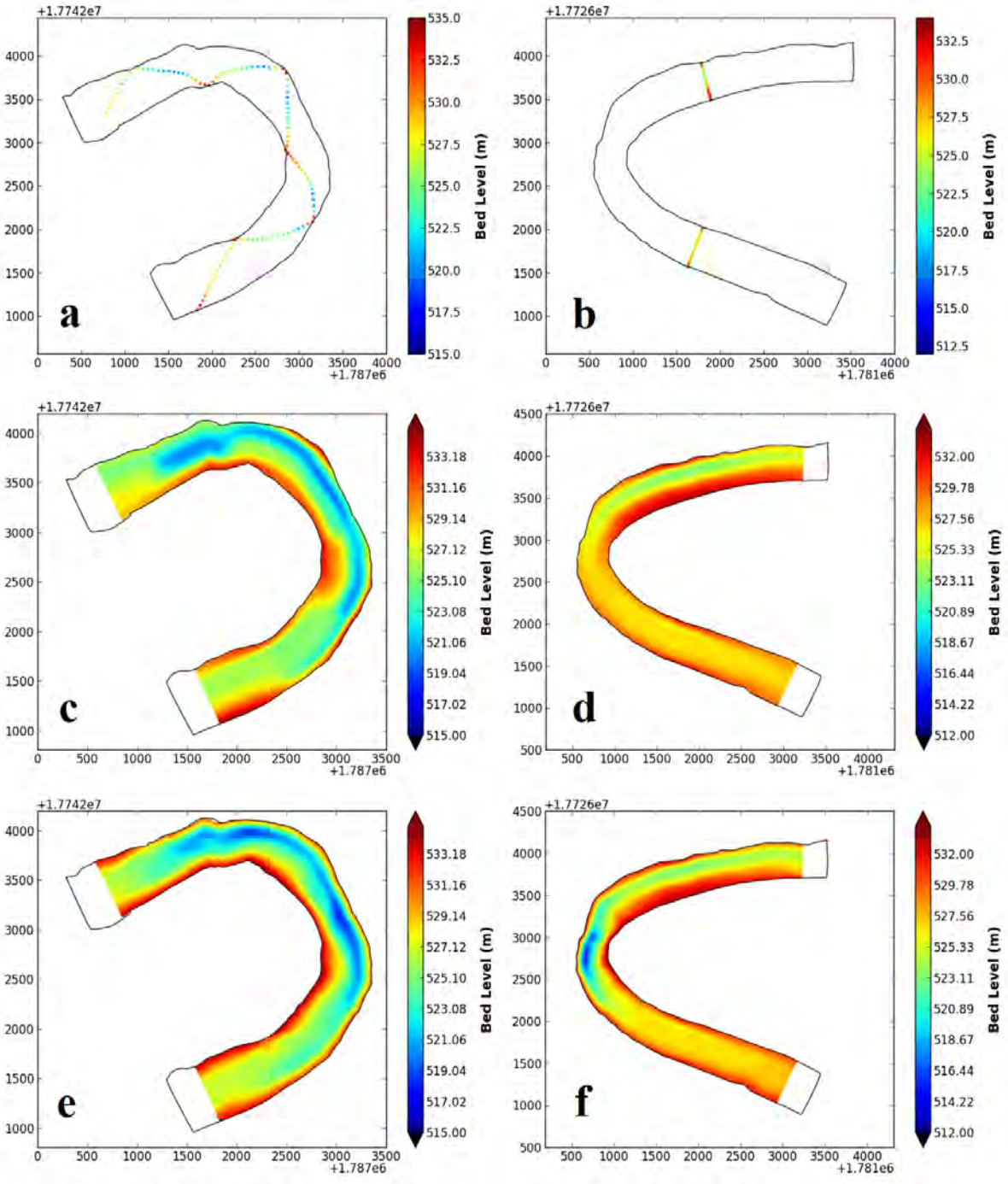

Figure 5.18. Kootenai river bends successful predictions by fusion method: (a,b) Tested datasets (tracklines: 0.14% data, cross-sections: 2, or 0.04% data), (c,d) EIDW partially failing result, (e,f) fusion result (EIDW and model).

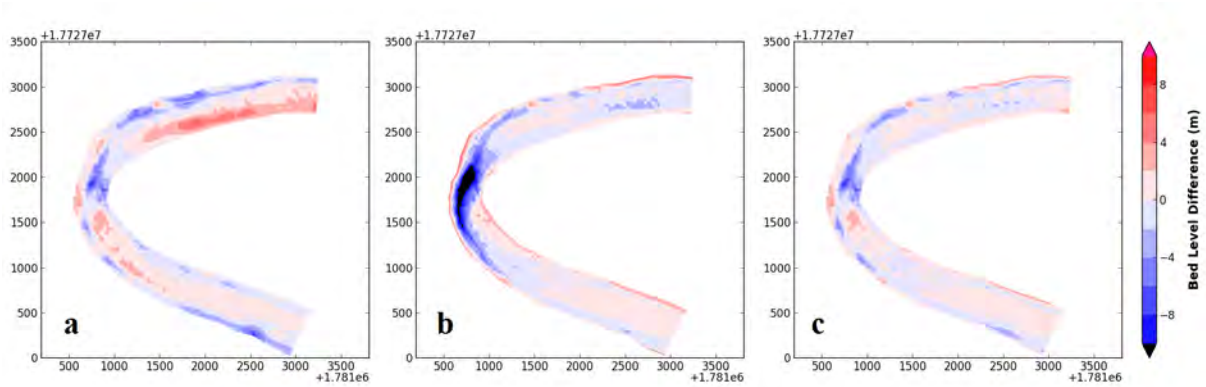

Figure 5.19. Error Maps for Kootenai #2, of 2 cross-sections as Test dataset (Figure 5.18 b): (a) Physics-based Model difference, (b) EIDW difference, (c) Fusion method difference.

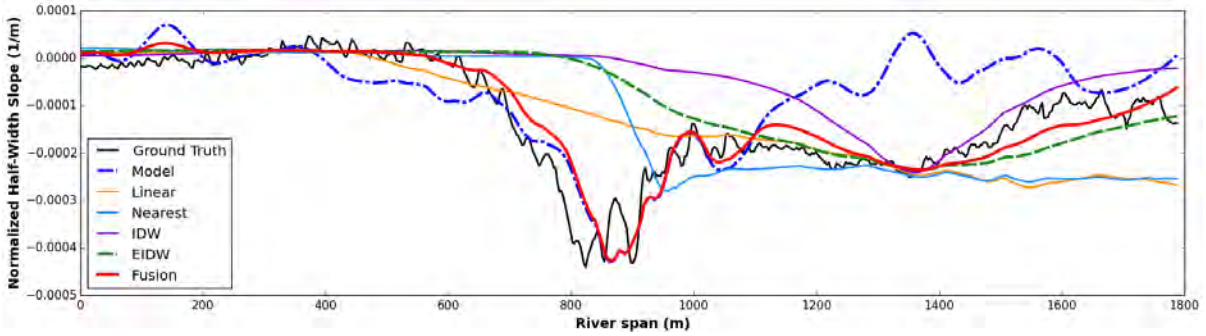

Figure 5.20. NHWS for Kootenai #2, with 2 sample cross-sections (Figure 5.18 b). All methods.

5.3 IJssel – Results

IJssel is a river affected by the human interference. In general, it holds very little variations in widths, but the chosen bends have a large difference in average channel width because of their far-apart locations. One of them lies north close to Zwolle where the river is wider (average width: 143 m) and the other to the south close to the beginning of the IJssel near the branching of the Nederrijn (average width: 80 m). It should be noted that although mediated in numbers by the initial choice selection, wherever present, groynes' and dikes' artefacts of local pools are impossible to simulate correctly, only partially. Neither the model nor the interpolation methods can capture the specific formation of these pools [Figure 5.21]. However, the general estimate is closer to the expected deepening of the outer bends. Furthermore, dune formations are of course not detectable both due to the model's assumptions and due to little data available for interpolation. The subsequent smoothing also erases any sharp detected areas.

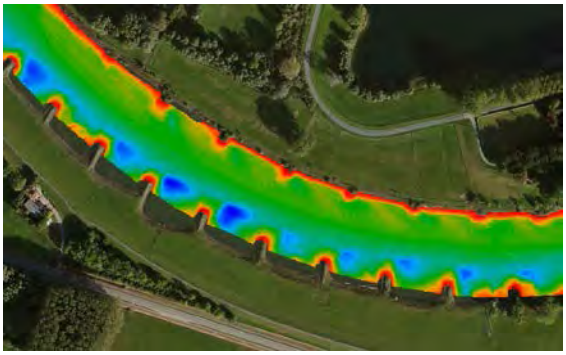

Figure 5.21. Interference of groynes at riverbed morphology, IJssel (Bing maps).

Larger spans of the river were chosen for the IJssel cases, therefore a higher number of cross-sections was tested (11 to 4 cross-sections). For IJssel bend #1 (North) the RMSE results in Figure 5.22 hold a similarity to the ones detected in Kootenai rivers, with EIDW and Linear interpolations showing very close patterns, but the Fusion method outperforms both for scarce data of less than 11 cross-sections (0.37% data coverage). This corresponds to cross-section spacing distances of more than 385 m. On the other hand, the southern bend of IJssel #2 presents a more linear display of features [Figure 5.23]. This can be attributed to the smaller average width of the channel and the higher water flow, and can also relate to its low curvature ratio. As a subsequence, the Linear interpolation is the most beneficial choice in terms of RMSE, although with little differences from the fused results. Without loss of generality of the foregoing, the fusion method could use instead of the EIDW, the results of the Linear computations to reach a better approximation in cases as these. Contradictorily, IDW fails in this case because of the large gaps between the cross-sections and the lack of any anisotropic considerations.

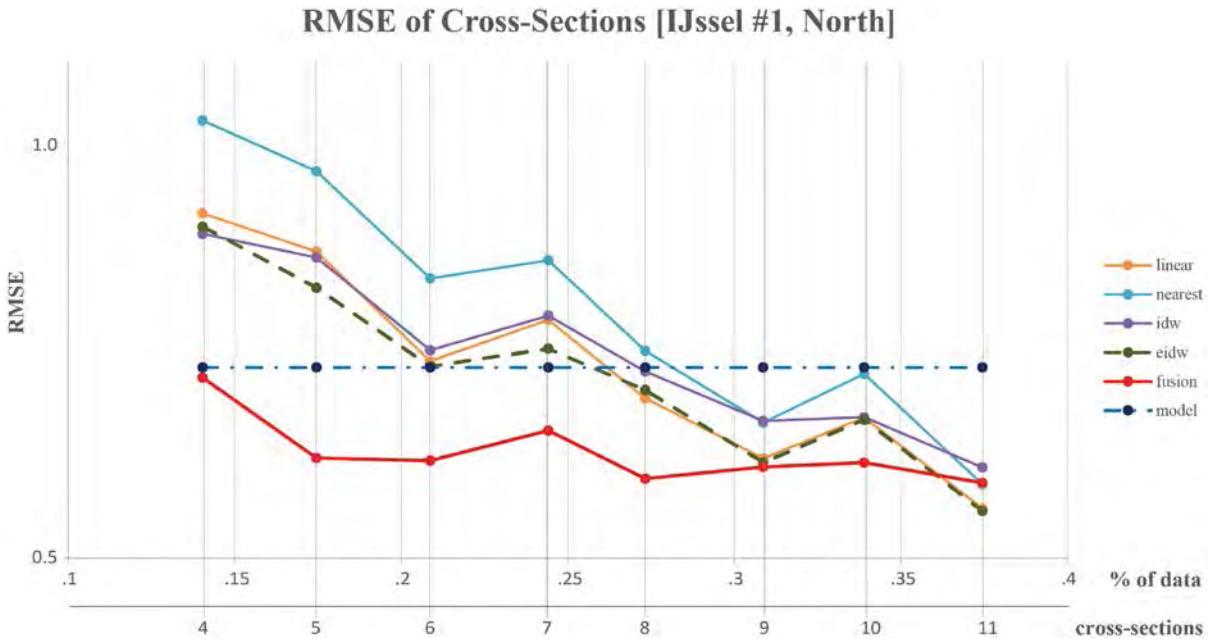

Figure 5.22. RMSE values for cross-sectional Test datasets for IJssel #1.

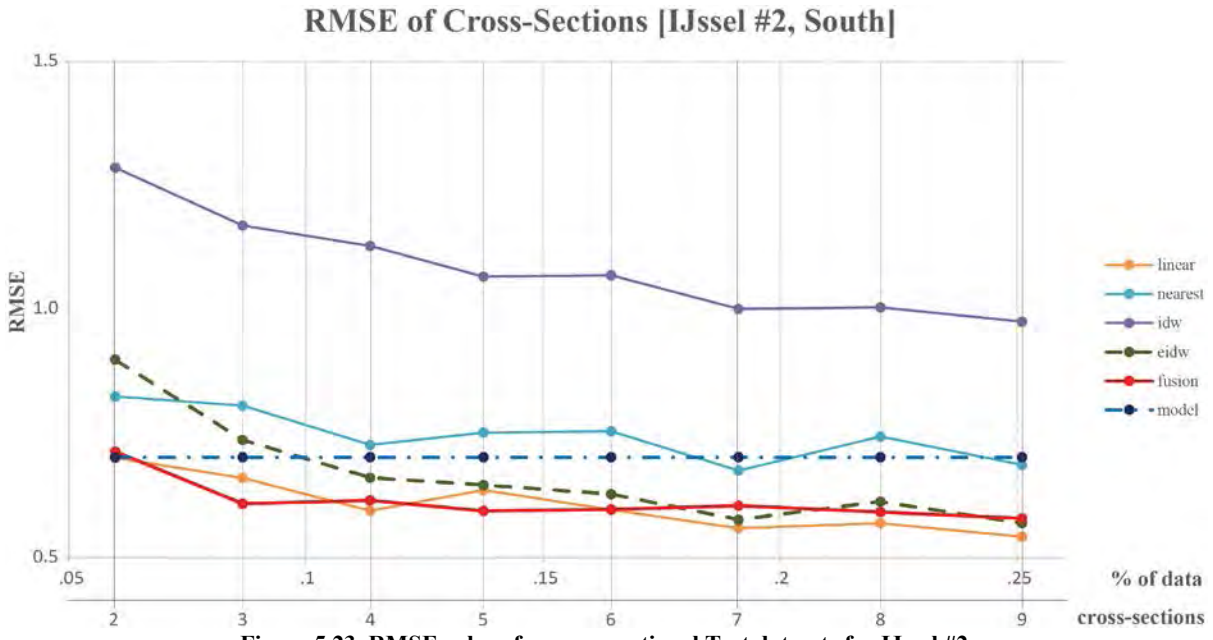

Figure 5.23. RMSE values for cross-sectional Test datasets for IJssel #2.

When the sampled data have a trackline pattern, there lies a certain distinction again between IDW / Nearest Neighbour and EIDW / Linear spatial interpolations. The first two are failing for the same reasons as mentioned in the Kootenai cases in § 5.2. The other two are interchanging in RMSE response, yet being very close in their values. As such, the fused results do not bear a much different profile, outperforming the rest only in scarcer dataset cases of IJssel #1 [Figure 5.24]. For IJssel #2 [Figure 5.25], the linear features of the bend match better to the EIDW results for denser samples, mainly due to the 'zig-zag' pattern of them. However, because of the bad general result from the model's estimations, the fusion method's output is not managing to outperform the rest. In general for the IJssel cases, the trackline Test dataset RMSE values are not better than the ones of the cross-sectional ones for a similar amount of data.

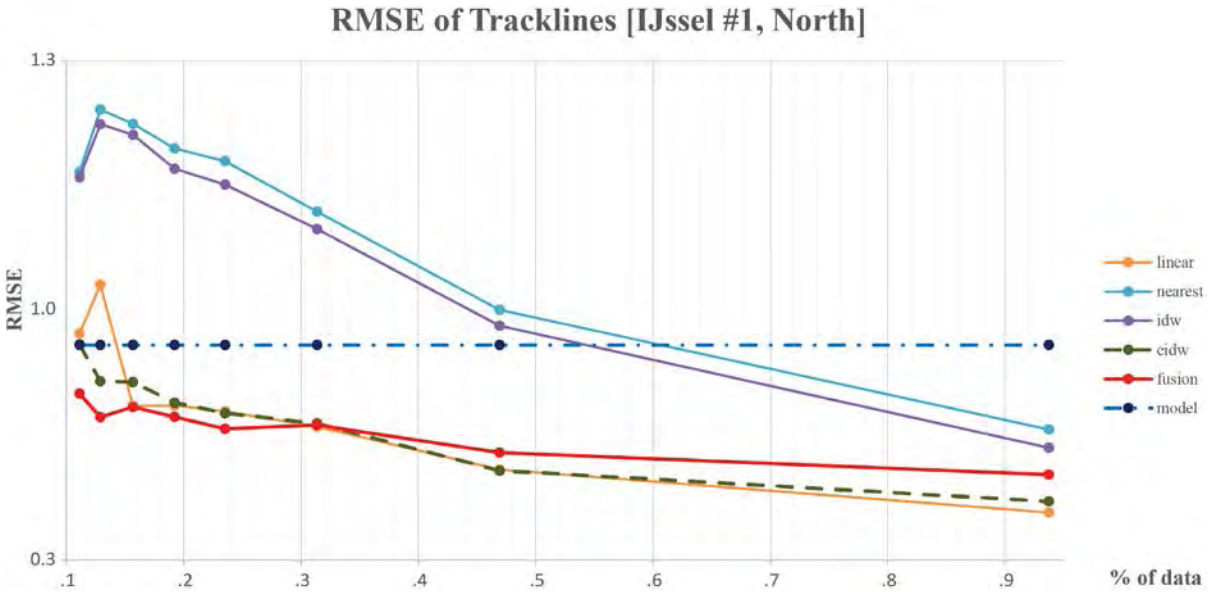

Figure 5.24. RMSE values for tracklines Test datasets for IJssel #1.

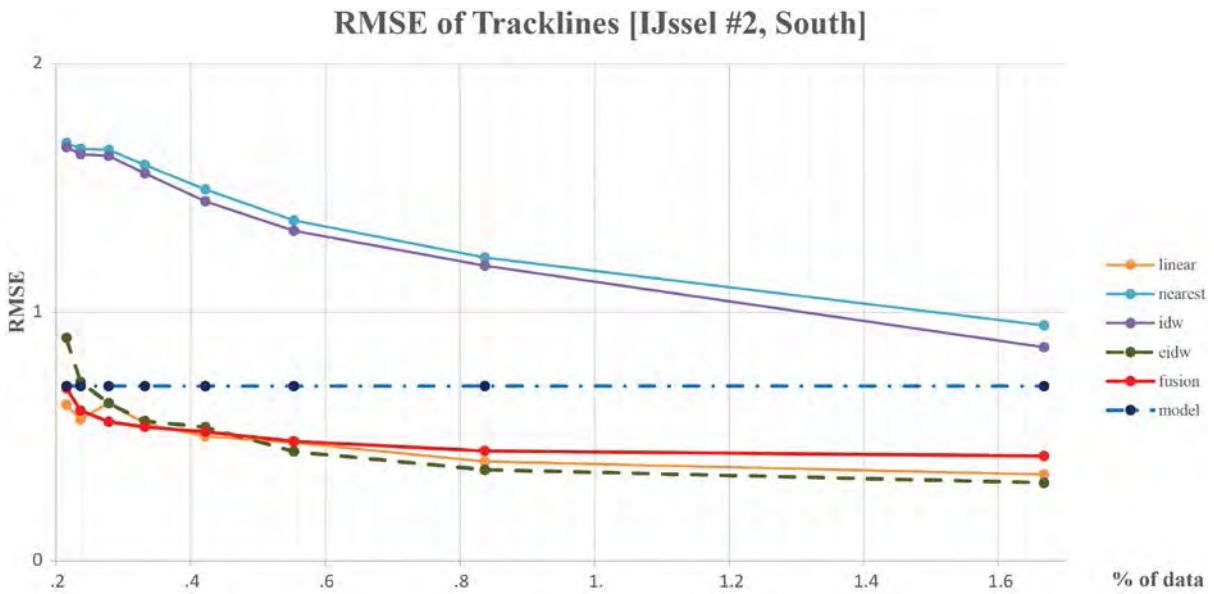

Figure 5.25. RMSE values for tracklines Test datasets for IJssel #2.

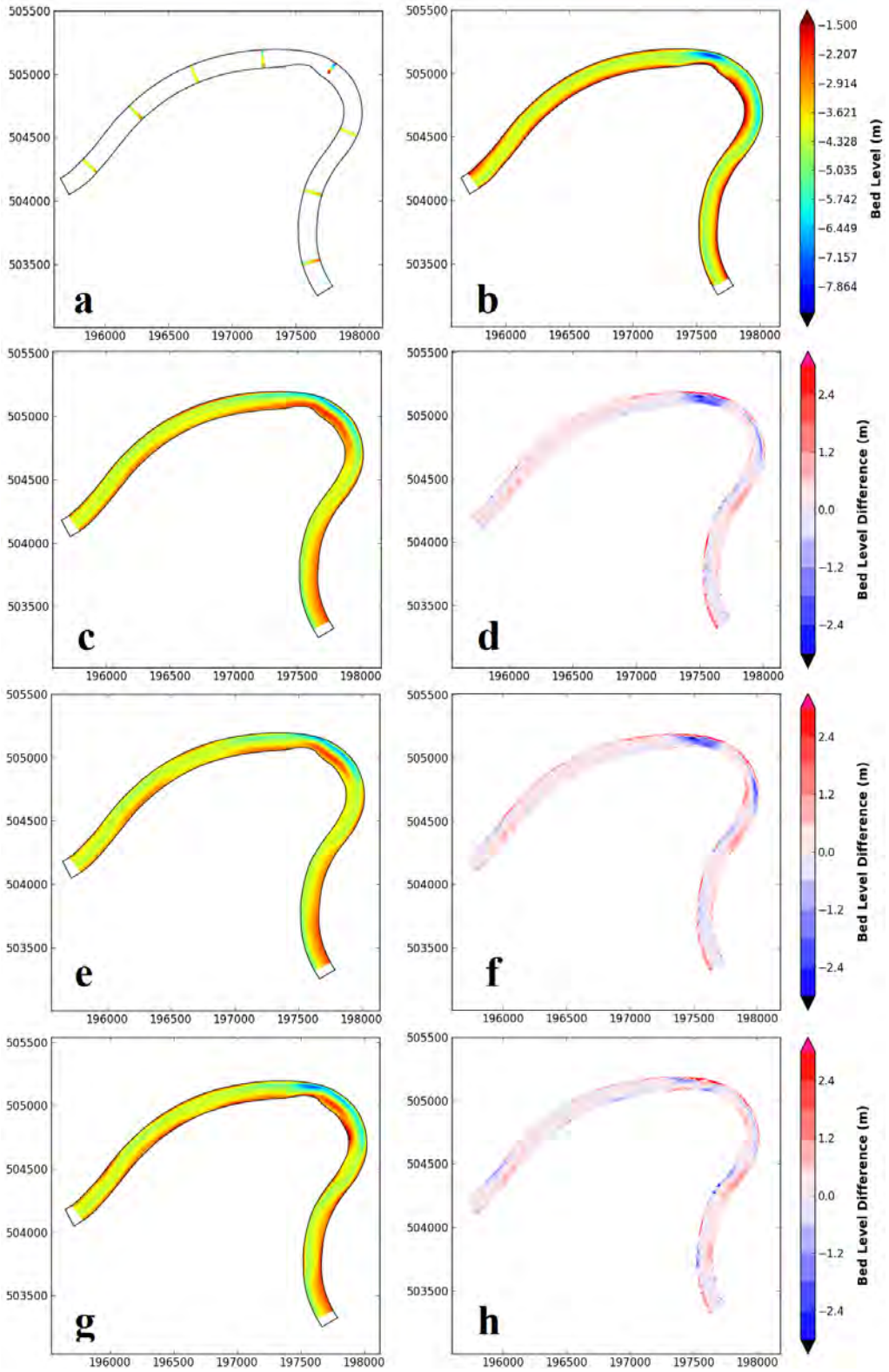

Figure 5.26. IJssel #1 computed bed levels for cross-sectional Test data: (a)Test dataset (8 cross-sections, 0.27% data coverage), (b)Physics-based model riverbed topography, (c,d) Linear interpolation and error map, (e,f) EIDW and error map, (g,h) Fusion method and error map.

In all of the RMSE graphs shown, the responses are similar for the EIDW, Linear interpolations and the fusion method, except in IJssel #1 for cross-sectional Test data, where the proposed method performs best. In Figure 5.26, for 8 cross-sections, the two spatial interpolation methods are displaying similar features, but at the same time failing at the bend's topography estimation. With the fusion method some parts are better reconstructed and the overall result shows less of differences on the corresponding error map. This is also reflected in Figure 5.27 of the NHWS, the slope from the Linear interpolation is also performing well. On the graph, the existence of some wrong peaks and troughs of the physics-based model's estimations are most probably a result of missing the "lag" factor estimation from the model. This factor is based on the assumption that certain features along the water flow of the river tend to appear later than expected by the model's equations. This can be viewed for example in between about 1750-2250 m of the channel's span.

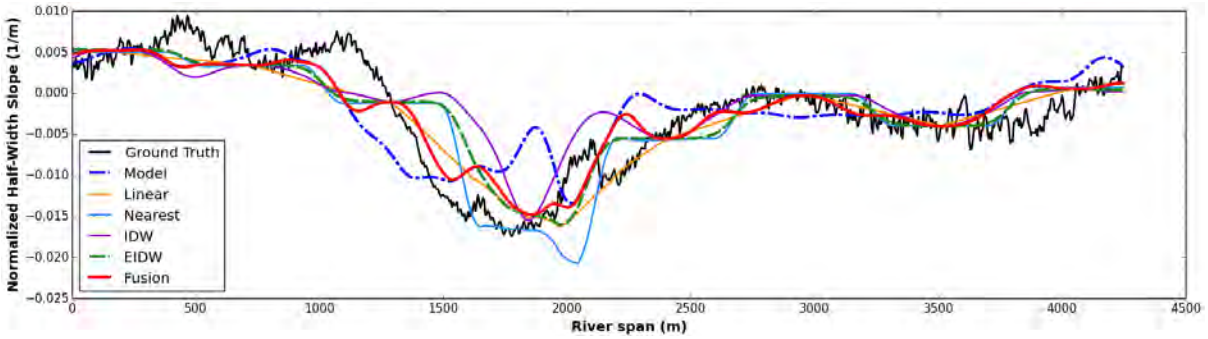

Figure 5.27. NHWS for IJssel #1, with 8 sample cross-sections (Figure 5.26 a). All methods.

On the contrary, the results of the IJssel #2 show an appeal towards the linear interpolated output. As mentioned above, this is probably because of the relatively straighter planform style of little curvature for that part of the IJssel and because of the stronger currents running though such smaller widths. In Figure 5.29, although small the differences, a better performance by the Linear interpolation can be viewed. The main errors of the fusion method can be attributed mostly to the physics-based model. This can be cross-checked in Figure 5.28 of the NHWS, where the "lag" effect is again visible along the whole span of the channel.

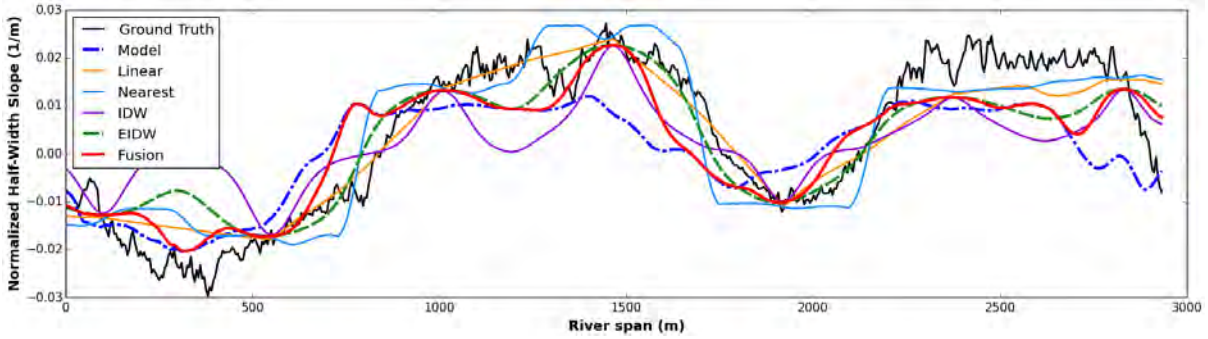

Figure 5.28. NHWS for IJssel #2, with 7 sample cross-sections (Figure 5.29 a). All methods.

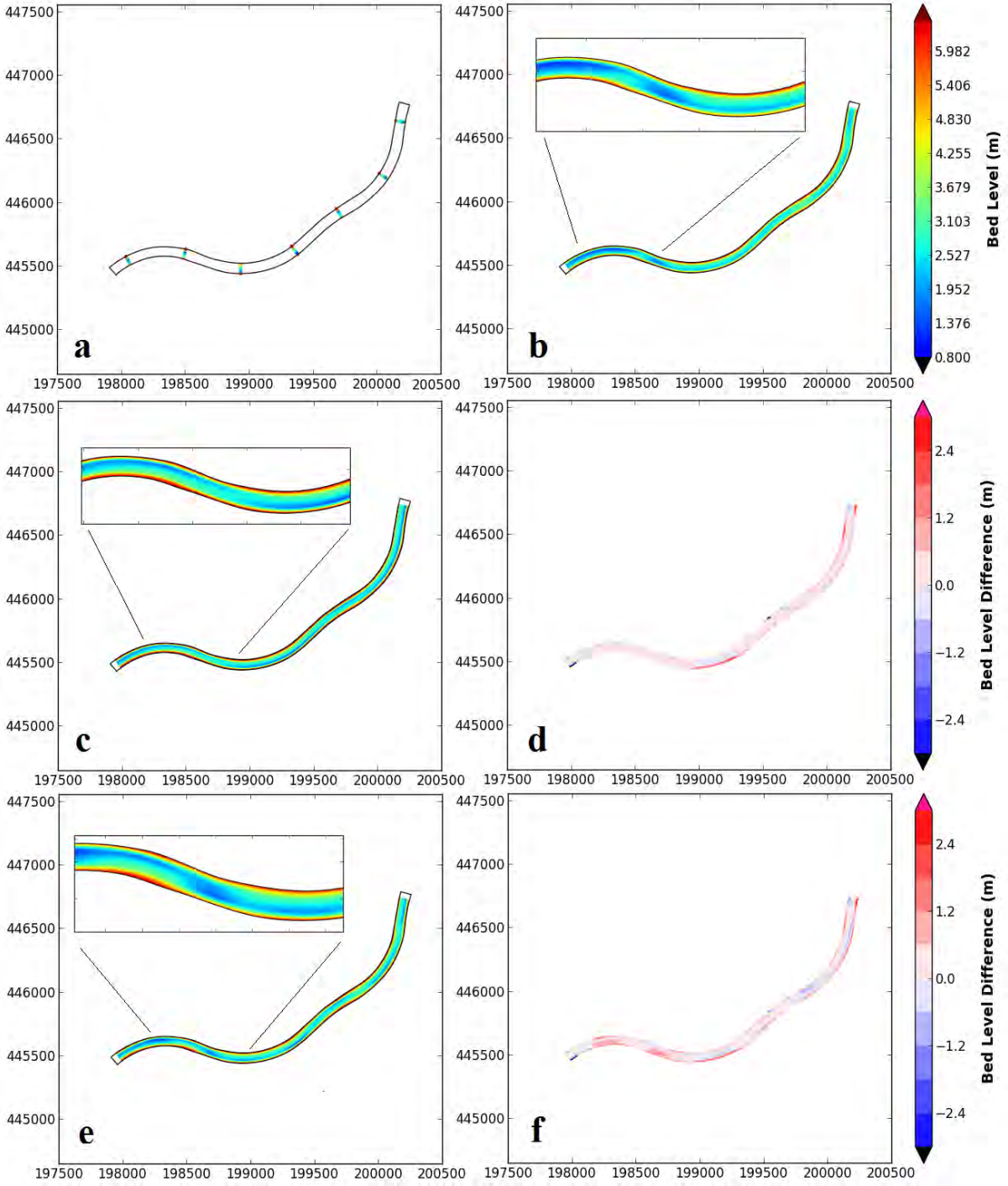

Figure 5.29. IJssel #2 computed bed levels for cross-sectional Test data: (a)Test dataset (7 cross-sections, 0.19% data coverage), (b)Physics-based model r iverbed t opography, (c,d) L inear i nterpolation a nd e rror map, (e,f) F usion method and error map.

5.4 Danube – Results

In the final study case, two areas close to the bifurcations in south and north of Borcea were chosen. The initial available data were in singlebeam form, random tracklines and cross-sections merged together in one dataset. In order to extract Test datasets, manual operations commenced. However, the data were not dense enough to have either cross-sections at regular distances or specific sinuous tracklines. Furthermore, since the whole of the riverbed was not covered, no "full" ground-truth dataset covered the whole extent of the grid. Nevertheless, the whole of the single-beam dataset is assumed to be the ground-truth dataset. A precise comparison cannot be made in terms of RMSE or inspecting the NHWS, but to the best possible extent, a discussion is made.

In the north, the Danube bend #1 has little available data [Figure 5.10]. From that only 2 Test datasets were able to be extracted; one of 9 cross-sections and one trackline dataset [Figure 5.30, Figure 5.31]. In both cases, the interpolated results are showing some extensive smoothed-out results. This is most obvious in the cross-sectional case where there is a large gap between two consecutive cross-sections. The fusion method's results are more natural-looking, with various gaps filled with predicted erosion/sedimentation patterns.

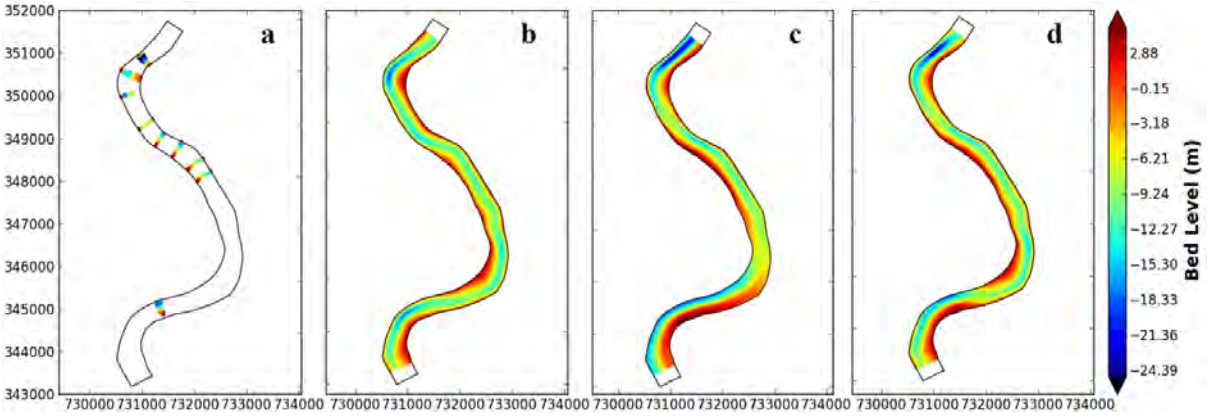

Figure 5.30. Danube #1 interpolation and fusion method results for cross-sectional Test dataset: (a) Test dataset, (b) model riverbed topography, (c) EIDW result, (d) fusion method result (EIDW and model).

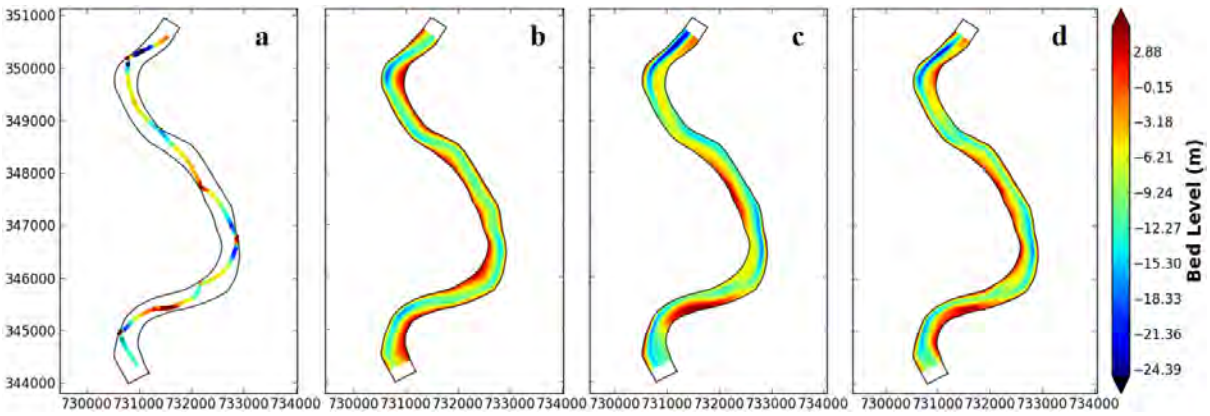

Figure 5.31. Danube #1 interpolation and fusion method results for trackline Test dataset: (a) Test dataset, (b) model riverbed topography, (c) EIDW result, (d) fusion method result (EIDW and model).

However, the above results could also be misleading. In order to view a more accurate representation of the river, all of the available data [Figure 5.10] are used for interpolation. The resulting EIDW dataset [Figure 5.32 a] shows some slightly unexpected patterns of "lag" effects, especially in the southern part. These would not be able to be assumed by the physics-based model, but once combined, the fused dataset displays a more "natural" look for rivers [Figure 5.32 b]. Because of the method's processes, some minor artefacts are inescapable.

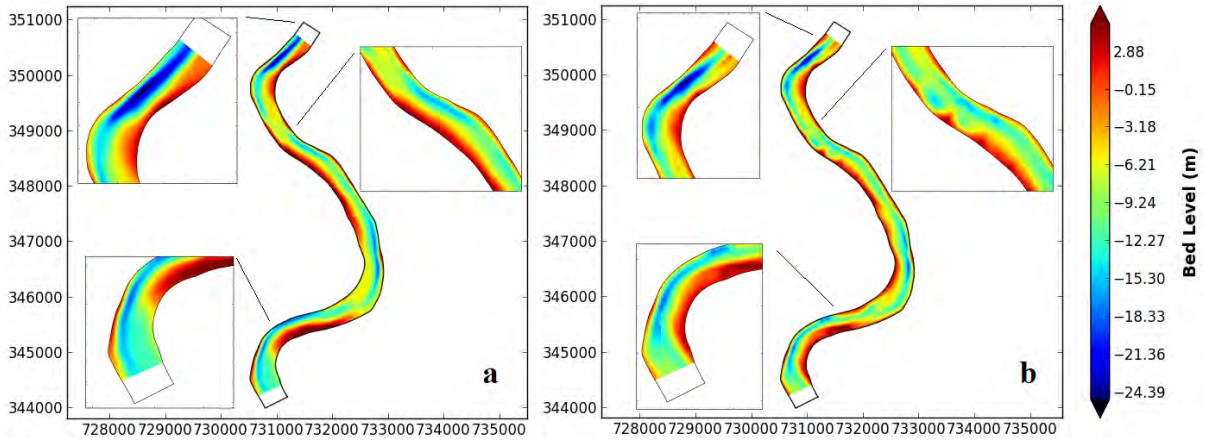

Figure 5.32. Danube #1 interpolated and fused datasets using the full single-beam dataset available: (a) EIDW, with smoothed-out riverbed estimations, (b) Fused method results, with some artefacts in the middle of the channel.

For Danube River bend #2, a denser single-beam dataset was available. As such, 9 cross-sections and 1 trackline pattern were extracted. The 9 cross-sections were thinned down, with as much as possible regular spacing between the remaining ones each time. The respective RMSE results [Figure 5.33] show a better output for the fused method for less than 5 cross-sections, corresponding to a large spacing of 1300 m. This can be attributed to the small curvature ratio of the channel, but also to the fact that again the lag effects on river morphology are present.

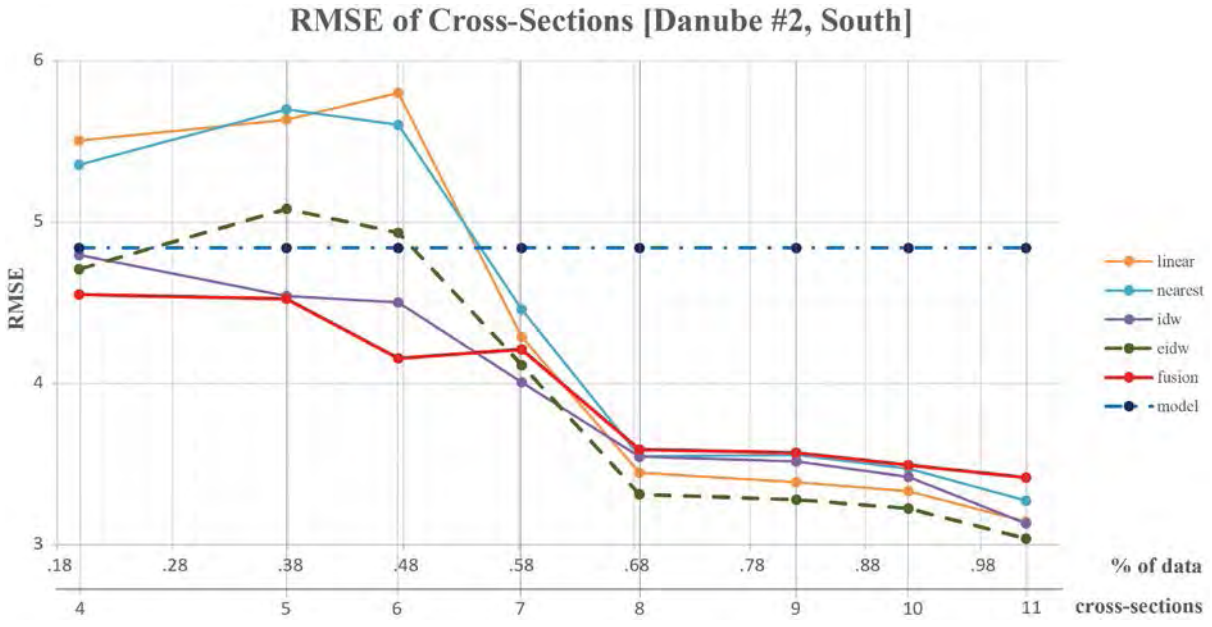

Figure 5.33. RMSE values for cross-sectional Test datasets for Danube #2.

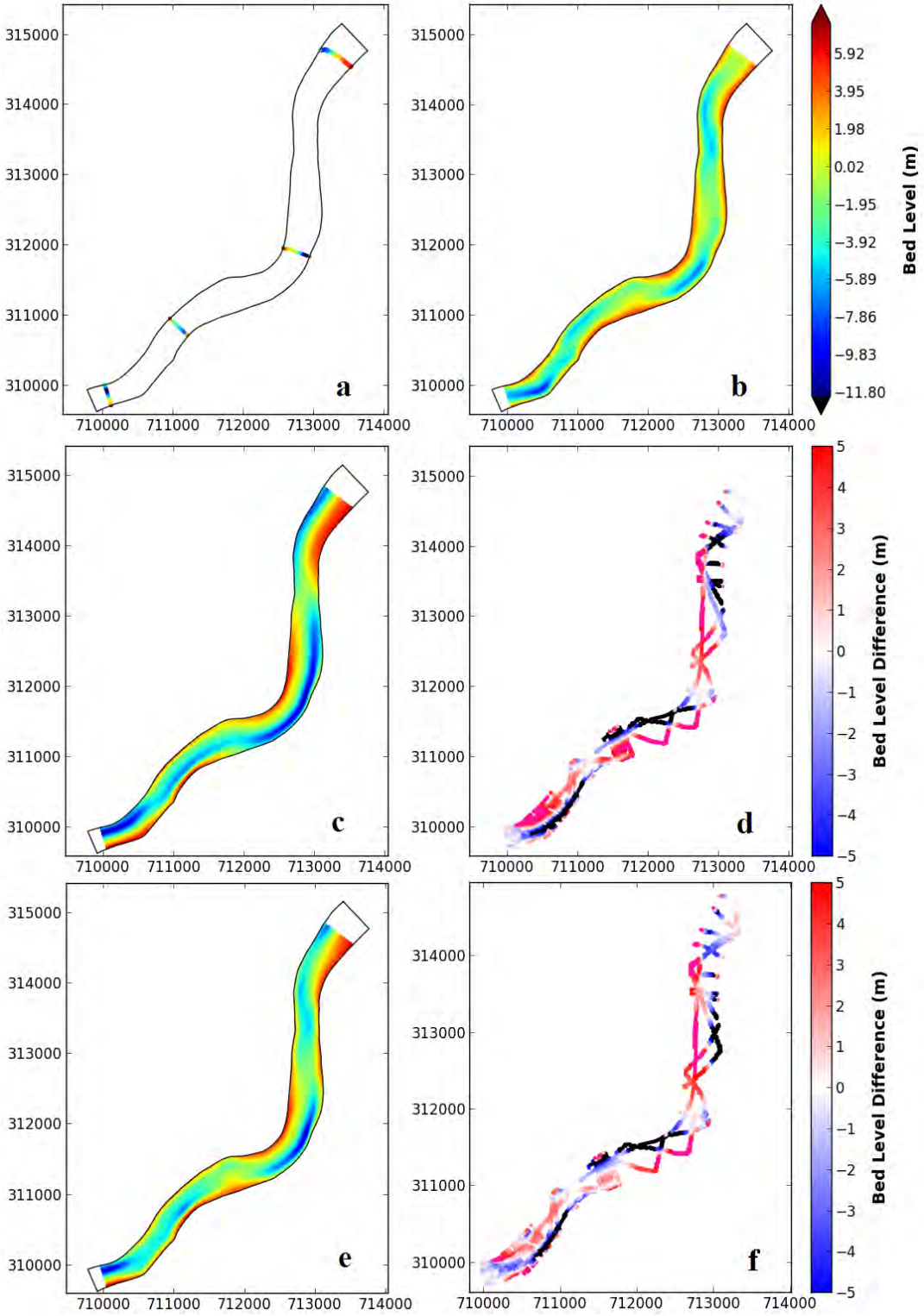

Figure 5.34. Danube #2 computed bed levels for cross-sectional Test data: (a) Test dataset (4 cross-sections, 0.48% data coverage), (b) Physics-based model, (c,d) EIDW and error map, (e,f) Fusion method and error map.

In such cases with limited data, the error maps can only show the difference of results for the points available [Figure 5.34 d,f]. In both the EIDW and the fused output, the depths are quite deviating from the ground-truth, but in the latter one less so. A few overestimated depths of EIDW (pink-colored points) are brought to more normal levels in the fused method. However, the underestimated parts (black points) do not have a better response.

Again, by using the full data coverage of the area [Figure 5.11], a better representation of what is the expected outcome can be retrieved [Figure 5.35]. There is again a definite lagging in the morphology of the river, which cannot be captured by the model, resulting in an intermediate outcome, which although might look more natural, it can have various shifting morphological artefacts.

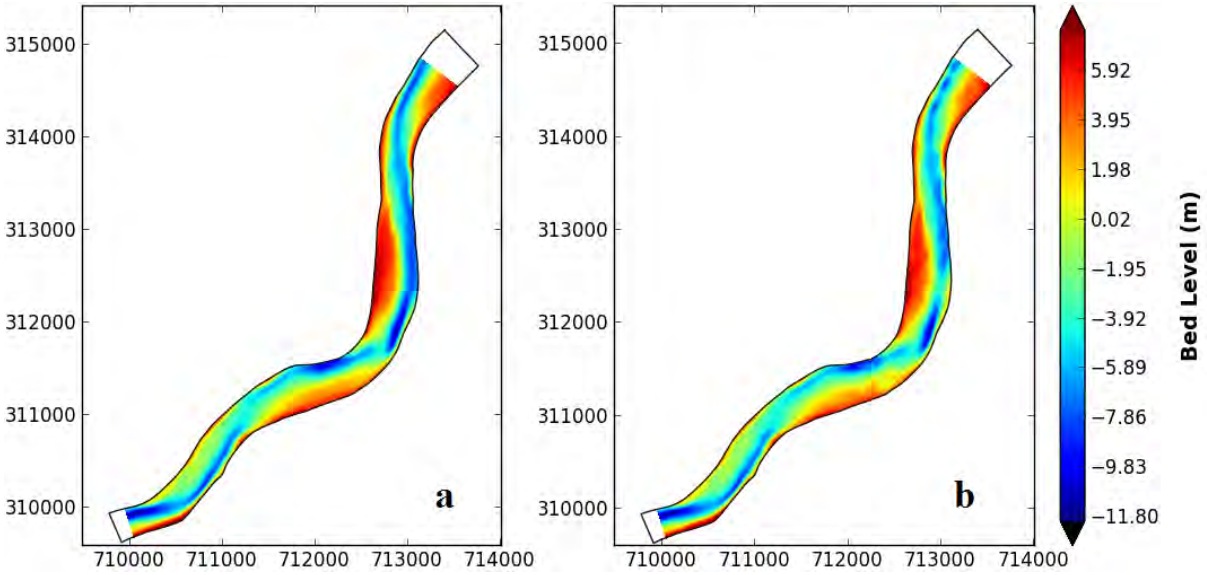

Figure 5.35. Danube #2 interpolated and fused datasets using the full single-beam dataset available: (a) EIDW, with smoothened-out riverbed estimations, (b) Fused method results, with some artefacts in the north part of the channel.

5.5 Summary of Results

The experiments performed involved river channels of different extents and with different types of sampled data, cross-sections and tracklines. The fusion method is composed of the weighted sum of EIDW interpolation and physics-based model results. Interestingly, in the cases of scarcer data, the fusion method outperformed the spatial interpolation methods and the physics-based model predictions. That was documented in the Ijssel and Kootenai rivers by RMSE values, visually inspected by error maps and by the general view of the NHWS along the channels' spans. For the Danube due to its limited ground-truth data, only one case could be assessed as such, whereas the rest were mainly visually inspected.

In relation to the RMSE graphs, any inconsistency in the trend as the data are thinned is to be attributed to the differences of the sampled regions. During the data thinning, same areas are not always sampled. Therefore, in some cases various unexpected morphological features are missed out, whereas in others they are included. If they cannot be reproduced by the physics-based model, they are totally omitted resulting in a general bad prediction by the fusion method. These irregularities can

cause the “jumps” in the graphs, evident in Figure 5.15 and Figure 5.16. The basic conclusion from this is that where data is gathered matters for both interpolation and subsequently fusion methods.

It was further noted that EIDW and Linear interpolations displayed better results than IDW and Nearest Neighbour interpolations, especially in the cases of trackline Test data [Figure 5.13, Figure 5.14, Figure 5.16, Figure 5.17, Figure 5.19, Figure 5.20, Figure 5.22, Figure 5.24, Figure 5.26]. That can probably be attributed to the spatial dependency of morphological features happening along the longitudinal direction in rivers. EIDW accounts for it by introducing the anisotropy factor and Linear interpolation for its directional implementation in the flow-oriented system. In fact, Linear interpolation was reported to be equally good or better than the fusion method for a tested straighter bend [Figure 5.23, Figure 5.25, Figure 5.28, Figure 5.29].

Additional differences can be noticed in between the two different types of datasets. Cross-sectional Test data can be thinned and preserve regular distances. Trackline Test data are more difficult to have regular thinning in size. Therefore, larger differences exist in the RMSE graphs. Due to the variations of data samples in between the thinning process, it was not easy to define specific percentage thresholds of data scarcity below which the fusion method performs the best.

Error maps were able to display specific regions on a river channel where predictions stated over- or under-estimations [Figure 5.19, Figure 5.26, Figure 5.29, Figure 5.34]. Even though the model’s predictions and EIDW results had obvious areas of problematic output, the fusion method allowed them to complement each other and the final error map had such areas reduced.

Because the fusion method is a result of the merged datasets of the physics-based model and EIDW outputs, the fusion’s NHWS varies between the two others. In some cases it was clear that the fusion’s result was following closer the ground-truth’s slopes along the river span [Figure 5.20]. However, quite often [Figure 5.28] it is ambiguous which method performs better according to this measure, which is why it must be used with care.

6 Conclusions and Recommendations

In this thesis, the problematic case of limited availability of bed topography data in rivers has been researched, focusing on meandering alluvial river channels. To deal with such "scarce" data, a method has been proposed which makes use of a physics-based model and spatial interpolation results, combining them to a complete solution. This solution can bear a more thorough and more natural representation of the riverbed topography than the smoothed-out results of interpolation methods. In addition to it, a number of steps have been presented, during which the overall implementation process has been elaborated on.

The knowledge gained from the research performed and the implementation results is divided into four subsections. First, conclusions are drawn (§6.1), with remarks concerning the field of work and answers to the initial research questions. What follows is a discussion on the limitations of the overall procedure (§6.2) and afterwards recommendations of use of the method in its current state are given (§6.3). Finally, closure is given by proposals for future work on the field of study (§6.4).

6.1 Conclusions

6.1.1 Conclusive Remarks

The most important remarks drawn from the research and experiments performed are the following:

- spatial interpolation techniques in river channels can fail when the available data are scarce or a natural trend exists in the riverbed (§2.2, §5.2, §5.4)
- a water-flow direction based interpolation can bear significantly better results (§4.6)
- anisotropy plays an important role in the bathymetric variability of river channels and bends (§4.6, §5.2 to 5.4)
- a physics-based model, even if simplified in its description, can help interpolation results reach a better outcome (§5.2 to 5.4)
- morphological lag effects in riverbed topography cannot be represented by the zero-order, axi-symmetric physics-based model (§5.4)
- smoothing operations are required to average out natural bed level variations at a smaller scale (§4.5, §4.6)

It has been shown that the case of scarce datasets can be a significant diminishing factor in the performance of spatial interpolation methods. The general fact is that with less data, unreliable estimates are retrieved, regardless of the interpolation method. Scarce trackline and cross-sectional data bear also a specific pattern, which does not allow for geostatistical interpolation techniques like Kriging to reach an acceptable estimation. Deterministic techniques like Natural Neighbour also outputs overly generalized results, whereas the ones by Thin Plate Splines may result in over or under-estimated representations. The methods tested in the thesis (Linear, Nearest Neighbour, IDW,

and EIDW) bear a higher relation to the spatial dependence of the data and distances between them and are therefore more preferable.

Concerning the flow directional dependence of data, rectangular Cartesian coordinates do not define a river channel's boundaries in the correct manner. Therefore, the direction followed by the main water flow can dictate a boundary-fitted curvilinear coordinate system to base the interpolation upon. To structure this in an applicable manner, a centerline to the river's polygon is drawn to describe the direction and a curvilinear grid is constructed upon which the interpolation is performed.

Furthermore, due to the natural processes issued by the water flow in channels and bends, the morphological features of the riverbed have a greater correlation along the water flow than transverse to it. This anisotropic dependence can influence the choice of interpolation. It has been shown that methods like EIDW and Linear interpolations can give a more accurate result, especially in the case of scarce data. Even more so, when the sampled scarce dataset has a trackline pattern, IDW and Nearest Neighbour are failing in their predictions, rendering their usage not recommended for scarce data.

Some natural features undetectable by spatial interpolation methods can be predicted by physics-based models, even if the underlying assumptions allow for a simplified one. In this thesis such simplified model is used to combine with the interpolated results. Additionally, bank-line profiles were used to cover the areas where the model equations cannot formulate the riverbed close to river banks.

However, space lag effects may be existent in parts of the river channels, especially close to bends or alternating bars regions. They affect the riverbed topography, changing the expected location of morphological patterns. As such, a simplified physics-based model that does not account for them, such as the one used in this thesis, cannot predict the correct topography in cases where the lag effects are evident. Therefore, higher levels of modelling are required.

Finally, smoothing has been proven to be an important consideration in acquiring a unified representation. In the transverse direction, it can allow for a better cross-sectional portrayal of the model's results, whereas in the longitudinal direction it can help interpolations without anisotropic considerations (i.e. IDW, Nearest Neighbour) reach a better estimation. However, it would require some further research insight to be able to define the correct smoothing method or degree of window smoothing. In addition, smoothing of the bed topography is generally dependent on its geology and sediment types present. Even if the general classification a river channel labels it as alluvial, there are variations to be considered while smoothing.

6.1.2 Answers to Research Questions

The main research question governing the thesis has been formulated in §1.6 as follows:

> *"How can a spatial interpolation method be coupled with river morphology physics in order to approximate better the riverbed topography when input data are scarce?"*

The answer to this question is the "fusion" method as described in §4.7. The fusion method is proposed to combine the datasets resulting from a spatial interpolation (EIDW) with the physics-based model riverbed topography result. In context with the research question stated above, the river morphology physics are incorporated by the use of two equations describing the water depth at the centerline (zero-order solution, Eq. 4.1) and the cross-sectional variations from it (axi-symmetric solution, Eq. 4.5). The spatial interpolation chosen to be used for the combination is EIDW, because it abides to the anisotropic expectations for river morphology and gives a more natural representation

devoid of artefacts compared to the other methods considered. Scarce data have the form of either tracklines or cross-sections. As such, in order to create a relation between the two datasets and the known data, the concept of weighting distances is brought forth. The further away an unknown point lies to a sampled point, the more the model's result for that location is considered. Vice versa, the closer an unknown point is to a sampled point, the more the interpolated result is considered. This concept is formulated in terms of weights in the range of [0,1] to apply to the two datasets results (Eq. 4.6). In the case of cross-sections the weighting is applied as a membership function (Eq. 4.7), whereas for trackline datasets the weights are acquired as fractions of distances from a threshold maximum distance (Eq. 4.8). The method is therefore named as "fusion" method because of combining the two datasets.

Along with the main research question, three more sub-questions have been posed for completeness:

1. *What is an objective function to measure 'goodness-of-fit' of the method?*

In order for the method to be evaluated, three ways of measuring the results have been presented. RMSE of the overall result has been chosen as a numerical evaluator, error maps are used for a visual qualitative assessment and the Normalized Half-Width Slope (NHWS) of the transverse cross-sections gives further insight into what happens along the longitudinal direction of the channels, targeted to the areas of interest. From the experimental results, the conclusions vary. RMSE can be arguably the most objective evaluator, since it is a measure that punishes both systematic error and error variance. In every case, it provides a single number that is scale dependent, but it allows a comparison in between the different prediction methods that are under evaluation. However, this measure can have a value that is smaller (better) for a result that in overall has a good response, but in a specific area of interest (i.e. a bend) the prediction fails. This is not notable by a single number, and as such not always desirable. That is why the more qualitative measure of error maps is deployed. With them, the depiction of problematic areas for the method's predictions can be easier to detect, however it relies on the evaluation by the spectator and does not provide a clear overall and objective result. The NHWS can partially give an understanding of the predicted result on a more centralized area of a river channel. The graph displays how well the predicted results' cross-sectional slopes follow the ground-truth ones, locating the areas of wrong predictions. However, it also cannot give a general statement for the state of the prediction. Based on the above, although the best course of action for each case would be to investigate all three evaluators, the more objective one and the one that should be considered at least as first definitive assessment is the RMSE value.

2. *What coordinate system allows for better predictions on riverbed topography?*

As shown in §4.6 and based on [*Merwade et al. 2006*], interpolation in the Cartesian field (x,y) for river environments is a wrong course of action. The boundaries given by the river's banklines direct the bathymetric variability and therefore the depth values. An assumption of equal value dispersion in the Cartesian plane is wrong. Therefore, a water flow-oriented system (s,n) is used. The assumption that governs its definition is that the main water flow direction that shapes the river itself can be approximated by the centerline of the river polygon. The flow-oriented coordinate system defines the data points on a plane that has corrected directional dependences and is fit for performing spatial interpolation methods. What was further noted is that the significance of using such a system is even higher with scarce data. Some data that lie closer in the Cartesian plane could actually be much further apart in the flow-oriented system and with scarce data, the interpolated values could be influenced by data samples that would otherwise have a smaller impact.

3. How much of the full data can be thinned out and still have a successful outcome?

During the experiments, the data have been iteratively thinned out in terms of number of cross-sections per river bend or sinusoidal lengths for tracklines. This was not possible for the Danube case due to only partial coverage of the riverbed by the sampled data, but nevertheless some conclusions can be drawn. The general assumption that the more data available the better the interpolated result will be can fall short in cases such as rivers where there are feature shaping trends due to natural processes or geometric characteristic of the river. For example, a larger number of cross-sections does not necessarily guarantee a better prediction, if a certain local erosion or sedimentation pattern is not sampled. On the contrary, even 3 cross-sections in one bend can be enough, assuming that at least 1 of them is in the middle or a little downstream of the highest curvature area, depending on the test case. It has been shown [Figure 5.18, Figure 5.19] that even with extremely limited data the fusion method can succeed in its predictions. In all cases, test data of less than 1% of the full channel coverage were used as scarce data. The method could perform well even when less than 0.3% data were used. This is ambiguous to translate into a clear global number of cross-sections or trackline lengths. However, some definite understanding can be drawn about the relation between the density of the data collection and the location of them on a bend or straight part of the river.

6.2 Discussion on Limitations

By performing the procedure followed in Chapter 4 on an application level, the manual labour required for achieving a good riverbed representation is significantly reduced from a few weeks of expert work to a number of hours. A single running of the procedure itself is a matter of minutes, since the usual computational time was within 2 to 4 minutes. However, including the pre-processing of data and definition of datasets, that time would expand. Furthermore, the user still has the task to tweak and change each procedure's output to his or her liking in order to reach the best result possible. However there are some limitations that need to be considered and understood before applying the process and fusion method.

The research performed in this thesis involved a larger number of considerations other than the main product solution of the fusion method proposed. At first, the problem of describing the data on a flow-oriented coordinate system spawned the need for the construction of a curvilinear grid. To acquire it, the centerline problem was visited, where not a single definitive solution exists. The approximated centerline with the Voronoi method used in this thesis is subject to the number of points that describe the river polygon and the distances in between them. That is the reason that the densification of the polygon geometry is required. If the user aims for an as perfect as possible centerline, the densification may result in a polygon with exceedingly large number of edge points and the subsequent Voronoi tessellation will demand higher computation times. A more graceful solution could be drawn from analysing the areas that require such densification.

The centerline is then used for constructing the curvilinear grid. The grid itself is an approximation of the river polygon and the way it is defined has a great impact on the representation and calculation of the whole method. The grid is the foundation of all processes taking place, like data aggregation, physics-based model bathymetry estimation, interpolation and evaluation. For the same river channel if a different grid is described, different outcomes may be drawn. This limitation poses an importance weight on describing the grid with a good resolution that fits the purposes of the user of the tool.

The physics-based model's prediction for the bathymetry is dependent on the hydrographical values inputted before calculation. Therefore, these values dictate the output. In this thesis, the assumption has been that these values are true and available from start. However, in the real world, some of them are difficult to be precisely described due to the ever-changing nature of rivers. It is proposed to advance these values with further investigation and theoretical considerations. As an example, in this thesis the Chézy roughness coefficient values have been chosen to alternate based on the local widths of the channels (Eq. 4.3). However, for much larger spans of rivers this measure could be misleading. An area or curve-based description of river parts could give a better conceptual answer to this issue.

Considering the experiments performed with spatial interpolation, it has been shown that IDW and Nearest Neighbour methods require extensive smoothing. Although the smoothing applied on the spatial interpolation results can be attributed to physical phenomena, the smoothing degree itself needs to be carefully inserted in order to not exceed the expected outcomes.

As far as the evaluation methods go, the NHWS poses some certain limitations in interpretation. In some cases, it can verify some outcomes or assumptions about the quality of the result, but quite often the response of the Linear interpolation would seem to be the most fitting result, especially with scarcer data or on straighter parts of rivers. This is to be expected, since the measure displayed relates to a best-fitting curve for cross-sectional data. A linearly interpolated result also has fewer variations and that allows for a smoother and seemingly less erred NHWS graph.

6.3 Recommendations for Use

Bearing in mind the limitations presented in the previous paragraph, some recommendations for use can be given regarding the method in its present form.

Firstly, it should be noted that the grid's resolution does not bear a hindrance in terms of running time. For the same stretches, no significant change in computation times was noted when a finer grid was used in comparison to a coarser one. The computations remained within a five-minute stretch. As such, it is recommended to use as fine grid as possible, close to the initial collected data resolution. However, it must also remain clear that since the experiments were performed on short spans of rivers, no clear conclusion can be made for running times for much larger stretches.

The physics-based model's results can be dependent on the extents of the bankline profiles chosen left and right on the grid. In a real-case scenario, the user would be able to manually assess the coverage of the scarce dataset; if the samples reach areas near the river banks, it is advised to take them into account and include the bankline profile choice. If the data are limited to more centralized parts of the river, the model should yield better predictions if the grid itself is adjusted to the data extents and these profiles are omitted.

Concerning the choice of spatial interpolation for the fusion method, in the overall described procedure in Chapter 4, EIDW was used. However, in cases where the river channel is relatively straight, it was shown that Linear interpolation can also have equally good or even better results. In such cases, it is advised that there is such change of choice based on the user's estimation. An automated distinction for which parts are straight and which are still curved is left for further research.

Concerning the fusion method, it can produce relatively stable outputs. The pattern of the sampled data however may vary. If the data are in clear, regular cross-sections, the automated calculation of weights is possible (§4.7.1). The more ambiguous case is when they are in trackline or even random

format. In these cases, the safest choice is to make an educated guess of the best distance threshold to be given (§4.7.2). The user defines as such from which distance and on the results of the interpolation are not to be trusted and the values opt for the model's calculations.

Finally, the study cases used in this thesis were just some smaller parts of larger river channels. The method itself can easily be used on larger stretches, however not ones that include bifurcations. Therefore only single channel stretches are recommended for use. Nevertheless, the user can still segment the river in parts and have a separate assessment for each of them.

6.4 Future Work

The overall process steps together with the fusion method proposed offer a complete way to mitigate the problem of data scarcity by combining interpolated and model results. There is still room though for further development. A number of topics are listed below, separated in further research to be made within the scope of this thesis and extended work beyond it.

6.4.1 Further Research

- **Validate Fusion method with more test cases.**

  Although a big number of tests were performed on the three chosen rivers, the method proposed would still require to be tested on an extended set of meandering alluvial rivers. These rivers could hold similar properties as the ones chosen here to validate the method further or vary in properties like width, length and curvature to extend the cases covered.

- **Implement the space lag factor in river bends.**

  It has been noted that in some river bends (i.e. Danube), there is a streamwise lag effect in the expected erosion and sedimentation patterns formed by the main water flow. This can be on a first level attributed to the geometric description of the meandering rivers, when there are multiple alternating bends in a short span of the river. This bears a problem, since the used physics-based model cannot predict such cases and if these areas are not sampled, interpolation also fails, leading to a subsequent bad estimation by the fusion method. A first simple recommendation would be to approach the issue from a geometric perspective and treat the water flow as particles. In this context, a ray-tracing algorithm can be applied, where vectors of expected water flow are defining the areas where the water particles "hit" and cause additional erosion. Areas devoid of these rays could be defined with smaller depths. The difficulty lies in defining the intensity or applied weights of this fix. Another recommendation would demand the use of a better described physics-based model. In [*Crosato 2008*] a steady-state situation is covered where the flow velocity adapts to depth variations with a certain spatial lag. An empirical space lag can also be assumed related to the curvature, like the kinematic meander models of [*Ferguson 1984, Howard 1984*].

- **Extend application to the whole river by piecewise implementation.**

  The method as is can be implemented on parts or areas of rivers. An extended implementation to a whole river stretch is not impossible though. It would require segmenting the river in specific

parts and by piecewise application all depths of the whole stretch of a river channel would be possible to be computed. However, bifurcations or cases with islands would require special treatment, mainly by redefining these areas by the grid basis.

- **Vary interpolation by semantically classifying river parts.**

Similar to the previous recommendation, the full river stretch could be segmented and classified by a certain geometrical or physical property. Then, based on that property, an automated choice could be made on which spatial interpolation to use for each segment. This property could be for example the curvature value, using Linear interpolation on straighter parts (small curvature) and EIDW close to bends (high curvature). The classification process however requires substantial research and possibly to consider the boundaries by fuzzy logics or perform customized interpolation at the boundary areas of the connecting parts.

- **Minimize cross-sectional data collection.**

A recommended course of action for the trackline data can be quite a difficult topic to assess. However some ideas in respect to the positioning of the cross-section data collection can minimize the number of the data required. Usually the areas of problematic or unexpected behaviour are closer to the sharper parts of channel bends. As such it is advised to focus the biggest number of cross-sections in these areas and only collect a few (1 or 2, depending on the river stretch) in straighter parts of the river. A first recommendation to automatize the assessment would be to classify the river by the local curvature ratio. Wherever the ratio is larger (mainly sharp bends and of smaller widths) the more cross-sections are required to have a better assessment.

6.4.2 Extended Work

Extending the project's scope one can reach a vast field for future work. An obvious first area of research would be to expand on the physics-based model's response with additional considerations such as non-linear effects, sharper bends, greater variations in widths and curvature, bifurcations and islands. Also a more scientific approach could be researched concerning the bankline profiles. A new complete model that would also assess these issues and also stay within logical limits of computations would be ideal for a rapid assessment and combination with the interpolated results.

Another way to approach the problem would be to implement the interpolation on an earlier level of computation within the physics-based model. The physics-based model's simplified equations could either be implemented as a bias for interpolating or offer the boundary conditions for a Thin Plate Spline interpolation. Assuming a data assimilation technique, the interpolation could also be guided by a set of rules defined by a hydrological model, trying in every step to minimize a set of values.

Finishing with the applicability of the method proposed, the fusion method could be researched further to reach a state where certain conclusions can be drawn concerning navigation using as scarce data as possible. Assuming a more detailed physics-based model and extended assumptions concerning the validity of the resulting depth values, navigational paths can be drawn and investigated whether they are usable by certain classes of vessels. That would give a more application-based result for the whole process and be a significant addition to the RAT-IN tool.

Appendix A: Centerline

This Appendix reviews three possible ways to create the centerline of a polygon. The implementation and running time for computation varies, however the results are relatively the same for the scale required by the project. As such, the more efficient and less time-consuming was chosen for use (§4.3.2). Nevertheless, all three were implemented and tested in QGIS and Python code.

In overview, §A.1 covers the implementation by rasterizing the polygon and iteratively thinning the non-zero raster cells towards the center. §A.2 presents the Medial Axis Transform (MAT), which is a more mathematical description of creating a polygon skeleton. Finally, §A.3 has the method eventually used in the project, which involves the use of a Voronoi tessellation of the river polygon.

A.1 Rasterization and Iterative Collapse

A common way to extract the centerline for a given polygon is through the process of rasterization and collapse. A raster is a spatial data model that, contrary to the continuous vector display, it defines space as an array of equally sized cells of regular rows and columns. As such, it is an approximated view of the real world and it depends on the specified resolution. The steps to follow in order to extract the centerline with this procedure are the following:

- Convert the polygon area to raster [Figure A.1]
- Iteratively thin the non-zero raster values [Figure A.2]
- Transform back to vector format and manually clean extended branches [Figure A.3]
- Smoothen the centerline and points' distances [Figure A.4]

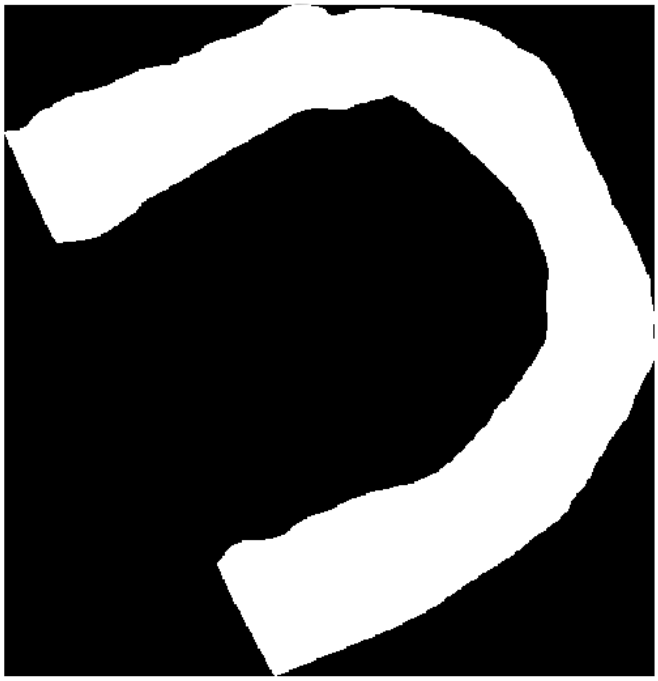

Figure A.1. Rasterization. White areas denote non-zero values (*QGIS*).

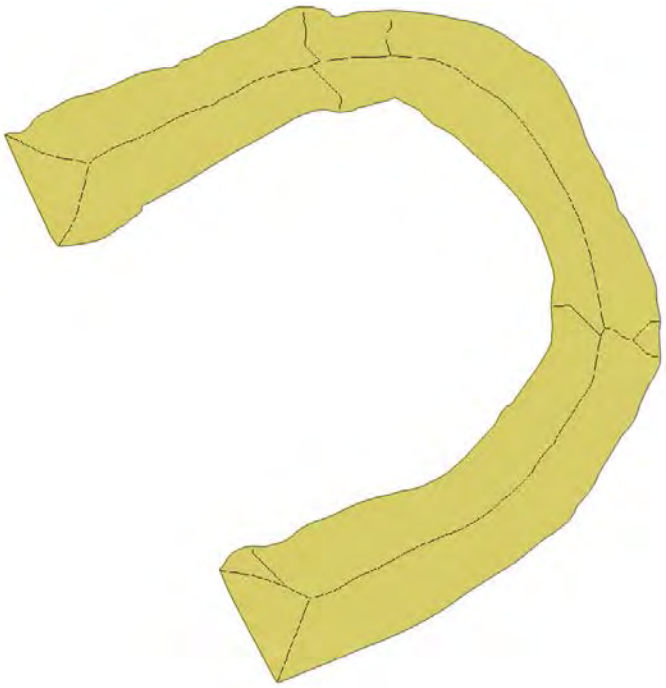

Figure A.2. Skeleton of the polygon after iterative thinning (*QGIS*).

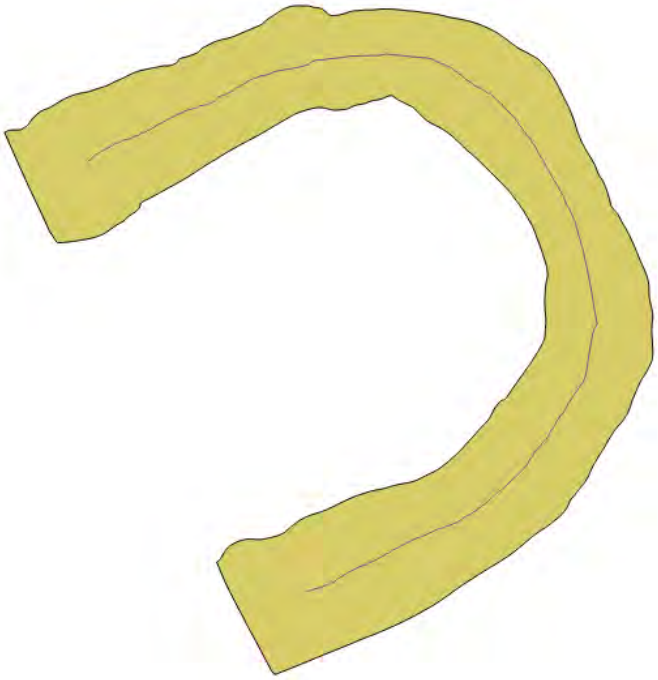

Figure A.3. Centerline after vectorization and manual removal of extra branches (*QGIS*).

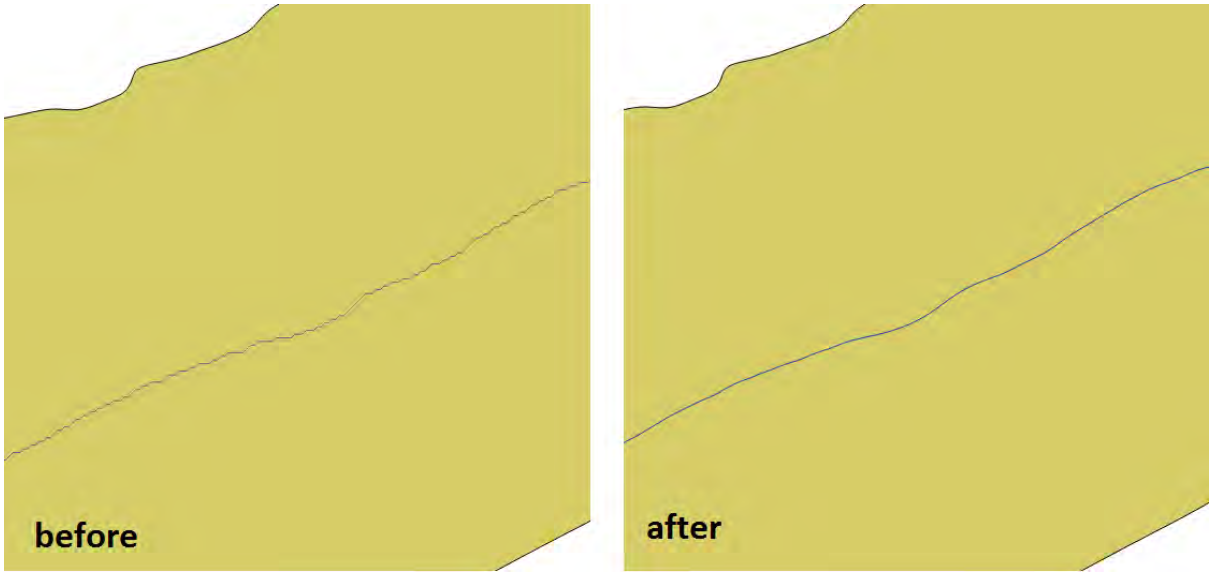

Figure A.4.Centerline smoothing (Snakes Algorithm, *GRASS* plugin - *QGIS*).

This method results in an approximation of a polygon's centerline, which is highly dependent on the initial resolution of the raster polygon and its thinned-out cell approximation. Its greater drawbacks are its increasing computational time at higher resolutions and the requirement for manual deletion of the skeleton branches, which depending on the case can be large in number. The final outcome requires smoothing, which is in all cases necessary due to the nature of raster cells being rectangular and the approximated centerline has a "zig-zag" pattern. Its main advantage is that all steps can be implemented in any nowadays GIS software or can also be coded. Because however of the drawbacks stated above, this method is not used in the current thesis.

A.2 Medial Axis Transform

The Medial Axis describes a topological skeleton and was initially introduced as a tool for biological shape recognition [*Blum, 1967*]. For a given polygon, together with the radius function of the maximally inscribed discs, the Medial Axis Transform (MAT) [*Vilaplana, 1996*] describes the points inside the polygon that are centers of circles tangent in two or more points to the polygon's boundary. For practical use a version was coded in Python, however the implementation required to define a starting point and direction along which the circles are fitted. Because a precise calculation of the skeleton is usually very computationally intensive, discs of varying thresholds are used to fit on the polygon's boundaries instead of the circles. The general steps are:

- Define thresholds and starting disc and direction.
- Compute skeleton, storing the network of bifurcation points [Figure A.5].
- Choose parts of network that describe the centerline.
- Smoothen the centerline and regularize points' spacing.

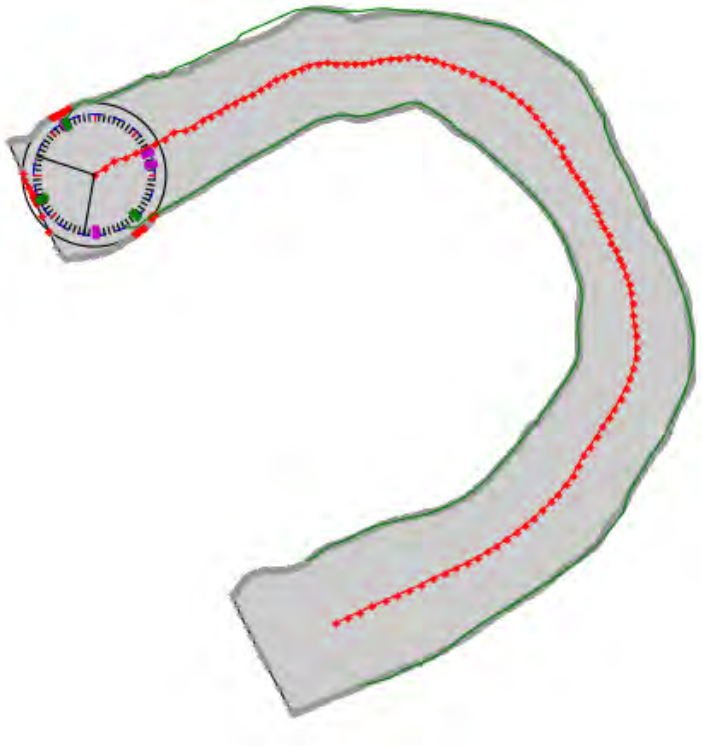

Figure A.5.Centerline construction through MAT. The "travelling" disc of specified threshold can be seen from the 2 equal-center cicles (*Python*).

As already stated above, this solution is very intensive computationally and requires a well-described algorithm to cover all cases of the different polygons. Furthermore, the threshold of the fitting discs defines the approximation of the centerline's points. However, the process may stumble across local bifurcations and may encounter issues if the threshold is not defined correctly. If the polygons are well-defined and without sudden bumps to their boundaries, this method can describe the best possible approximation for the centerline. However, due to its requirement for user interaction and necessity for precise description, together with the fact that the coded procedure is prone to failure, it is not used in this thesis.

A.3 Voronoi Method

A more practical and efficient method to use for calculating the centerline is the Voronoi Method. A Voronoi Diagram is retrieved by partitioning a plane based on equal distances from the given points [Figure A.6]. Given the river polygon's outer boundary nodes as points, the Voronoi tessellation can approximate the polygon's centerline [*Roberts et al., 2005*]. The Voronoi polygon's edges which lie inside the polygon can be chosen by intersection and the resulting skeleton is trimmed to extract the centerline. The procedure requires however a densification of the polygon boundary geometry in cases there are big gaps in between its nodes (long polygon edges). As such the general steps for this method are:

- Densification of polygon geometry (define maximum distance between points and add points in case of exceeding it).
- Calculation of the Voronoi tessellation [Figure A.7].
- Intersection with the polygon geometry to acquire the skeleton [Figure A.8].
- Definition of start-end branch points.

- Trimming of extra skeleton branches based on given points to acquire the centerline [Figure A.9].
- Regularization of points' spacing along the centerline.

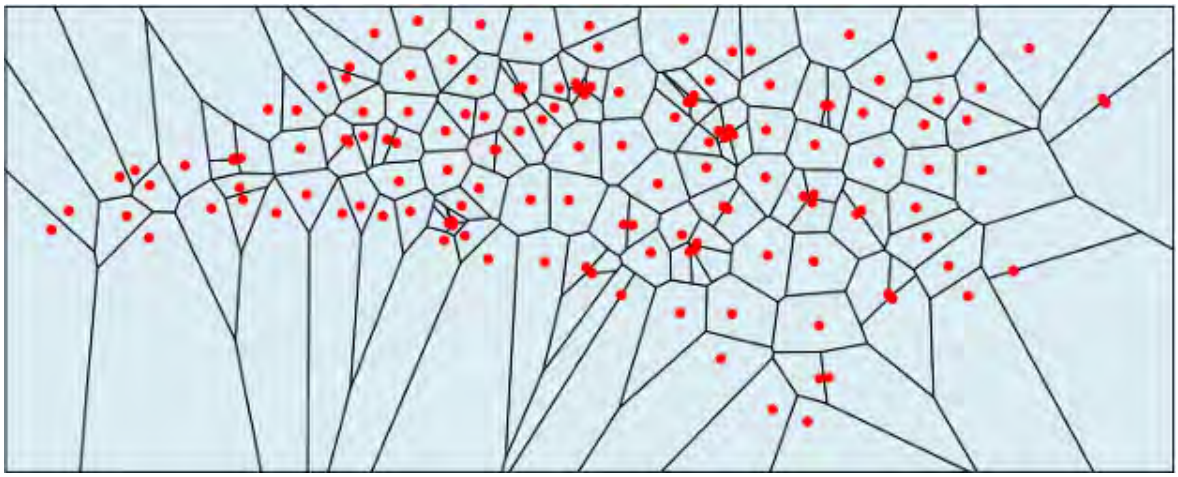

Figure A.6.Voronoi Tesselation example (*Grass, OSgeo*).

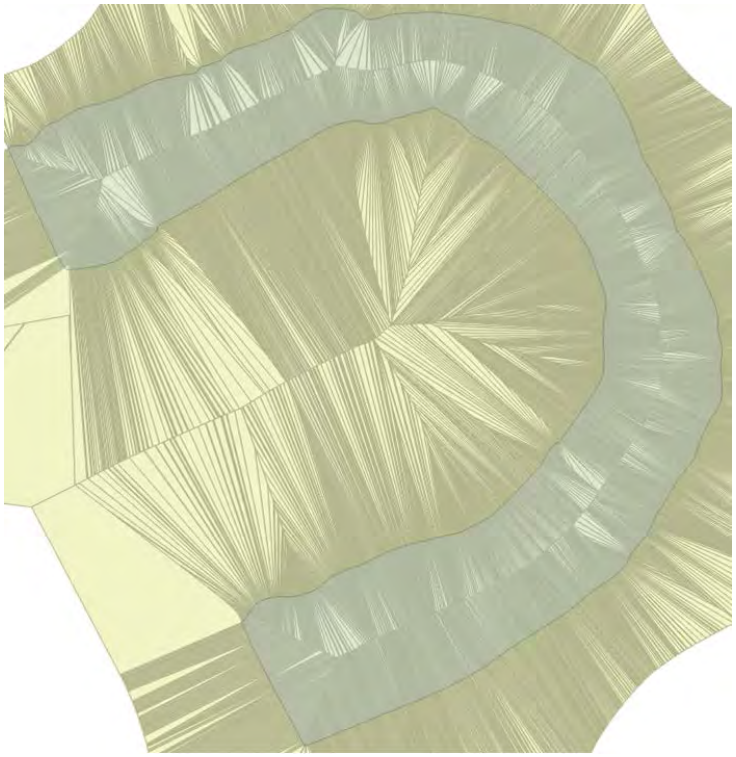

Figure A.7. Voronoi Tesselation and respective river polygon (*Python*, representation in *QGIS*).

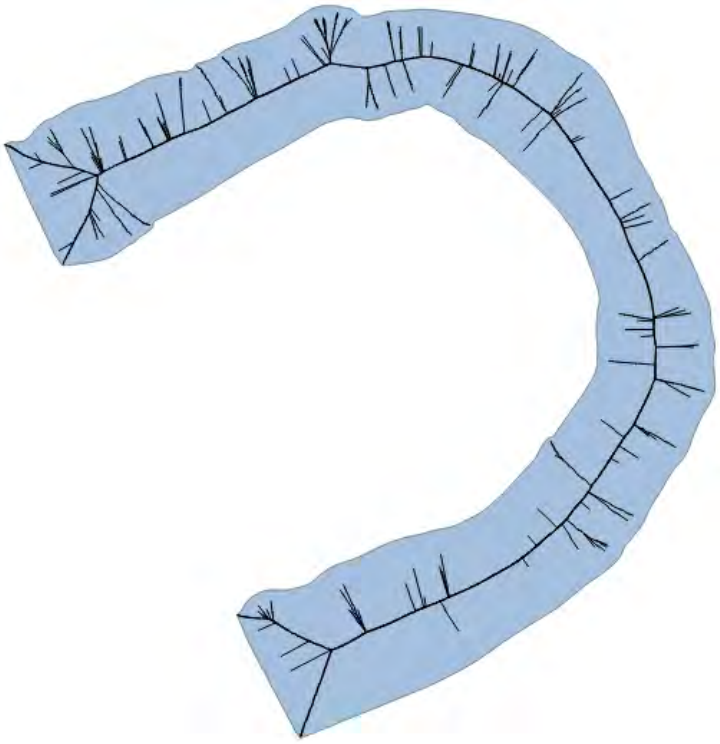

Figure A.8. Voronoi skeleton extracted from Figure A.7(*Python*, representation in *QGIS*).

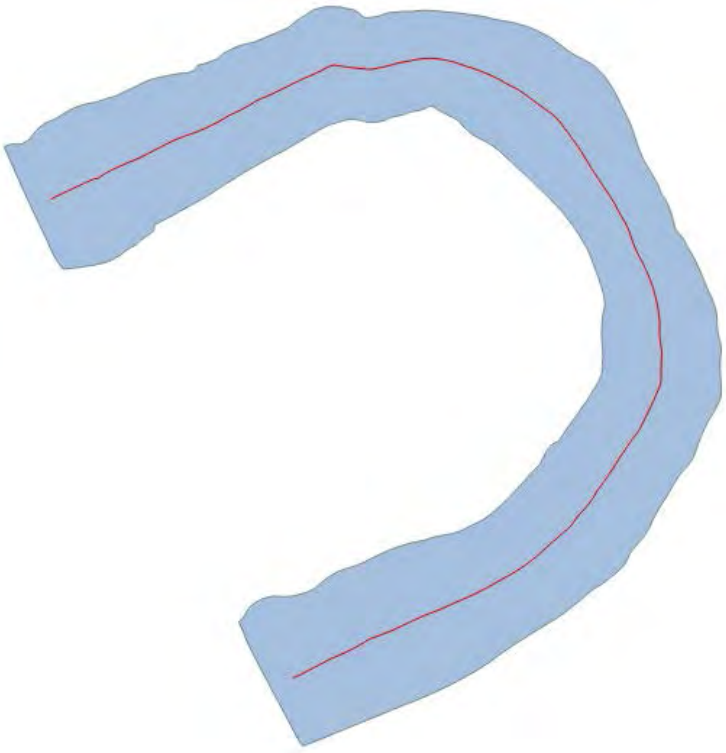

Figure A.9. Voronoi-defined centerline (*Python*, representation in *QGIS*).

Other than the river polygon, in order to acquire one continuous centreline, the endpoints need to be defined by the user. By setting the coordinates of the start and the end points of the polygon's extents, the algorithm can simply choose the closest skeleton branch points and keep those branches in order to clean the remaining off from the skeleton. At least 2 points are required to have one continuous centerline, but if more are set, the algorithm breaks the new branches as separate parts of multiple centerlines [Figure A.10]. In the river bends explored, none includes bifurcations, therefore such cases are not prominent.

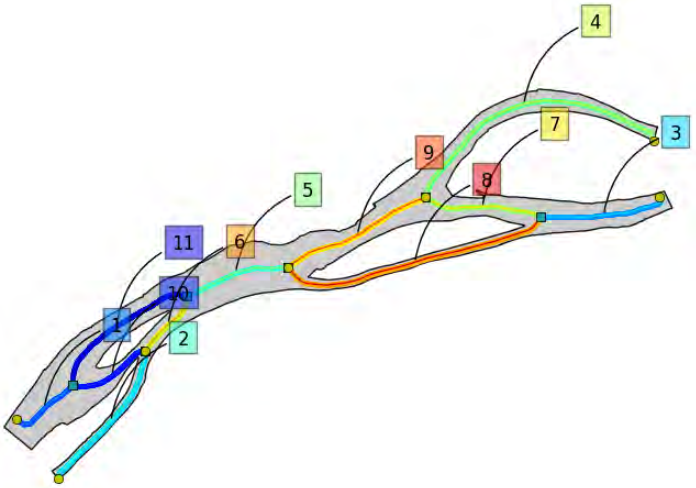

Figure A.10. Example of multiple branched centrelines in a braided river part of Danube (*Python*).

This procedure was implemented in Python code and has been chosen as the one to use in the thesis. The results are approximating very well the centreline of a given polygon and can easily be extended to include bifurcations and holes in the polygon. It is notable to say, that the output is fully automated just by defining a polygon and the starting and ending points. A regular spacing of the centreline points can be chosen in the end, by defining the distance in between two consecutive points.

Appendix B: Data Aggregation

In this Appendix, three options are presented concerning point data aggregation on a specified curvilinear grid. The implementation is solely based on Python programming language.

The process of discretizing a denser point dataset covering an area to a grid cell area is a well-known procedure in GIS. It is essentially a rasterization procedure through which the given dataset is averaged on grid cells. This can be achieved either by simply snapping to the closest point value (§B.1), averaging all point values that fall within a raster cell (§B.2) or by performing an interpolation technique to the points defining the grid cells (§B.3).

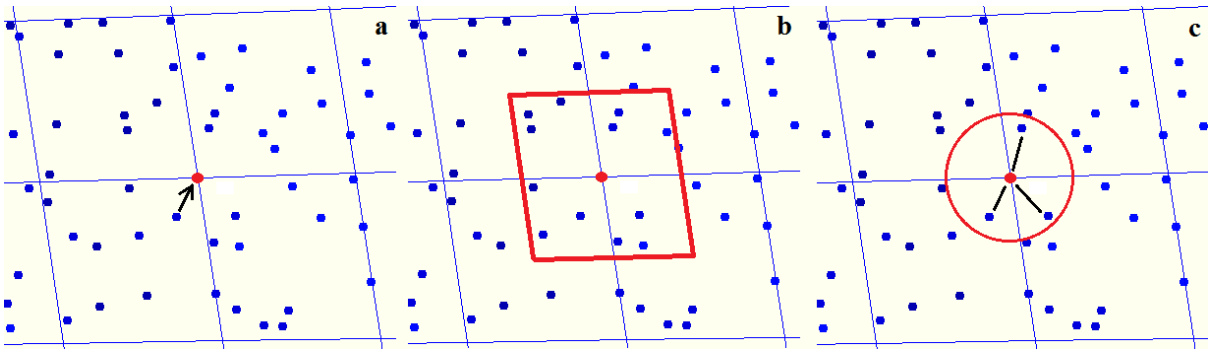

Figure B.1. Aggregation of data on the grid: (a) Snapping, (b) Averaging by cell centres, (c) Interpolating by radius distance.

B.1 Snapping

In the current context, each intersection node of the grid requires a value. If snapping is the chosen process [Figure B.1 a], the depth value of the closest point to a node is appointed as the depth for that grid point. This method is fit for use when the grid is covered in whole by the data extent and has relatively larger resolution than the sampled data spacing.

B.2 Averaging

If the grid is greatly larger than the data spacing, an averaging method can be adequate. This is performed by calculating the mean value of the points' depths within a raster cell. In the case of grid intersection nodes, this area can be defined by the centers of the surrounding grid cells [Figure B.1 b]. This averaging can be quite a big generalizing factor in cases where the grid is fine and data have not been cleaned out of outliers.

B.3 Interpolating

Finally, an interpolation scheme can be applied. Assuming an IDW interpolation, a circular neighbourhood area can be measured using as center the grid's intersection nodes [Figure B.1 c]. All points that fall within the area are weighted by distance and the respective node point receives the interpolated value. The output of this aggregation can be similar to the averaging or snapping stated above, depending on the radius and weighting applied.

B.4 Further Considerations

In the latter two cases (§B.2, B.3) a k-closest version can be performed, where instead of using all the points within the chosen area, at most (or at least) k point values are used. This can moderate the averaging that could happen if the neighbourhood is large, but also to make sure each grid's intersection node point receives a value.

Furthermore, in order to have an efficient data search amongst a huge number of data points, a spatial tree data structure can be used. By doing so, the sampled points are organized by their minimum bounding rectangles in space. Nearby object points to the current grid's intersection node point can be queried much faster and the overall aggregation process is much less time consuming. In this project, a KD-tree data structure is used for simplicity, since the only operation required is nearest neighbours search.

In all of the above cases, a geostatistical analysis of the standard deviations of the initial data can be performed as a first step in order to apply a quadrant-oriented data selection or surface analysis to define the neighbourhood areas. However, this is a complex process, which would require a higher computational time than necessary, especially for aggregating a multibeam dataset onto the grids. This step is anyways trivial to the method proposed, supposing that in a real-case scenario the data points are scarce and only few, where simple snapping on a fine grid would be sufficient.

Appendix C: Test Results

In this Appendix, additional results are displayed from testing the proposed method. Additionally, in the following tables the overall outputted RMSE values are documented. All Fusion methods use EIDW and the Physics-based model results.

C.1 RMSE

Table C.1. RMSE values for Kootenai #1. Cross-sections graph: Figure 5.13. Tracklines graph: Figure 5.16.

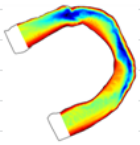

KOOTENAI #1 (North)	1600m (~1.6km)								
	CROSS-SECTIONS	2	3	4	5	6	7	8	9
	%data	0.0432286	0.064843	0.0851064	0.1080716	0.128335	0.1499493	0.1715637	0.1945289
	method								
	linear	4.2436614	2.949933	3.0536622	2.5365587	2.4256594	1.904817	1.958348	1.6290041
	nearest	4.6219415	3.3616601	3.0984101	2.6083854	2.6682389	1.9262469	2.0472681	1.6850786
	idw	5.0530941	3.2764984	3.2786773	2.5205234	2.5759931	2.0183505	2.0734231	1.760091
	eidw	4.4894821	2.942939	3.0505614	2.3574314	2.5594327	1.9228579	2.0531721	1.7466082
	model	2.3373918	2.3373918	2.3373918	2.3373918	2.3373918	2.3373918	2.3373918	2.3373918
	fusion	3.2489694	2.141623	2.1303921	2.0317551	2.0768343	1.8701408	1.9121938	1.8487507
	TRACKLINES						auto	auto	auto
	Dthres (m)	120	120	120	120	120	133.23401	86.096519	89.515878
	%data	0.0472813	0.1013171	0.1188788	0.1404931	0.1783181	0.2350557	0.3525836	0.7038163
	method								
	linear	3.5698706	2.1730463	2.4201634	2.312789	2.0253747	1.7242778	1.1298538	1.1858778
	nearest	5.6099305	5.0456128	5.3481007	5.1644154	4.4206056	4.1715819	3.1190485	2.3250306
	idw	5.4370888	4.4977395	4.6470916	4.7475793	3.7204416	3.6113853	2.7158891	2.1703281
	eidw	3.7241129	2.2558646	2.4364445	2.7221526	1.9562642	1.8142495	1.2886409	1.2401263
	model	2.3373918	2.3373918	2.3373918	2.3373918	2.3373918	2.3373918	2.3373918	2.3373918
	fusion	2.4424672	1.8447409	1.9570665	2.2292185	1.6751223	1.7089946	1.4445092	1.32847

Table C.2. RMSE values for Kootenai #2. Cross-sections graph: Figure 5.14. Tracklines graph: Figure 5.17.

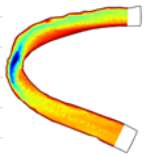

KOOTENAI #2 (South)	1788m (~1.8km)								
	CROSS-SECTIONS	2	3	4	5	6	7	8	9
	%data	0.0386628	0.0579941	0.0773255	0.0966569	0.1159883	0.1353196	0.154651	0.1739824
	method								
	linear	2.5803262	2.3529879	2.3351813	1.7429546	1.88274	1.3539432	1.7180435	1.2300773
	nearest	2.7559343	2.8651292	2.4090008	1.9456665	1.9266192	1.4881508	1.7374226	1.3018323
	idw	3.2441605	3.0986331	2.7178294	2.1335557	2.1430031	1.6854145	1.8298806	1.4779224
	eidw	2.8632716	2.4985846	2.4083053	1.7958381	1.9481916	1.4753913	1.7271308	1.3513412
	model	2.0945676	2.0945676	2.0945676	2.0945676	2.0945676	2.0945676	2.0945676	2.0945676
	fusion	1.4973226	1.7468734	1.7202824	1.5857557	1.6370687	1.5040332	1.7053329	1.4828827
	TRACKLINES						auto	auto	auto
	Dthres (m)	120	120	120	120	120	108.11102	82.047369	62.108776
	%data	0.0797419	0.1014897	0.1171965	0.1425689	0.177607	0.2343929	0.3540058	0.7055952
	method								
	linear	2.8500341	1.855414	2.065667	1.8919773	1.5757738	1.1878707	0.9471311	0.6926972
	nearest	3.9922456	3.6300948	3.7263478	3.8644911	3.276736	2.9940492	2.418696	1.3104411
	idw	3.8489792	3.2738142	3.3472453	3.5468238	2.8197893	2.5330639	2.1040249	1.2491678
	eidw	2.6998667	1.7081937	1.6380351	2.0856902	1.5400604	1.1754504	1.0006415	0.7425358
	model	2.0945676	2.0945676	2.0945676	2.0945676	2.0945676	2.0945676	2.0945676	2.0945676
	fusion	1.9896679	1.60302	1.48487	1.6875137	1.5010075	1.1475771	1.1521862	0.9492353

Table C.3. RMSE values for IJssel #1. Cross-sections graph: Figure 5.22. Tracklines graph: Figure 5.24.

IJSSEL #1 (North)	4246m (~4.25km)							
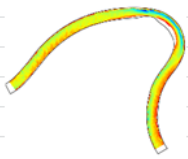								
	CROSS-SECTIONS	4	5	6	7	8	9	10	11
	%data	0.1404175	0.1745731	0.2087287	0.2441493	0.2732448	0.3086654	0.3390259	0.3744466
	method								
	linear	0.9168577	0.8704998	0.7382316	0.7880902	0.6935434	0.6208883	0.6699817	0.5603921
	nearest	1.0289368	0.9677441	0.838212	0.859906	0.7506972	0.663886	0.7229266	0.5897475
	idw	0.892211	0.8635813	0.7513983	0.7931126	0.7258772	0.6660093	0.6705661	0.6099093
	eidw	0.9006568	0.8268095	0.7318929	0.7532791	0.7034852	0.6158652	0.6675155	0.5573618
	model	0.730816	0.730816	0.730816	0.730816	0.730816	0.730816	0.730816	0.730816
	fusion	0.7183247	0.6213795	0.6180092	0.6544942	0.5962351	0.6104704	0.615815	0.5912044
	TRACKLINES			auto	auto	auto	auto	auto	auto
	Dthres (m)	150	150	145.6021	141.90335	136.44651	126.83515	109.78015	71.423221
	%data	0.1113219	0.1290323	0.1568627	0.1922834	0.2352941	0.3137255	0.4693232	0.9373814
	method								
	linear	0.7540026	0.8515621	0.6089567	0.609523	0.597751	0.567207	0.4813582	0.3954345
	nearest	1.0774605	1.201829	1.1739127	1.124511	1.0987516	0.9978704	0.8012673	0.561474
	idw	1.0664379	1.1731017	1.1518867	1.0839007	1.0521118	0.9631346	0.7693983	0.52479
	eidw	0.731691	0.6580082	0.6564689	0.615008	0.5943061	0.5738424	0.4792577	0.4177164
	model	0.730816	0.730816	0.730816	0.730816	0.730816	0.730816	0.730816	0.730816
	fusion	0.6336806	0.5864149	0.6064321	0.5866389	0.5628547	0.5703056	0.5154925	0.4713284

Table C.4. RMSE values for IJssel #2. Cross-sections graph: Figure 5.23. Tracklines graph: Figure 5.25.

IJSSEL #2 (South)	2932m (~3km)							
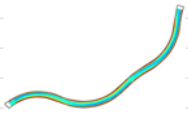								
	CROSS-SECTIONS	2	3	4	5	6	7	8	9
	%data	0.0597746	0.0866732	0.1135718	0.1374817	0.1643803	0.1912789	0.2211662	0.2510535
	method								
	linear	0.7012146	0.6607456	0.594715	0.6363663	0.5967207	0.5594351	0.5695326	0.5420997
	nearest	0.8251581	0.8063602	0.7275241	0.7521644	0.7546622	0.6755994	0.7440056	0.6873369
	idw	1.2863189	1.1695774	1.1283774	1.0665529	1.0692112	1.0013748	1.0044748	0.975814
	eidw	0.8992826	0.7372845	0.6611798	0.6465324	0.6280014	0.5767142	0.6129075	0.5696189
	model	0.7025324	0.7025324	0.7025324	0.7025324	0.7025324	0.7025324	0.7025324	0.7025324
	fusion	0.7142629	0.6087281	0.6156116	0.5940783	0.5973592	0.6050567	0.5921152	0.5793922
	TRACKLINES				auto	auto	auto	auto	auto
	Dthres (m)	85	85	85	81.31098	80.062939	74.057146	62.771683	40.332658
	%data	0.2151887	0.2361099	0.2779521	0.3317493	0.4214113	0.5529155	0.8368451	1.6677127
	method								
	linear	0.6277082	0.5681113	0.6344115	0.5530237	0.5013713	0.4755203	0.3999343	0.3477861
	nearest	1.6809837	1.6573945	1.6533268	1.5924488	1.4944675	1.3694983	1.2205673	0.9469169
	idw	1.6636186	1.635782	1.6285956	1.5589169	1.4460789	1.3278575	1.1870394	0.8590929
	eidw	0.8972035	0.7201127	0.6339701	0.5622417	0.5381545	0.4399545	0.366096	0.3140975
	model	0.7025324	0.7025324	0.7025324	0.7025324	0.7025324	0.7025324	0.7025324	0.7025324
	fusion	0.6943248	0.6051346	0.5600544	0.5383877	0.5188472	0.4808507	0.4423547	0.421997

Table C.5. RMSE values for Danube #2. Cross-sections graph: Figure 5.33.

DANUBE #2 (South)	6521m (~6.5km)							
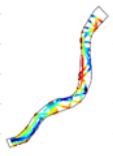								
	CROSS-SECTIONS	2	3	4	5	6	7	8	9
	%data	0.1990195	0.3786224	0.4757051	0.582496	0.6844328	0.8203485	0.9174312	1.019368
	method								
	linear	5.5061695	5.6359447	5.8015049	4.289012	3.4455476	3.3872579	3.3316505	3.141795
	nearest	5.3562444	5.6999983	5.60353	4.4584879	3.5487182	3.5562579	3.4721749	3.2733746
	idw	4.7963067	4.5420313	4.5029714	4.0076001	3.5451085	3.5173184	3.4204172	3.1308344
	eidw	4.7082648	5.0825747	4.935297	4.1134435	3.3120796	3.278931	3.2242525	3.0376708
	model	4.8403539	4.8403539	4.8403539	4.8403539	4.8403539	4.8403539	4.8403539	4.8403539
	fusion	4.5518383	4.5245972	4.155883	4.2109919	3.5904091	3.5704381	3.4938092	3.4160427

C.2 Additional Results

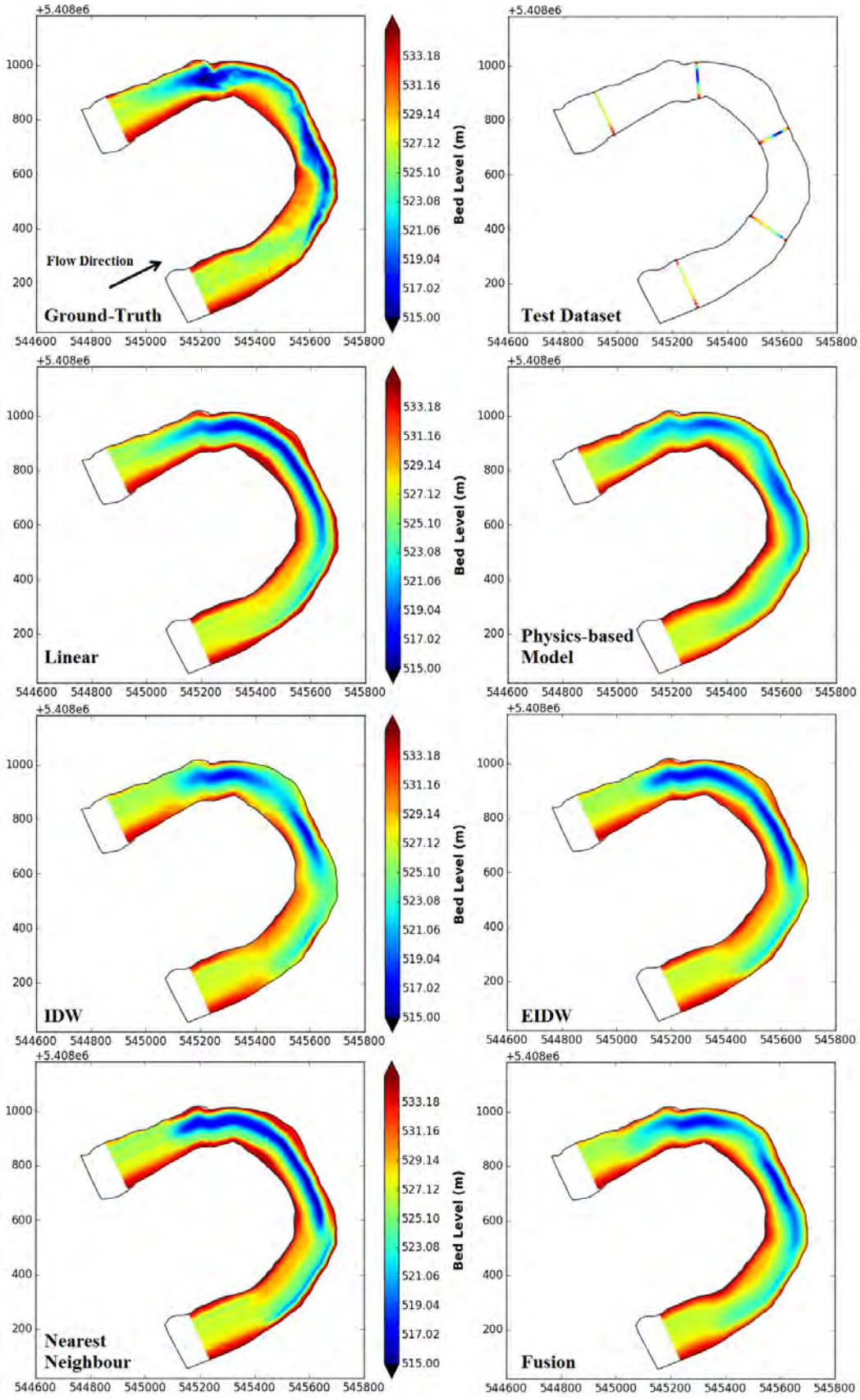

Figure C.1. Kootenai #1 results with Test data of 5 cross-sections.

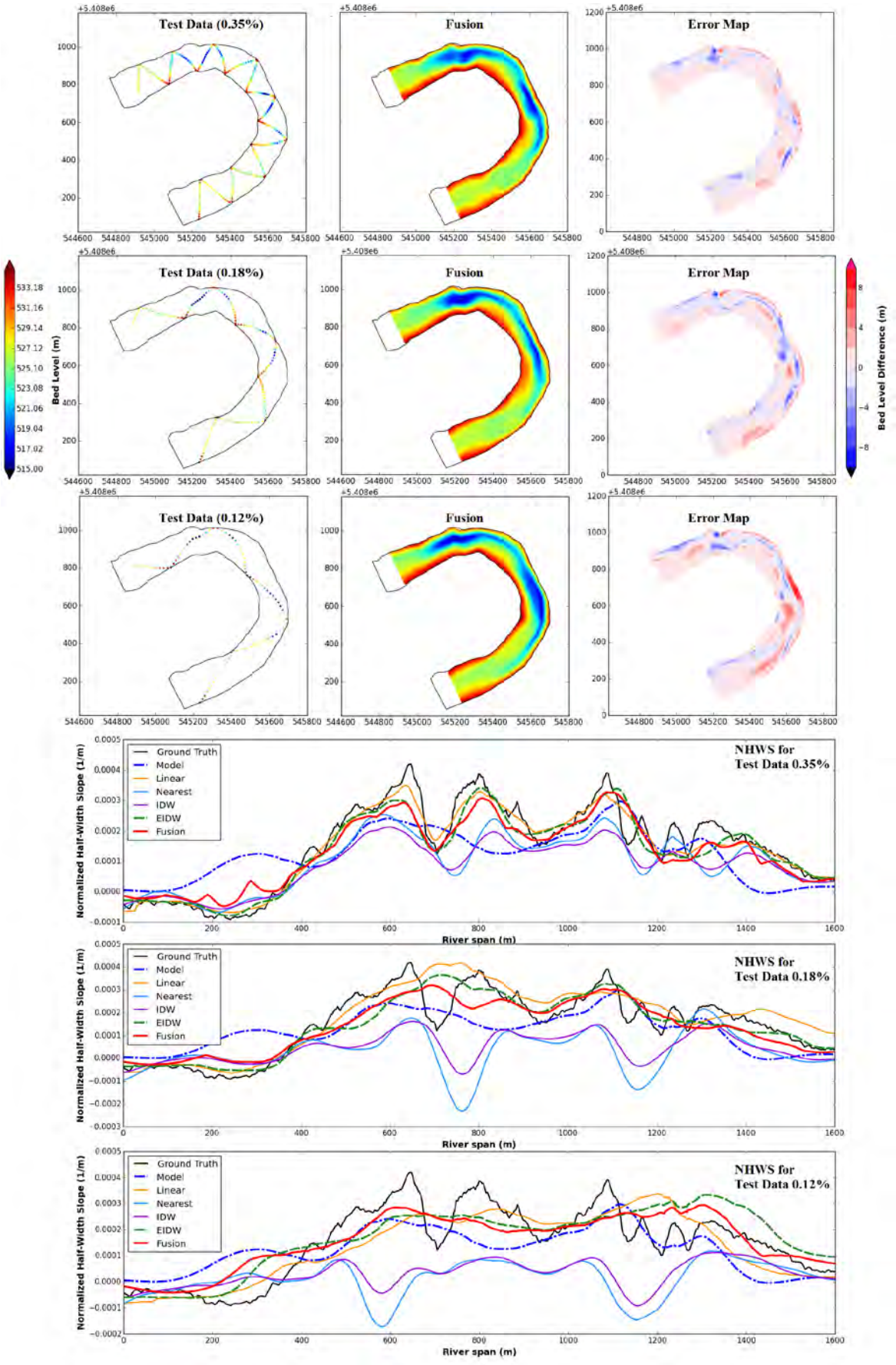

Figure C.2. Iterative thinning of trackline Test data for Kootenai #1 and results of Fusion method.

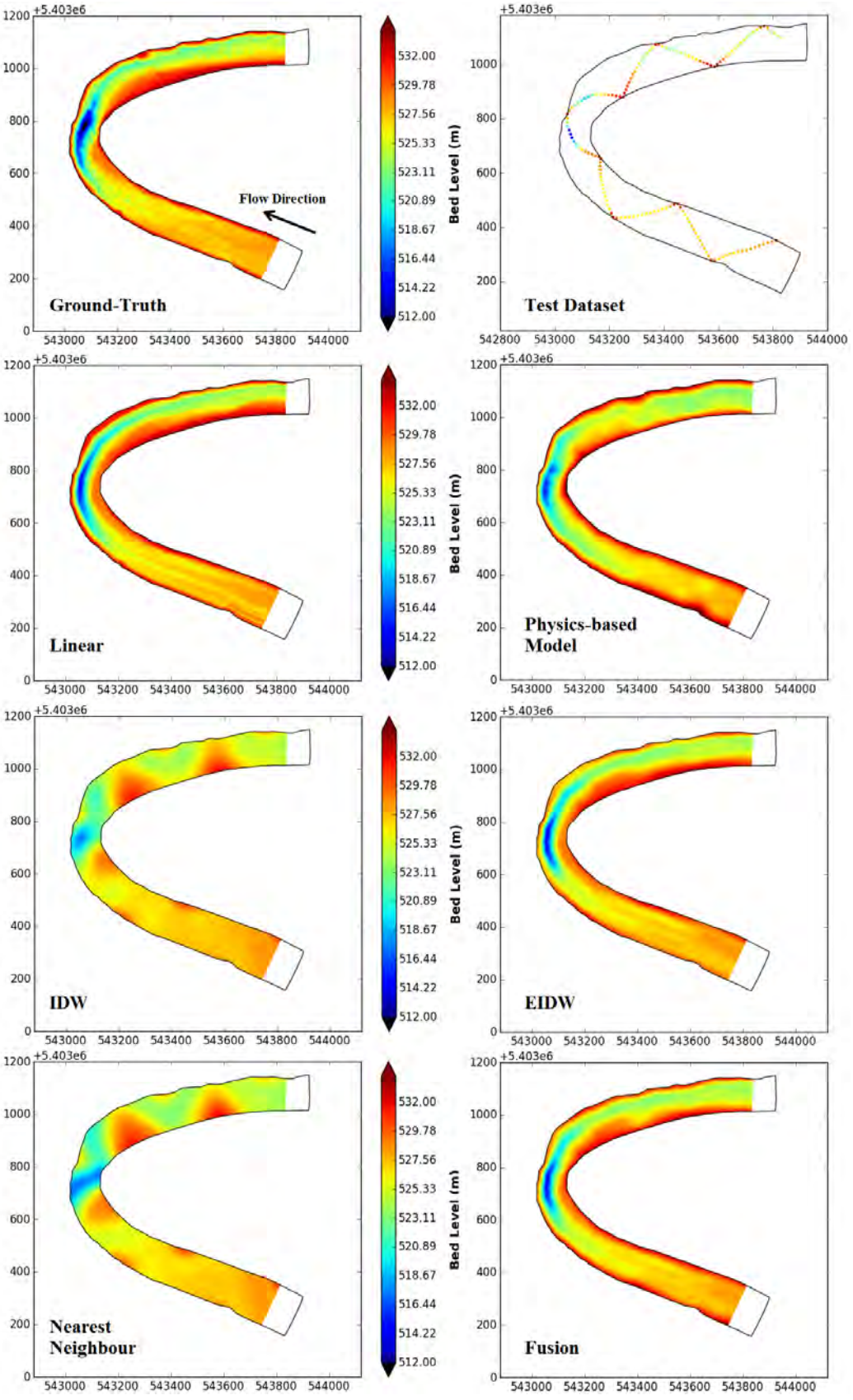

Figure C.3. Kootenai #2 results with trackline Test data (0.18% grid coverage).

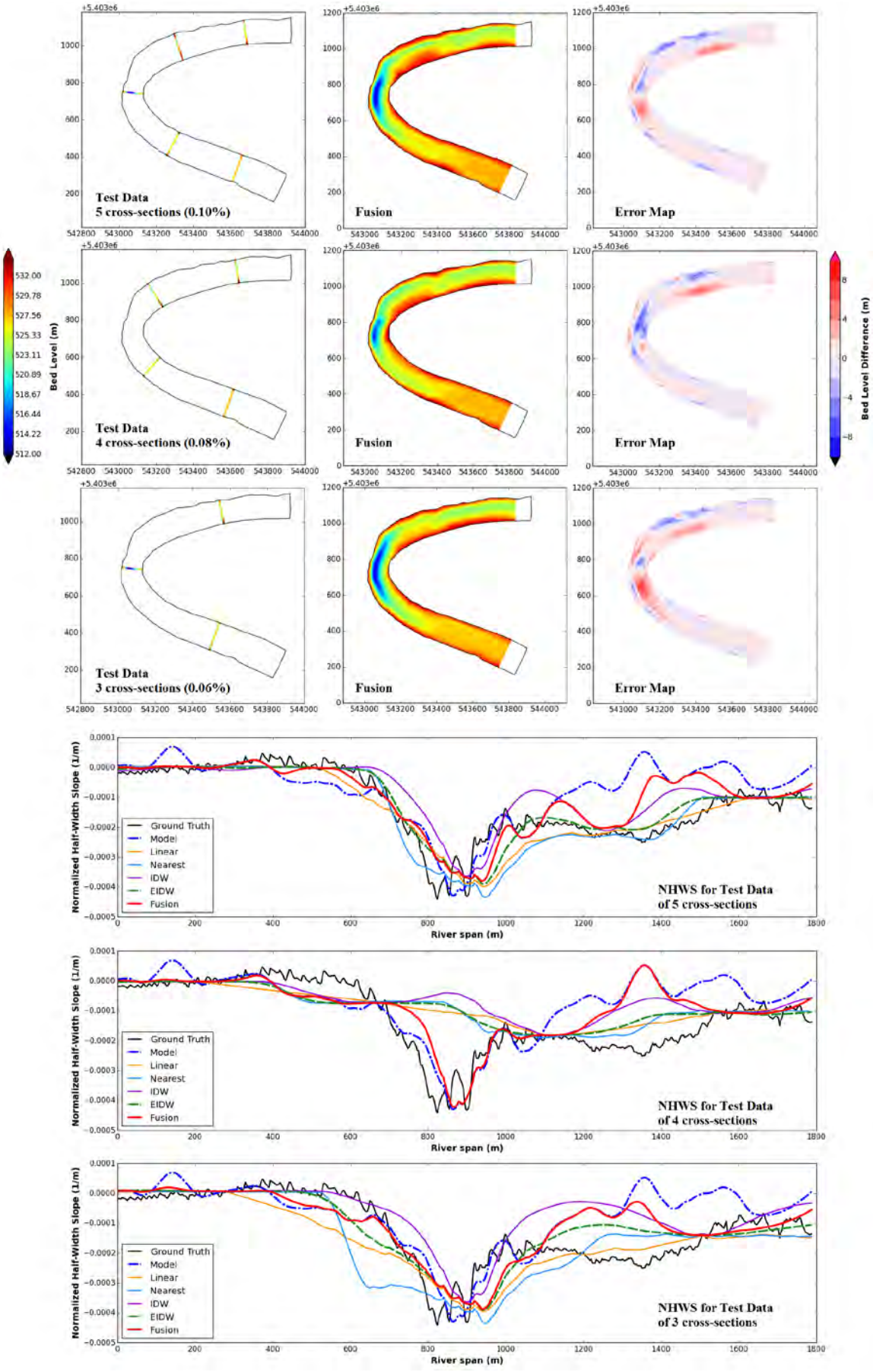

Figure C.4. Iterative thinning of cross-sectional Test data for Kootenai #2 and results of Fusion method.

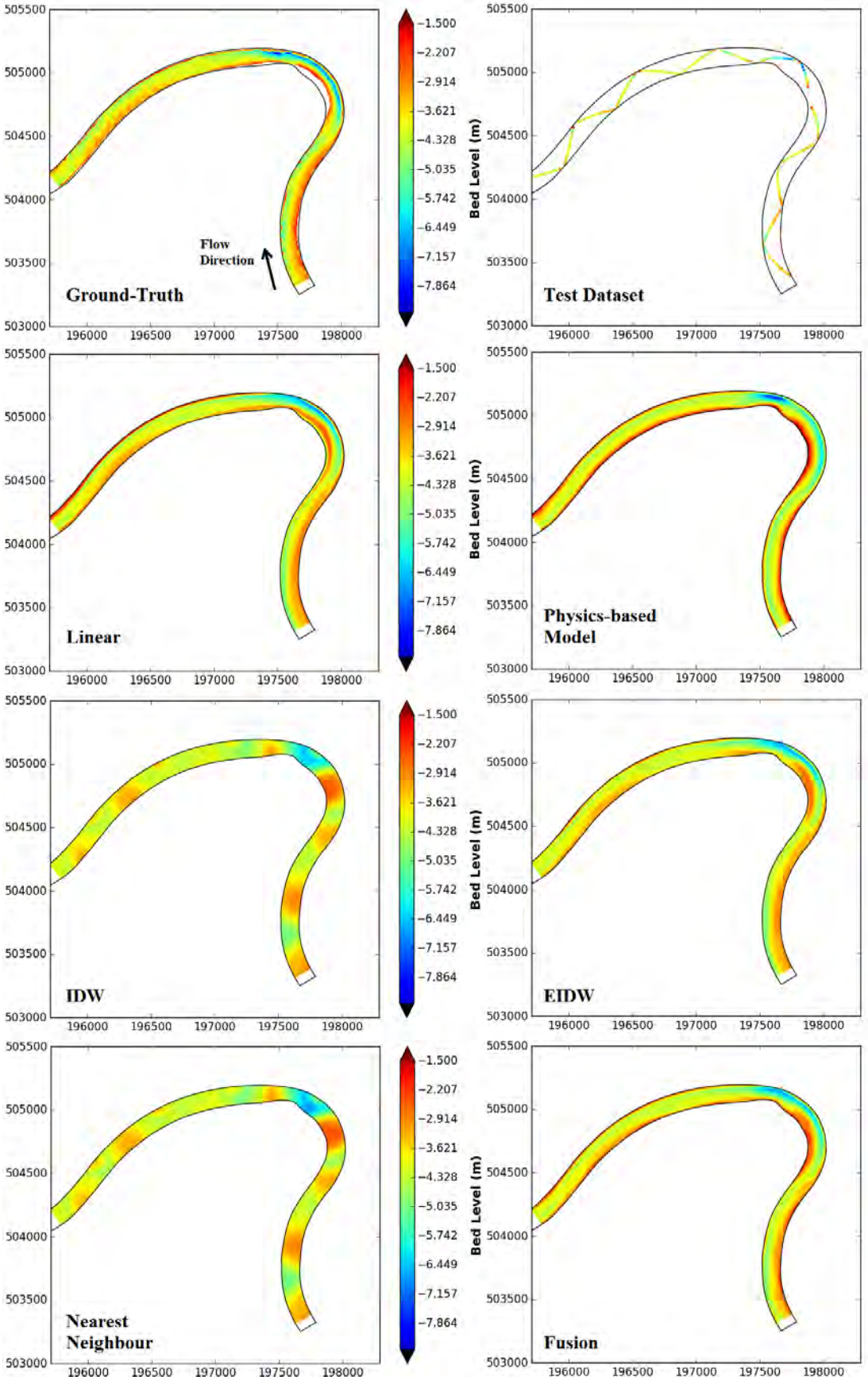

Figure C.5. IJssel #1 results with trackline Test data (0.24% grid coverage).

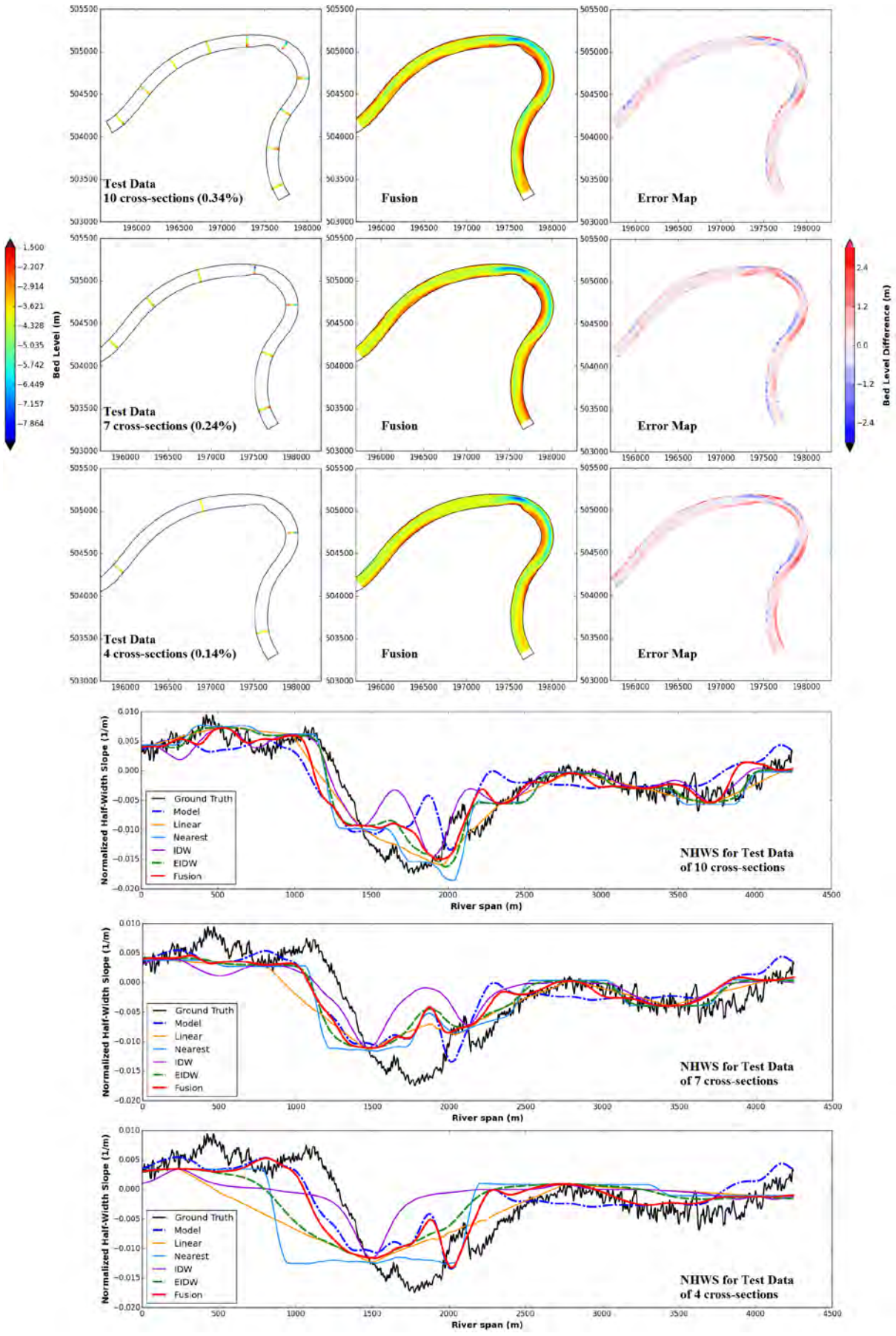

Figure C.6. Iterative thinning of cross-sectional Test data for IJssel #1 and results of Fusion method.

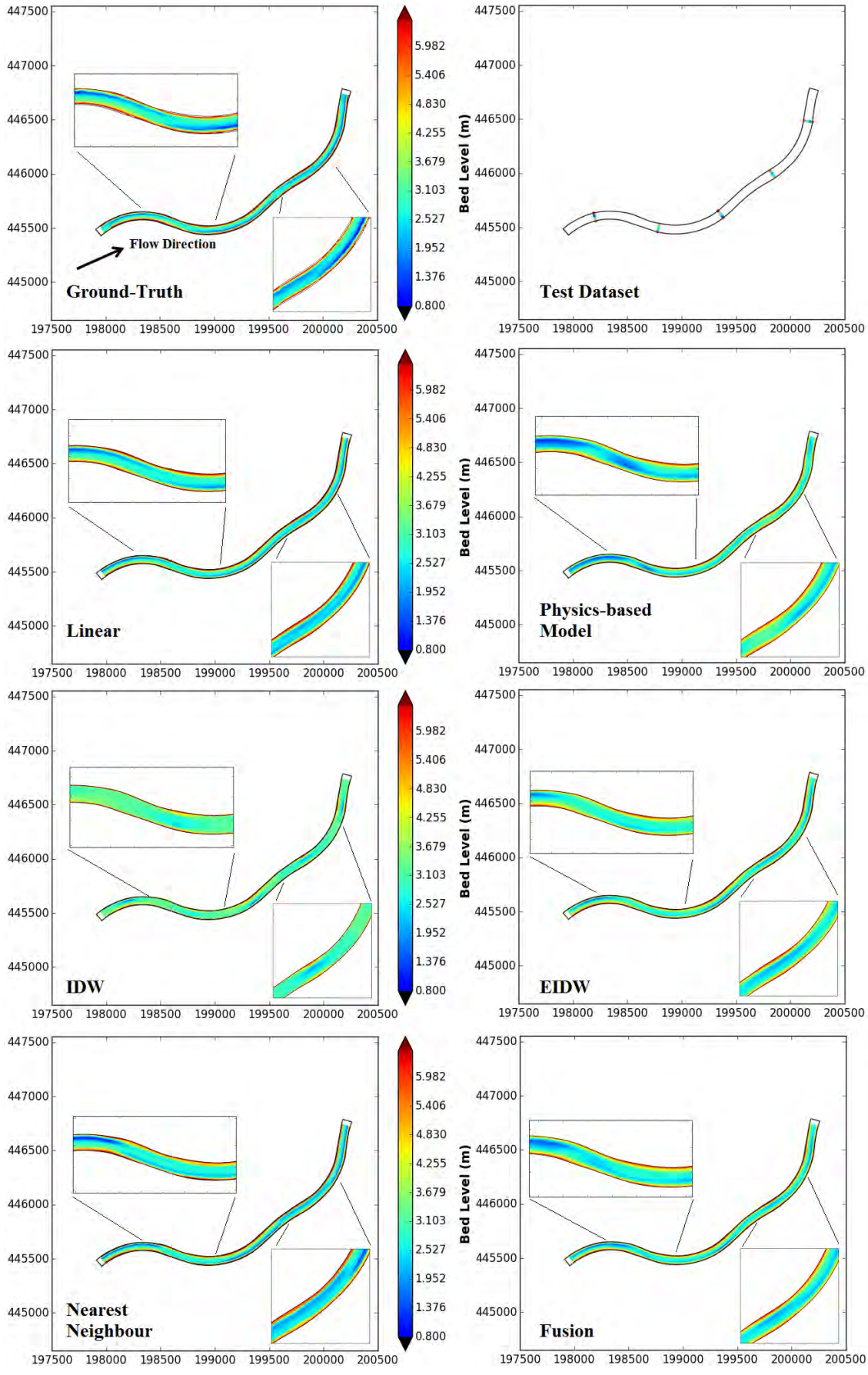

Figure C.7. IJssel #2 results with Test data of 5 cross-sections.

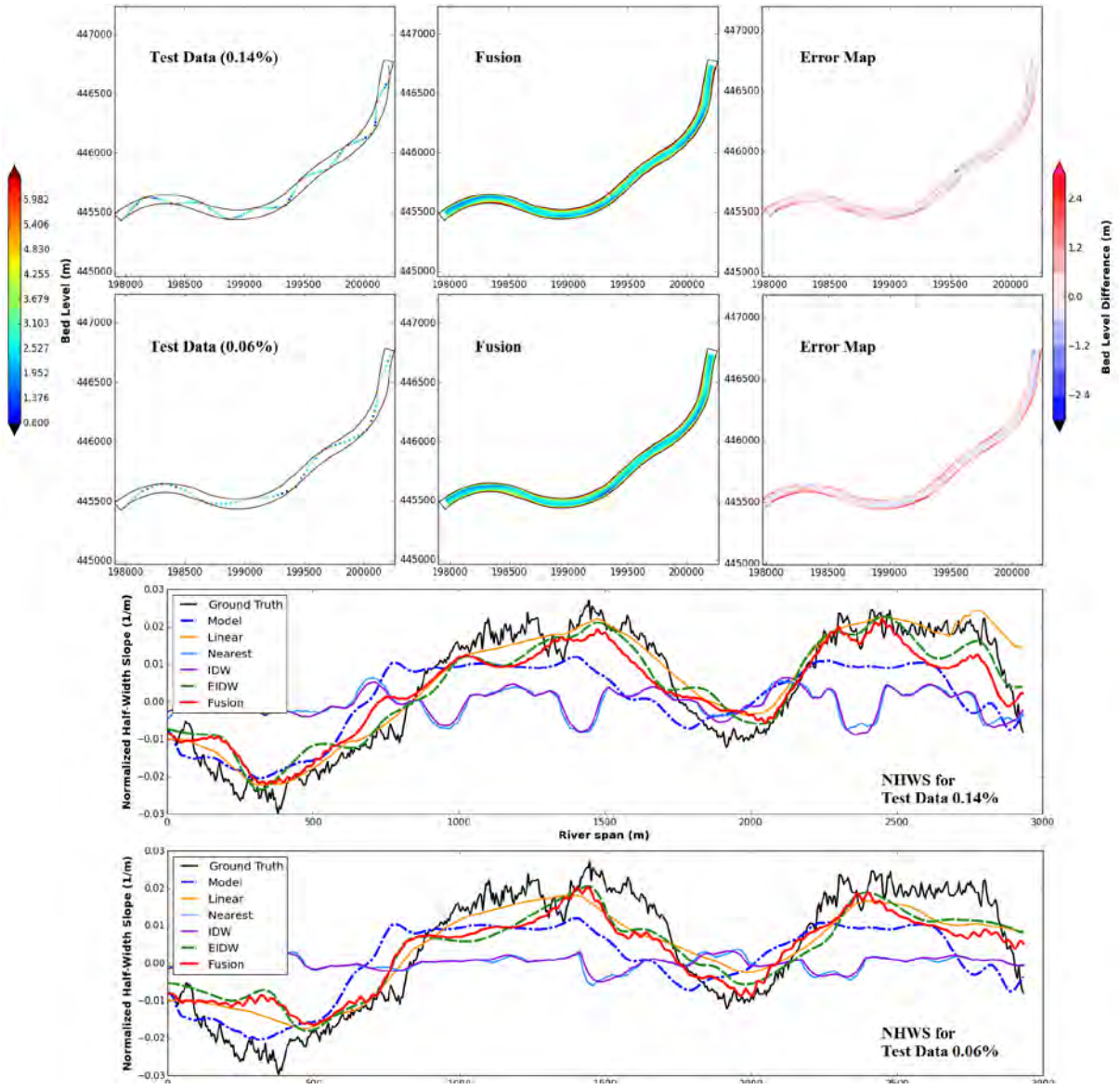

Figure C.8. Iterative thinning of trackline Test data for IJssel #2 and results of Fusion method.

In the latter case of the IJssel river #2 further examples are unnecessary to show, since there are no striking differences. For the Danube river all cases of interest are already covered in the thesis document (Chapter 5).

References

Abebe H.E., (2011). *Reconstruction of 2D riverbed topography from sarce data*. MSc thesis, UNESCO-IHE, Institute for Water Education.

Allmendinger N.E., Pizzuto J.E., Potter N.JR., Johnson T.E., Hession W.C. (2005). *The influence of riparian vegetation on stream width, eastern Pennsylvania*. USA GSA Bulletin, Vol. 117, No ½, pp.229-243, doi: 10.1130/B25447.1.

Bagnold R.A., (1960). *Some Aspects of the Shape of River Meanders*. Physiographic and Hydraulic Studies of Rivers, Geological Survey Professional Paper 282-E.

Barton G.J., (2004). *Characterization of Channel Substrate, and Changes in Suspended-Sediment Transport and Channel Geometry in White Sturgeon Spawning Habitat in the Kootenai River near Bonners Ferry, Idaho, Following the Closure of Libby Dam*. Water-Resources Investigations Report 03-4324, U.S. Department of the Interior, U.S. Geological Survey.

van Bendegom L., (1947). *Some considerations on river morphology and river improvement*. De Ingenieur, 59(4), B1–B11.

Berry J.K (2013). *Beyond Mapping III*. (Compilation of Beyond Mapping columns appearing in GeoWorld magazine 1996 to 2013).

Beven K., (2006). *A manifesto for the equifinality thesis*. Journal of Hydrology 320 (2006) 18–36, doi:10.1016/j.jhydrol.2005.07.007.

Blanckaert K., De Vriend H.J. (2004). *Secondary flow in sharp open-channel bends*. Journal of Fluid Mechanics, 498, 353–380, doi:10.1017/S0022112003006979.

Blum H. (1967). *A transformation for extracting new descriptors of shape*. Models for the perception of speech and visual form, 01/1967; 19:362-380.

Borkowski A., Meier S., (1994). *A procedure for estimating the grid cell size of digital terrain models derived from topographic maps*. Geo-Informations-System, 7 (1) (1994), pp. 2–5.

Burroughes, J.E., George, K.J., Abbott, V.J., (2001). *Interpolation of hydrographic survey data.* The Hydrographic Journal (99), 21–29.

Chai T., Draxler R.R., (2014). *Root mean square error (RMSE) or mean absolute error (MAE)? – Arguments against avoiding RMSE in the literature*. Geosci. Model Dev., 7, 1247–1250, doi:10.5194/gmd-7-1247-2014.

Crosato A., (1987). *Simulation model of meandering processes of rivers*. Extended Abstracts of the International Conference: Euromech 215 -Mechanics of Sediment Transport in Fluvial and Marine Environments, European Mechanics Society, Sept. 15 -19, Santa Margherita Ligure-Genoa, Italy, printed by the University of Genoa, pp. 158-161.

Crosato A., (1989). *Meander migration prediction*. Excerpta, G.N.I., Vol. 4, pp. 169-198, Publisher Libreria Progetto, Padova, Italy.

Crosato, A., (2008). *Analysis and modeling of river meandering*, PhD Thesis, TUDelft.

Crosato, A. (2012). *River Morphodynamics - Morphological Response at the Reach Scale*. Lecture Notes LN0381 , UNESCO IHE, Delft, The Netherlands.

De Vriend H.J., (1981). *Velocity redistribution in curved rectangular channels*. Journal of Fluid Mechanics, Vol.107, pp 423-439.

Einstein A., (1926). *Die Ursache der Mäanderbildung der Flußläufe und des sogenannten Baerschen Gesetzes*. Naturwissenschaften, 12 März 1926, Volume 14, Issue 11, pp 223-224.

Eriksson, M., Siska P.P., (2000). *Understanding anisotropy computations*. Mathematical Geology 32 (6), 683-700.

Fargue L., (1868). *Etude sur la correlation entre la configuration du lit et la profondeur d'eau dans les rivieres a fond mobile*. Annales Des Ponts Et Chaussees.

Ferguson R.I., (1984). *Kinematic model of meander migration.* In: River Meandering, Proc. of the Conf. Rivers '83, 24-26 Oct. 1983, New Orleans, Louisiana, U.S.A., ed. Elliott C.M., pp. 942-951, ASCE, New York. ISBN 0-87262-393-9.

Foley J.D., (1995). *Computer Graphics: Principles and Practice*. Addison-Wesley Professional. p. 13. ISBN 0-201-84840-6.

Fosness R.L., (2013). *Bathymetric surveys of the Kootenai River near Bonners Ferry, Idaho*, water year 2011: U.S. Geological Survey Data Series 694, 26 p.

Franke R., (1982). *Smooth interpolation of scattered data by local thin plate splines*. Computers and Mathematics with Applications 8 (4), 237–281.

Frascati, A., Lanzoni, S. (2010) *Long-term river meandering as a part of chaotic dynamics? A contribution from mathematical modeling*. Earth Surf. Process. Landf. 35 (7), 791 –802, doi:10.1002/esp.1974.

Frascati , A., Lanzoni, S. (2013) *A mathematical model for meandering rivers with varying width*. J. Geophys. Res. Earth Surf. 118 (3), 1641–1657.

Fukoka, S., Sayre, W.W. (1973) *Longitudinal dispersion in sinuous channels.* Journal of Hydraulics Division, ASCE Proceedings 99, 195–217.

Goff, John A., Nordfjord, Sylvia, (2004). Inter*polation of fluvial morphology using channel-oriented coordinate transformation: A case study from the New Jersey Shelf.* Mathematical Geology 36 (6), 643–658.

Hengl T., (2006). *Finding the right pixel size*. Computers & Geosciences Volume 32, Issue 9, Pages 1283–1298, doi:10.1016/j.cageo.2005.11.008.

Hoehn L., Niven I., (1985). *Averages on the Move.* Math. Mag. 58, 151-156.

Holley E.R., Jirka G.H., (1986). *Mixing in rivers.* Technical Report E-86-11, U S Army Engineer Waterways Experiment Station, Vicksburg, Mississippi.

Howard A.D., (1984). *Simulation model of meandering*. In: River Meandering, Proc. of the Conf. Rivers '83, 24-26 Oct. 1983, New Orleans, Louisiana, U.S.A., ed. Elliott C.M., pp. 952-963, ASCE, New York. ISBN 0-87262-393-9.

Ikeda S., Parker G. & Sawai K., (1981). *Bend theory of river meanders. Part 1: linear development*. Journal of Fluid Mech., Vol. 112, pp. 363-377.

Institute: *Deltares* (http://www.deltares.nl)

Jansen P. Ph, Van Bendegom L. & Van Den Berg J. (EditorS), (1979). *Principles of river engineering*. Pitman Publishing Ltd., London, Great Britain, ISBN 90-6562-146-6.

Kalkwijk J.P.Th & De Vriend H.J., (1980). *Computation of the flow in shallow river bends*. Journal of Hydraulic Research, IAHR, Vol. 18, No. 4, pp. 327-342.

Kenney J.F., Keeping E.S., (1962). *Root Mean Square.* §4.15 in Mathematics of Statistics, Pt. 1, 3rd ed. Princeton, NJ: Van Nostrand, pp. 59-60.

Koch F.G. & Flokstra C., (1980). *Bed level computations for curved alluvial channels*. In: Proc. of the XIX IAHR Congress, New Delhi, India, Vol. 2, p. 357.

Kummu M., de Moel H., Ward P.J., Varis O. (2011), *How Close Do We Live to Water? A Global Analysis of Population Distance to Freshwater Bodies.* PLoS ONE 6(6): e 20578. doi:10.1371/journal.pone.0020578

Lemmens M. (2011). *Geo-information: Technologies, Applications and the Environment*. Springer Science+Business Media, ISBN 978-94-007-1666-7, doi: 10.1007/978-94-007-1667-4.

Lecture notes: ENV 208 – Environment, Transport And Fate, Chapter 2 – Dartmouth, Thayer School of Engineering, (http://engineering.dartmouth.edu/~d30345d/courses/engs43/Chapter2.pdf)

Lecture notes: Environmental Fluid Mechanics 1, Chapter 3 – Institut für Hydromechanik, University of Karlsruhe, (http://www.ifh.uni-karlsruhe.de/lehre/envflu_i/Downloads/course_script/ed2/ch3.PDF)

Leopold, L.B. (1994). *A View of the River*. Harvard University Press, Cambridge, MA.

Lesser G.R., Roelvink J.A., Van Kester J.A.T.M., Stelling G.S. (2004). *Development and validation of a three dimensional morphological model*. Coastal Engineering, Vol. 51/8-9, pp. 883-915.

Manning R., (1889). *On the flow of water in open channels and pipes*. Transactions of the Institution of Civil Engineers in Ireland, Vol. 20, pp.161-195.

Merwade V., Maidment D.R., & Goff J.A. (2006). *Anisotropic considerations while interpolating river channel bathymetry*. Journal of Hydrology, 331(3–4), 731–741.

Merwade V., Cook A., Coonrod J., (2008). *GIS techniques for creating river terrain models for hydrodynamic modeling and flood inundation mapping*. Journal of Environmental Modelling & Software 23 (2008) 1300–1311.

Merwade, V. (2009). *Effect of spatial trends on interpolation of river bathymetry*. Journal of Hydrology 371, 169–181.

Ministry: Rijkswaterstaat (http://www.rijkswaterstaat.nl/water/vaarwegenoverzicht/ijssel.aspx)

Mosselman E., (1992). *Mathematical modelling of morphological processes in rivers with erodible cohesive banks*. PhD Thesis, Communications on Hydraulic and Geotechnical Engineering, No.92-3, Delft University of Technology, ISSN 0169-6548.

Navier C.L.M.H., (1822). "*Memoire sur les lois du mouvement des fluides*", Mem. Acad. Sci. Inst. France, 6, 389-440.

Odgaard, A.J., (1981). *Transverse bed slope in alluvial channel bends.* Journal of the Hydraulics Division, ASCE, 107(HY12, Proc. Paper 16750), 1677–1694.

Olesen K.W., (1984). *Alternate bars in and meandering of alluvial rivers*. In: River Meandering, Proc. of the Conf.Rivers '83, 24-26 Oct. 1983, New Orleans, Louisiana, U.S.A., ed. Elliott C.M., pp. 873-884, ASCE, New York. ISBN 0-87262-393-9.

Olesen K.W., (1987). *Bed topography in shallow river bends*. Ph. D. Thesis, Communications on Hydraulic and Geotechnical Engineering, No. 87 1, Dept. of Civil Engineering, Delft University of Technology, The Netherlands.

Oliver M.A., (1990). *Kriging: A method of interpolation for geographical information systems.* International Journal of Geographic Information Systems 4, 313–332.

Olsen N.R.B. (2003). *3D CFD Modeling of a Self-Forming Meandering Channel*. ASCE, Journal of Hydraulic Engineering, ASCE, Vol. 129, No. 5, pp. 366-372.

Osting T.D., (2004). *An improved anisotropic scheme for interpolating scattered bathymetric data points in sinuous river channels*. CRWR Online Report 04-01,Center for Research in Water Resources, University of Texas at Austin.

Ottevanger W., (2013). *Modelling and parameterizing the hydro- and morphodynamics of curved open channels*. PhD Thesis, TU Delft.

Parker G. (1978). *Self-formed straight rivers with equilibrium banks and mobile bed (Part 1, The sand-silt river and Part 2, The gravel river).* Journal of Fluid Mechanics, Vol. 89, pp. 109-125 (Part 1), pp. 127-146 (Part 2).

Philip G.M., Watson D.F. (1982). *A precise method for determining contoured surfaces*. Australian Petroleum Exploration Association Journal 22, 205–212.

Roberts S.A., Hall G.B., Boots B. (2005). *Street Centreline Generation with an Approximated Area Voronoi Diagram*. Developments in Spatial Data Handling, 2005, pp 435-446, ISBN: 978-3-540-22610-9.

Shields A. (1936). *Anwendung der Aehnlichkeitsmechanik und der Turbulenzforschung auf die Geschiebebewegung [Application of similarity principles and turbulence research to bed-load movement]*. Mitteilungen der Preußischen Versuchsanstalt für Wasserbau 26. Berlin: Preußische Versuchsanstalt für Wasserbau.

Sibson R. (1981). *A brief description of natural neighbor interpolation*. In: Barnet, V. (Ed.), Interpreting Multivariate Data. John Wiley & Sons, Chicester, pp. 21–36.

Struiksma N.; Olesen K.W.; Flokstra C. & De Vriend H.J., (1985). *Bed deformation in curved alluvial channels*. Journal of Hydraulic Research, IAHR, Vol. 23, No. 1, pp. 57-79.

Struiksma N. & Crosato A., (1989). *Analysis of a 2 D bed topography model for Rivers. In: River Meandering, Water Resources Monograph*, AGU, Vol. 12, eds. Ikeda S. & Parker G., pp. 153-180, ISBN 0-87590-316-9.

Talmon A.M., Struiksma N., Van Mierlo M.C.L.M. (1995). *Laboratory measurements of the direction of sediment transport on transverse alluvial-bed slopes*. Journal of Hydraulic Research, IAHR, Vol.33, No.4, pp. 495-517.

Tobler W., (1970) *A computer movie simulating urban growth in the Detroit region*. Economic Geography, 46(2): 234-240.

USGS (2013). *Multibeam Echosounding Survey in Meander Reach, Kootenai River near Bonners Ferry, Idaho - Water Year 2011*. Dataset publication date: January 01, 2013 . (https://catalog.data.gov/dataset/multibeam-echosounding-survey-in-meander-reach-kootenai-river-near-bonners-ferry-idaho-wa-2011)

Valenzuela C., Baumgardner M., (1990). *Selection of appropriate cell sizes for thematic maps*. ITC Journal, 3 (1990), pp. 219–224.

Vilaplana J., (1996). *Computing the Medial Axis Transform of Polygonal Objects by Testing Discs.*

Wang Y., Chen Z., Cheng L., Li M., Wang J., (2013). *Parallel scanline algorithm for rapid rasterization of vector geographic data.* Computers & Geosciences, Volume 59, September 2013, Pages 31–40.

Wahba G., (1990). *Spline Models for Observational DataCBMS-NSF Regional Conference Series in Applied Mathematics*. Society for Industrial and Applied Mathematics, Philadelphia, 169pp.

Watson D.F., Phillip G.M., (1987). *Neighbor Based Interpolation*. Geobyte 2 (2), 12–16.

Willmott C.J., Ackleson S.G., Davis R.E., Feddema J.J., Klink K.M., Legates D.R., O'Donnell J., Rowe C.M., (1985). *Statistics for the evaluation and comparison of models*. Journal of Geophysical Research, 90(C5), 8995–9005.

Zimmermann C., Kennedy J.F., (1978). *Transverse bed slopes in curved alluvial streams.*ASCE J. Hydraul. Div., 104(1), 33–48.